Advancing Bioprocess Development for Filamentous Fungi

Von der Fakultät für Mathematik, Informatik und Naturwissenschaften der RWTH Aachen University zur Erlangung des akademischen Grades einer Doktorin der Ingenieurwissenschaften genehmigte Dissertation

vorgelegt von

Master of Science (M. Sc.)

Katja Rohr

aus Bad Kreuznach

Berichter: Univ.-Prof. Dr. rer. nat. Marco Oldiges
Univ.-Prof. Dr. rer. nat. Ulrich Schwaneberg
Univ.-Prof. Dr. rer. nat. Wolfgang Wiechert

Tag der mündlichen Prüfung: 23.05.2025

„Engage“

Captain Kathryn Janeway

Eidesstattliche Erklärung

Ich, Katja Rohr,

erkläre hiermit, dass diese Dissertation und die darin dargelegten Inhalte die eigenen sind und selbstständig, als Ergebnis der eigenen originären Forschung, generiert wurden.
Hiermit erkläre ich an Eides statt

1. Diese Arbeit wurde vollständig oder größtenteils in der Phase als Doktorandin dieser Fakultät und Universität angefertigt;
2. Sofern irgendein Bestandteil dieser Dissertation zuvor für einen akademischen Abschluss oder eine andere Qualifikation an dieser oder einer anderen Institution verwendet wurde, wurde dies klar angezeigt;
3. Wenn immer andere eigene- oder Veröffentlichungen Dritter herangezogen wurden, wurden diese klar benannt;
4. Wenn aus anderen eigenen- oder Veröffentlichungen Dritter zitiert wurde, wurde stets die Quelle hierfür angegeben. Diese Dissertation ist vollständig meine eigene Arbeit, mit der Ausnahme solcher Zitate;
5. Alle wesentlichen Quellen von Unterstützung wurden benannt;
6. Wenn immer ein Teil dieser Dissertation auf der Zusammenarbeit mit anderen basiert, wurde von mir klar gekennzeichnet, was von anderen und was von mir selbst erarbeitet wurde;
7. Teile dieser Arbeit wurden zuvor veröffentlicht. Eine vollständige Auflistung ist auf den folgenden Seiten zu finden.

Aachen, 26. Mai 2025

Katja Rohr

Published work

This work was conducted at the Forschungszentrum Jülich GmbH at the Institute of Bio- and Geosciences, IBG-1: Biotechnology. Parts of this thesis have been published in peer-reviewed journals, were presented at conferences as posters or talks and were parts of supervised student's work.

Figures taken from existing own publications are cited in the text. Any thought, methodology, result, or conclusion that is part of an existing proprietary publication is not specifically mentioned, but is considered properly cited by the following listings.

Journal articles

I. K. Rohr, L. Gremm, B. Geinitz, E. Jourdier, W. Wiechert, F. Ben Chaabane, and M. Oldiges. "Optimizing microbioreactor cultivation strategies for *Trichoderma reesei*: from batch to fed-batch operations". In: *Microbial Cell Factories* 23 (2024), p. 112. DOI: 10.1186/s12934-024-02371-8

II. K. Rohr, B. Geinitz, J. Seiffarth, A. Anbarani, S. Bernauer, M. Moch, J. Tenhaef, W. Wiechert, K. Nöh, and M. Oldiges. "Insights into the morphology-productivity relationship of filamentous fungi through small-scale cultivation and automated microscopy of *Thermothelomyces thermophilus*". In: *Biotechnology Progress* (2025), e3528. DOI: 10.1002/btpr.3528

Scientific talks

I. K. Rohr, L. Gremm, H. Morschett, B. Geinitz, W. Wiechert, and M. Oldiges. *Microscale cultivation of Trichoderma reesei strains enables strain phenotyping and bioprocess development in batch and fed-batch mode with higher throughput*. Jahrestagung der Vereinigung für Allgemeine und Angewandte Mikrobiologie, virtual, 20.–23.02.2022

II. K. Rohr, B. Geinitz, J. Seiffarth, K. Nöh, W. Wiechert, A. Golabgir Anbarani, S. Bernauer, and M. Oldiges. *Automated morphology analysis for filamentous fungus Thermothelomyces thermophilus - combining small-scale cultivation, lab automation and machine learning*. Final project meeting, Ludwigshafen, Germany, 03.05.2023

Conference posters

I. K. Rohr, L. Gremm, B. Geinitz, W. Wiechert, and M. Oldiges. *Microscale cultivation of Trichoderma reesei RutC30 enables strain phenotyping and bioprocess development in batch and fed-batch mode with higher throughput*. Himmelfahrtstagung on Bioprocess Engineering 2022, Mainz, Germany, 23.–25.05.2022

II. K. Rohr, L. Gremm, B. Geinitz, W. Wiechert, and M. Oldiges. *Microscale cultivation of Trichoderma reesei RutC30 enables strain phenotyping and bioprocess development in batch and fed-batch mode with higher throughput*. Recent Advances in Fermentation Technology 14, Orlando, USA, 06.–09.11.2022

III. K. Rohr, L. Gremm, B. Geinitz, W. Wiechert, and M. Oldiges. *Microscale cultivation of Trichoderma reesei RutC30 enables strain phenotyping and bioprocess development in batch and fed-batch mode with higher throughput*. 6. BioProcessingDays 2023, Recklinghausen, Germany, 27.02.–01.03.2023

IV. K. Rohr, B. Geinitz, J. Seiffarth, K. Nöh, W. Wiechert, A. Golabgir Anbarani, S. Bernauer, and M. Oldiges. *Automated morphology analysis of industrially relevant filamentous fungus Thermothelomyces thermophilus*. 14th ECCE and 7th ECAB, Berlin, Germany, 17.–21.09.2023

Students' projects

I. L. Gremm. *Automating and characterizing the cultivation of Aspergillus niger ANip7-MCS-gfp2*. Research internship, RWTH Aachen University, 2021

II. L. Gremm. *Development of a microscale cultivation workflow for cellulase producing Trichoderma reesei strains*. Master's thesis, RWTH Aachen University, 2021

III. L. van Balen. *Automation and influence of pH, shaking frequency and temperature on microscale cultivation of protein-secreting fungus Thermothelomyces thermophila*. Research internship, FH Aachen, 2021

Danksagung

Diese Dissertation ist das Ergebnis vieler Stunden harter Arbeit, aber ohne die Unterstützung vieler wunderbarer Menschen wäre sie nicht möglich gewesen. Zuerst möchte ich mich ganz herzlich bei meinem Doktorvater Prof. Marco Oldiges für die Betreuung und seinen fachlichen Rat bedanken. Du bist mir immer auf Augenhöhe begegnet und prägst mit deiner offenen Art die produktive und kollegiale Atmosphäre, die ich an den BioPros so schätze. Mein besonderer Dank gilt auch Prof. Wolfgang Wiechert, dem Leiter unserer Hälfte des IBG-1. Du setzt dich mit großem Engagement für den Austausch unter den PhDs am Institut ein, was nicht nur die wissenschaftliche Arbeit fördert, sondern auch das Gemeinschaftsgefühl stärkt. Sowohl bei Marco als auch bei Wolfgang möchte ich mich außerdem ausdrücklich für die große Freiheit bedanken, die wir PhDs genießen dürfen.
Prof. Ulrich Schwaneberg danke ich für die Begutachtung meiner Arbeit und Jun.-Prof. Lisa Fürtauer herzlich dafür, dass sie als Prüferin mitgewirkt hat. Außerdem vielen Dank an Prof. Tony Heitkam für den Prüfungsvorsitz. Mein gesamtes Komitee hat mir während der Verteidigung eine angenehme Atmosphäre ermöglicht, wofür ich ebenfalls sehr dankbar bin.
Die kollegiale Unterstützung, die ich von allen BioPros und Microphens erfahren habe, hat mich während der gesamten Promotionszeit begleitet. Besonders hervorheben möchte ich Holger und Bertram, deren Engagement und fachlicher Rat von unschätzbarem Wert waren. Ich hatte außerdem das Glück, während meiner Promotionszeit in zwei großartigen Büros zu arbeiten: in 252 mit Valentin und Hütti sowie in 257 mit Laura und Max. Eure Gesellschaft hat die Arbeitstage deutlich bereichert und so manchen stressigen Labortag erträglich gemacht. Bedanken möchte ich mich außerdem bei Julia Tenhaef, Michael Osthege, Matthias Moch und Christian Wagner für ihre Unterstützung im Labor, ihren fachlichen Rat oder einfach für ein offenes Ohr. Mein ganz besonderer Dank gilt auch meinen Studentinnen Lisa Gremm und Lisa van Balen für ihre motivierte Mitarbeit und unseren produktiven fachlichen Austausch.
Abschließend gilt mein größter Dank Thomas und meiner Familie: meinen Eltern, Sarah, Stefan und Toni. Ohne euch wäre diese Promotion nicht möglich gewesen. Danke für ganz viel Liebe.

Contents

Abstract I

Zusammenfassung III

Abbreviations V

1. Introduction 1

1.1. The evolution of biotechnology: from early practices to industrial applications . . . 1
1.2. Filamentous fungi . . . 2
1.2.1. Micromorphology and life cycle . . . 4
1.2.2. Macromorphology in submerged cultivation . . . 5
1.2.3. Important industrial producers used in this thesis . . . 6
1.2.4. Selected important enzymes produced by filamentous fungi . . . 9
1.3. Small-scale cultivation and laboratory automation . . . 11
1.3.1. Microbioreactors . . . 12
1.3.2. Laboratory automation . . . 15
1.3.3. Automated microscopy and image analysis . . . 18
1.4. Aim and outline of this thesis . . . 20

2. Optimizing microbioreactor cultivation strategies for *T. reesei* 23

2.1. Development of batch cultivation protocols . . . 24
2.1.1. Plate geometry . . . 24
2.1.2. Cultivation medium . . . 28
2.1.3. Correlation of scattered light and cell dry weight . . . 31
2.2. Applying industrially relevant conditions: fed batch cultivation . . . 33
2.2.1. Ratio of batch to fed batch substrate . . . 33
2.2.2. Fed batch cultivation . . . 37
2.3. Conclusion Chapter 2 . . . 39

3. Automating microbioreactor workflows for *A. niger* 41
3.1. Applying state-of-the-art methods: microbioreactor cultivation workflow for *A. niger* . . . 42
3.2. Automated liquid handling of *A. niger* . . . 44
3.3. Simplifying the inoculation procedure for efficient robotic implementation 45
3.4. Reducing processing time of the pre-culture . . . 48
3.5. Evaluating the influence of the reduced robotic pipet tip size . . . 50
3.6. Applying wide bore robotic pipet tips . . . 52
3.7. Analyzing the variance of manual biological replicates . . . 55
3.8. Weighing the risks and rewards of automation . . . 57
3.9. Conclusion Chapter 3 . . . 59

4. Unraveling the morphology-productivity relationship of *T. thermophilus* 61
4.1. Cultivation and analysis workflow . . . 62
4.2. Microscopy settings . . . 64
4.3. Batch cultivation . . . 66
4.4. Bridging laboratory screening and industrial production: applying fed batch conditions . . . 68
4.5. Evaluating workflow insights: a side-by-side comparison of batch and fed batch results . . . 73
4.6. Automated image analysis . . . 74
4.6.1. Training and validation of the algorithm . . . 74
4.6.2. Application and analysis of cultivation data . . . 77
4.7. Conclusion Chapter 4 . . . 81

5. Conclusion and outlook 83

6. Material and methods 89
6.1. Devices, software and consumables . . . 89
6.2. Microorganisms and strains . . . 90
6.3. Cultivation media, reagents and buffers . . . 91
6.3.1. Cultivation media for *T. reesei* . . . 91
6.3.2. Cultivation media for *A. niger* . . . 92
6.3.3. Cultivation media for *T. thermophilus* . . . 93
6.3.4. Reagents and buffers for cellulase assay . . . 94
6.3.5. Reagents and buffer for phytase assay . . . 94
6.4. Cryo preservation . . . 94

6.5. Microbioreactor cultivation 95
6.5.1. Pre-culture procedure 95
6.5.2. Main culture procedure 96
6.6. Automated liquid handling 97
6.7. Microbioreactor sample processing and product analysis 97
6.7.1. Cell dry weight estimation and correlation with scattered light . 97
6.7.2. Cellulase activity measurement 98
6.7.3. Phytase activity measurement 99
6.7.4. Space-time yield calculation 100
6.8. Automated microscopy 100
6.9. Data processing and display 100

References **103**

List of figures **120**

List of tables **121**

A. Appendices **123**
A.1. Supporting material for Chapter 3 123
A.2. Supporting material for Chapter 4 125
A.3. Supporting material for Chapter 6 129

Abstract

Biotechnology has advanced industrial sectors such as bio-pharmaceuticals, animal feed and nutrition by harnessing the power of microorganisms to produce essential compounds. Among these microbial producers, filamentous fungi have proven indispensable due to their remarkable capacity for enzyme production. Important examples of enzymes produced by filamentous fungi are cellulases, which are used in bioethanol production and textile processing, and phytases, which increase the bioavailability of phosphorous in animal feed. However, bioprocess development for filamentous fungi is hampered by their complex morphology and its significant impact on productivity, making strain selection and process optimization inefficient and time-consuming. Conventional small-scale cultivation approaches often fail to replicate large-scale industrial process conditions, further complicating bioprocess development for filamentous fungi.

This work addresses these limitations by advancing small-scale cultivation techniques through the use of high-throughput microbioreactor systems, integrated laboratory automation and automated microscopy. Specifically, the methodology was developed for *Trichoderma reesei*, *Aspergillus niger* and *Thermothelomyces thermophilus* due to their industrial relevance and distinct morphological characteristics.

First, microbioreactor cultivation strategies were optimized for *T. reesei*, closely aligning small-scale conditions with industrial environments. Subsequently, automated workflows significantly improved the efficiency and throughput of *A. niger* cultivation. Furthermore, a detailed analysis of images of *T. thermophilus* obtained by automated microscopy revealed specific morphological features associated with enhanced enzyme production. These results contribute to a deeper understanding of the relationship between fungal morphology and productivity.

The methods and results presented in this thesis greatly accelerate fungal bioprocess development by reducing both the time and manual effort required. Overall, this framework provides a more efficient approach to optimizing fungal bioprocesses, ultimately advancing industrial enzyme production and contributing to the broader field of industrial biotechnology.

Zusammenfassung

Die Biotechnologie hat Industriezweige wie Biopharmazeutika, Tierfutter und Ernährung vorangebracht, indem sie sich die Fähigkeit von Mikroorganismen zunutze macht, wichtige Produkte herzustellen. Filamentöse Pilze haben sich dabei aufgrund ihrer bemerkenswerten Kapazität, Enzyme wie Cellulasen und Phytasen zu produzieren, als unentbehrlich erwiesen. Die Entwicklung von Bioprozessen für diese Pilze wird jedoch durch ihre komplexe Morphologie und deren Einfluss auf die Produktivität erschwert, was die Stammauswahl und Prozessoptimierung ineffizient und zeitaufwändig macht. Darüber hinaus reproduzieren konventionelle Kultivierungsmethoden im kleinen Maßstab oft nicht die Bedingungen im industriellen Maßstab.
Die vorliegende Arbeit adressiert diese Limitierungen durch die Weiterentwicklung von Kultivierungstechniken im kleinen Maßstab mithilfe von Mikrobioreaktorsystemen, integrierter Laborautomation und automatisierter Mikroskopie. Diese Methodik wurde speziell für die industriell relevanten Pilzarten *Trichoderma reesei*, *Aspergillus niger* und *Thermothelomyces thermophilus* entwickelt.
Zunächst wurden Kultivierungsstrategien für *T. reesei* in Mikrobioreaktoren optimiert, wobei die Bedingungen im kleinen Maßstab eng an die industriellen Bedingungen angelehnt wurden. Anschließend konnte durch die Automatisierung von Arbeitsabläufen die Effizienz und der Durchsatz bei der Kultivierung von *A. niger* deutlich gesteigert werden. Zudem zeigte eine detaillierte Analyse der durch automatisierte Mikroskopie gewonnenen Bilder von *T. thermophilus* spezifische morphologische Merkmale, die mit einer erhöhten Enzymproduktion einhergehen. Diese Ergebnisse tragen zu einem besseren Verständnis der Beziehung zwischen der Morphologie und Produktivität von Pilzen bei.
Die in dieser Arbeit vorgestellten Methoden und Ergebnisse beschleunigen die Entwicklung von Bioprozessen mit Pilzen erheblich, da sie sowohl den zeitlichen als auch den manuellen Arbeitsaufwand reduzieren. Insgesamt bietet dieses Konzept einen effizienteren Ansatz zur Optimierung von Pilz-Bioprozessen, was letztendlich die industrielle Enzymproduktion vorantreibt und einen Beitrag zum gesamten Bereich der industriellen Biotechnologie leistet.

Abbreviations

ALE	Adaptive Laboratory Evolution
A. niger	*Aspergillus niger*
BGL	β-glucosidase
CBH	cellobiohydrolase
CDW	cell dry weight
DBTL	Design-Build-Test-Learn
DO	dissolved oxygen
d_0	shaking diameter
EG	endoglucanase
FP	FlowerPlate
FTU	Phytase Unit
HTP	high-throughput
k_La	volumetric oxygen transfer coefficient
MBR	microbioreactor
MTP	microtiter plate
n	rotational frequency
n_{bio}	number of biological replicates
n_{tec}	number of technical replicates
O_2	oxygen content of the inlet air
RWP	round well plate
PDA	potato dextrose agar

PES	polyethersulfone
pNP	4-nitrophenol
pNPG	4-nitrophenyl-β-D-glucopyranoside
pNPL	4-nitrophenyl-β-D-lactopyranoside
σ	standard deviation
STY	space-time yield
t	(cultivation) time
T	temperature
T. thermophilus	*Thermothelomyces thermophilus*
T. reesei	*Trichoderma reesei*
$\mathbf{V_L}$	filling volume of cultivation wells
$\mathbf{V_W}$	total volume of cultivation wells
WT	wild type

1. Introduction

1.1. The evolution of biotechnology: from early practices to industrial applications

The evolution of biotechnology spans from ancient Egyptian practices of bread, beer and wine making to contemporary industrial applications such as the production of enzymes and pharmaceuticals [1–3]. Initially, these cultivations relied on naturally occurring microorganisms, with no understanding of the underlying microbial mechanisms [4, 5]. The existence of microbes was not discovered until the late 17th century by Antonie van Leeuwenhoek [6]. However, it was only in the late 19th and early 20th centuries that an understanding of the biological processes behind fermentation began to emerge [7].

In 1919, Karl Ereky coined the term 'biotechnology', marking the rise of a new scientific discipline [8]. That same year, Pfizer opened a pilot plant for the production of citric acid from sugar through a fermentation process utilizing *Aspergillus niger* [9]. The biotechnological process was continuously optimized and by 1926, the production of citric acid through fermentation far surpassed the traditional method of extraction from lemons and limes. This innovative process marked a significant turning point, making the citric acid production independent of Italian citrus supplies, which were disrupted during World War I [10].

Since these early developments, biotechnology has flourished into a multi-billion dollar industry. For example, in 2022, the global market for industrially relevant enzymes reached USD 12 billion, with enzymes produced by microorganisms accounting for 86 % of the market revenue [11, 12]. Moreover, this market is expected to reach USD 20 billion by 2030 [13]. This growth is driven by the numerous advantages of biotechnological enzyme production over traditional methods of enzyme extraction from plant materials and animal tissues: biotechnological enzyme production is fast, cost-effective, scalable and microorganisms can be genetically engineered [14].

1.2. Filamentous fungi

Biotechnology has advanced various industries by harnessing the power of microorganisms. Among these microbial producers, filamentous fungi have stood out for their remarkable production capabilities for more than a century [15]. Today, the applications of fungi and fungal products are diverse and span a wide range of industries, as illustrated in Fig. 1.1.
These applications include traditional products such as organic acids, antibiotics and enzymes, as well as the production of food through fungal fermentation. In addition, filamentous fungi are used in the production of pharmaceuticals and polyunsaturated fatty acids [16]. More recent and future applications with great potential include the production of meat alternatives, vegan leather and the use of fungi as composite materials. Visionary concepts even suggest the possibility of building houses and furniture from fungal hyphae [17]. Industries benefiting from fungal biotechnology include food and feed, pharmaceuticals, pulp and paper, textiles, transportation, chemicals, agriculture, automotive, construction and even aerospace [18].

Despite the undeniable value of filamentous fungi, research on these microorganisms still lags behind that of yeasts and bacteria. Several factors contribute to this discrepancy. One is the lower efficiency and longer time required for genetic transformation of filamentous fungi compared to yeasts and bacteria [19]. In addition, the enormous diversity of unique fungal species, numbering in the millions, poses a severe challenge.
Transitioning from academic research to industrial applications, the complex morphology of these different species is an additional critical factor, as it significantly influences bioprocess productivity [20, 21]. Therefore, understanding and eventually controlling their morphology is crucial for optimizing their industrial applications.
The morphology of filamentous fungi can be loosely grouped into their micro- and macromorphology. While micromorphology refers to the microscopic structural features of fungal growth, macromorphology refers to the larger scale forms of fungal organization, visible to the naked eye [22].

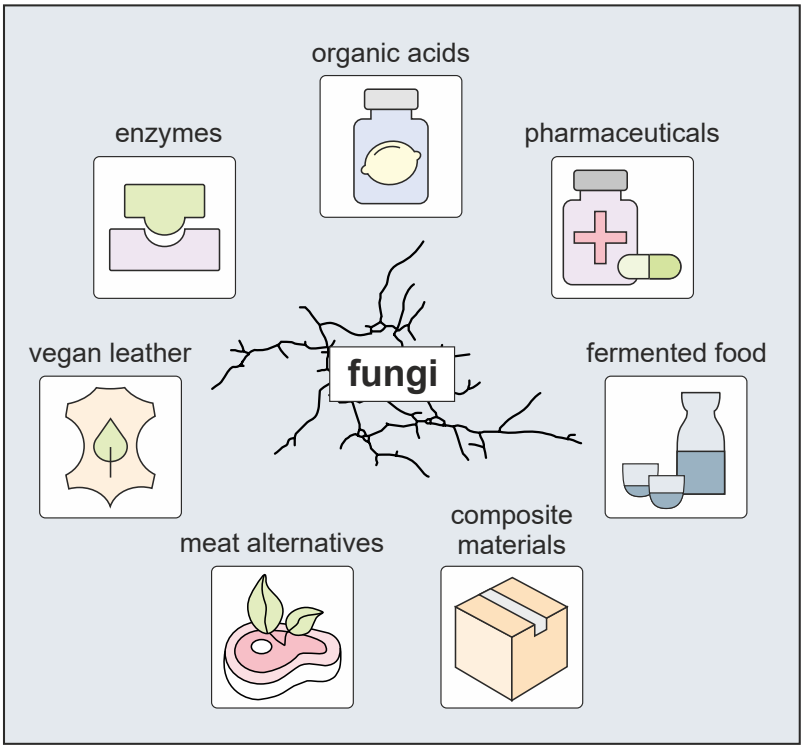

Fig. 1.1. **Product groups produced by filamentous fungi.** Filamentous fungi are key microbial producers, with applications in various industries. Their products include organic acids, pharmaceuticals, enzymes and fermented food. More recent and potential future applications include the production of meat alternatives, vegan leather and composite materials.

1.2.1. Micromorphology and life cycle

One aspect of the complex morphology of filamentous fungi is their distinct life cycle, illustrated in Fig. 1.2. The growth process typically begins with spores less than 10 µm in diameter. In a nutrient-rich environment, these spores begin to swell, increasing in size up to four times due to water uptake. This is followed by the formation of germ tubes, which continue to elongate and eventually develop into thread-like filamentous cells known as a hyphae [22].
As the hyphae elongate, they also form lateral branches. These branches form a network of interconnected hyphal threads called a mycelium [23]. When nutrients become limited, the mycelium begins to form spores. These spores are products of either sexual or asexual reproduction and are known as ascospores or conidia, respectively [24]. The spores remain dormant until favorable environmental conditions return, allowing the life cycle to begin anew.

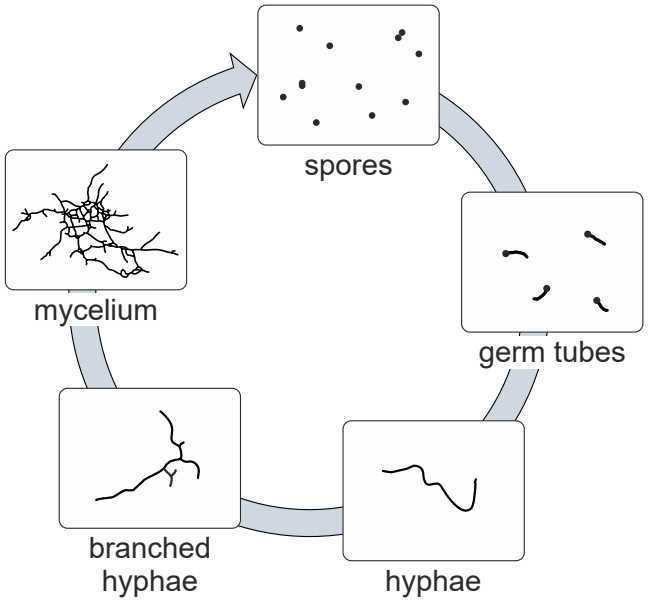

Fig. 1.2. **Life cycle of filamentous fungi.** The life cycle begins with spores that swell and form germ tubes in a nutrient-rich environment. These germ tubes elongate into hyphae, which branch out to form a mycelium. Under nutrient-limited conditions, the mycelium produces spores, which remain dormant until favorable environmental conditions return.

1.2.2. Macromorphology in submerged cultivation

In addition to the micromorphological structures shown in Fig. 1.2, the submerged cultivation of filamentous fungi produces larger scale organizational forms. These macromorphologies, illustrated in Fig. 1.3 A, range from a homogeneous suspension of dispersed hyphae to dense, spherical pellets up to several millimeters in diameter [25].

As shown in Fig. 1.3 B, the prevalent macromorphology is dependent on a wide variety of environmental factors, including agitation speed or rotational frequency, dissolved oxygen (DO) concentration, medium composition, pH or inoculum concentration [26]. In addition, different species of filamentous fungi may have varying responses to the influence of the same environmental conditions with respect to their morphological manifestations.

The morphology, in turn, significantly affects the physical properties of the culture suspension [27, 28]. For example, the mycelial morphology used in cultivations of *Trichoderma reesei* for enzyme production results in a highly viscous culture suspension. High viscosity can lead to temperature and nutrient gradients within bioreactors and reduces the maximum oxygen transfer capacity in stirred tank reactors, which can lead to oxygen limitations if not compensated by increased agitation or aeration [29]. In shaken systems, viscosities above $\simeq$80 mPa·s also reduce the maximum oxygen transfer capacity. In extreme cases, high viscosities can lead to the 'out-of-phase' phenomenon, where the fermentation suspension no longer follows the rotating motion of the shaker table. This leads to an undefined decrease of mixing efficiency and mass transfer of gas and liquid [30].

In contrast to a mycelial morphology, pellets offer a better heat and mass transfer within the bioreactor. Easier agitation and aeration result in lower operating costs due to reduced power requirements [31]. However, concentration gradients within the pellet can result in nutrient and oxygen depletion in the core, possibly even causing hollow cores [32, 33].

The morphology of filamentous fungi is often closely linked to their productivity and has a significant impact on bioprocess productivity (Fig. 1.3 B) [34, 35]. However, the best morphological configuration cannot be predicted a priori when developing a new process, as the optimal morphology is highly dependent on the specific fungus and the target product [21, 36]. For instance, filamentous growth of *A. niger* is preferred for pectic enzyme production, whereas pellet formation is more advantageous for citric acid production [37]. This variability necessitates extensive research

when establishing new bioprocesses to ensure the selected morphology enhances productivity and efficiency.

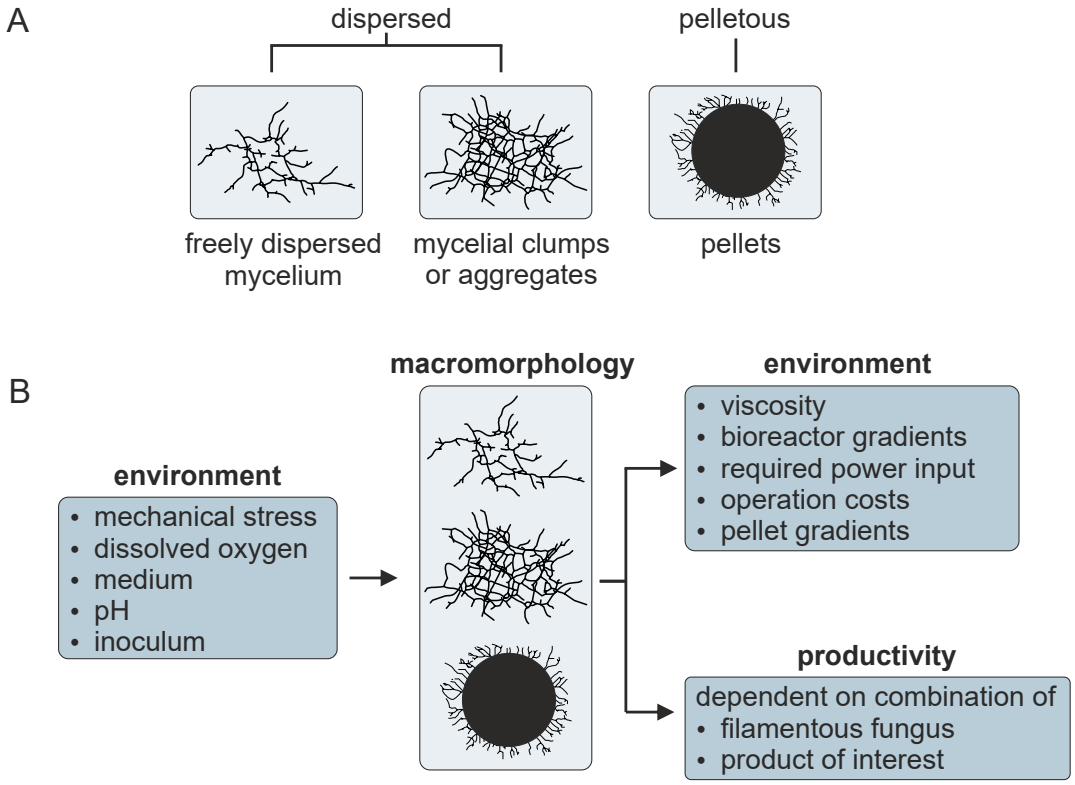

Fig. 1.3. **Morphology of filamentous fungi in submerged cultivation.** (A) Macromorphology. The macromorphology of filamentous fungi ranges from freely dispersed mycelium to mycelial clumps or aggregates and dense pellets. (B) Influences on the macromorphology and resulting effects. The prevalent morphology of filamentous fungi depends on the given environmental factors and in turn influences the environment. In addition, the productivity of filamentous fungi depends on the combination of their morphology and the product of interest. Subfig. A adapted from [38].

1.2.3. Important industrial producers used in this thesis

In the context of industrial biotechnology, the selection of a suitable filamentous fungus for a specific product is critical to achieving efficient bioprocesses. Moreover, a thorough understanding of each microorganism is essential to optimize production. For this work, *T. reesei*, *A. niger* and *Thermothelomyces thermophilus* were selected due to their established capabilities in organic acid and enzyme production. The following section provides an in-depth exploration of these fungi, highlighting their historical development and current relevance in the field.

T. reesei is a mesophilic ascomycete fungus that has attracted considerable attention since its discovery [39]. About 80 years ago, during World War II, *T. reesei* was first isolated from rotting US Army equipment on the Solomon Islands [40]. Initially identified as *Trichoderma viride* and named QM6a, it was later recognized as a distinct species and renamed *T. reesei* after researcher Elwyn T. Reese [41]. The genome sequence of wild type (WT) QM6a was published in 2008 [42].
T. reesei QM6a gained prominence as a robust producer of homologous cellulases, sparking interest in its potential for alternative fuel production [43]. The concept focused on the hydrolysis of cellulose-rich biomass to glucose, which could then be fermented to produce ethanol [44]. To economically produce enzymes for bioethanol production, researchers aimed to create catabolite derepressed mutants with high cellulolytic activity. Through three rounds of random mutagenesis of the WT, the hypercellulolytic and catabolite-derepressed strain RutC30 was successfully developed [45]. In addition to QM6a and RutC30, this work employs the strain TR3158, which has a lower viscosity compared to its parental strain RutC30 [46].
Today, *T. reesei* is not only known for the production of homologous cellulases, but has also become a prominent producer of heterologous enzymes [47]. With these advances in its use as a recombinant host, *T. reesei* is used for the production of various technically relevant enzymes, including amylase, catalase, glucosidase, laccase, phytase, pectinase, xylanase. In 2015, approximately 243 commercially available enzymes were produced by microbial fermentation, with 21 of these enzymes using *T. reesei* as a recombinant host [48].

In 1917, food chemist James Currie published a ground breaking discovery: any strain of the mesophilic ascomycete fungus *A. niger* could produce high concentrations of citric acid when grown in a sugar medium [49]. Just two years later, the American company Pfizer opened a pilot plant for the industrial production of citric acid with *A. niger*, heralding the birth of industrial biotechnology [10].
Initial research on *A. niger* primarily focused on optimizing citric acid production [7]. By the late 1950s, however, researchers discovered that *A. niger* was also a prolific producer of a variety of useful enzymes, including glucoamylases, proteases, oxidases, cellulases and pectinases, amongst others [50]. The publication of the *A. niger* genome in 2007 further marked a significant milestone in understanding its metabolic capabilities and genetic potential [51].
Today, citric acid production remains a multi-billion-dollar industry [52]. In addition, the fungus is a versatile platform for the production of a wide range of acids and

enzymes [53]. For example, it is common to achieve production titers of 30 $g \cdot l^{-1}$ of glucoamylase [54]. The strain *A. niger* ANIp7-MCS-gfp2 used in this work, which is derived from the protease deficient strain *A. niger* AB1.13, further enhances the utility of this platform by featuring the expression of GFP [55, 56].
In recent years, there has been a significant increase in research focused on establishing *A. niger* as an industrial platform for drug discovery and the production of secondary metabolites [57, 58]. These efforts are aimed at countering the alarming rise of drug-resistant microbes in both medicine and agriculture.

Alongside well-established biological systems such as *A. niger* and *T. reesei*, the ascomycete fungus *T. thermophilus* has emerged as a particularly promising organism for industrial applications [59, 60]. The WT, ATCC 42464, was first described in 1963 as *Sporotrichum thermophilum* [61]. Since then, it has been reclassified three times: in 1974 to *Chrysosporium thermophilum* or *thermophile* [62], in 1977 to *Myceliophthora thermophila* [63] and finally in 2015 to *T. thermophilus* [64]. In 2011, the genome sequence of the WT was published, greatly advancing research on this filamentous fungus [65].
This thermophilic fungus, with an optimal growth temperature of 45-50 °C, is particularly known for its natural secretion of a number of thermostable enzymes, including cellulases and hemicellulases [16, 66, 67]. In addition to those enzymes, *T. thermophilus* is recognized for its ability to produce phytase, an enzyme of significant importance in the animal feed sector. Accordingly, a phytase-secreting strain of *T. thermophilus* is employed in this thesis.
While academic research focuses on the WT of *T. thermophilus* and its thermostable enzymes, an important industrial strain has been developed since the early 1990s: the strain C1. This strain was originally discovered in alkaline soil in a forest in eastern Russia during a screening of fungal isolates for cellulase production, intended for applications in the textile industry [68]. Since its discovery, Dyadic International (Jupiter, US) has improved the strain in several random mutagenesis rounds. Initial steps resulted in strain HC, which has a high cellulase production capacity and 50-fold lower viscosity than the parental strain [69]. Subsequent development led to two key protease-deficient strains. A high cellulase strain producing up to 100 $g \cdot l^{-1}$ extracellular protein and a low cellulase strain serving as a platform for heterologous protein production [69]. These developed strains have been licensed by Dyadic to third parties such as Codexis, BASF and Abengoa Bioenery, enabling their use in various biotechnological applications [70].

1.2.4. Selected important enzymes produced by filamentous fungi

Filamentous fungi are well known for their ability to produce a wide range of enzymes that are vital to numerous industries. In the following section, two key enzymes, cellulases and phytases, produced by the filamentous fungi studied in this thesis are discussed. Their biological functions and industrial importance are reviewed to highlight their critical role in biotechnological applications.

Cellulases are a group of enzymes that facilitate the hydrolysis of cellulose, breaking it down into glucose [71]. As illustrated in Fig. 1.4, at least three different types of cellulases are required for the hydrolysis of cellulose to glucose: endoglucanase (EG, EC 3.2.1.4), cellobiohydrolase (CBH, EC 3.2.1.91) and β-glucosidase (BGL, EC 3.2.1.21) [72]. EG randomly cleaves the β-1,4-glycosidic bonds in the amorphous regions of cellulose, creating new chain ends. CBH, an exoglucanase, then attacks these newly exposed ends, cleaving off the disaccharide cellobiose. Specifically, CBH I cleaves cellobiose from the reducing ends of the cellulose chains, while CBH II targets the non-reducing ends. Finally, BGL hydrolyzes the resulting cellobiose into glucose [73].
The industrial relevance of cellulases is vast and includes applications in sectors such as pulp and paper, textiles and detergents, bioethanol production, brewing and winemaking, food processing, animal feed, agriculture and waste management [74]. In the textile industry, cellulases are used in the bio-stoning of denim, where the enzymes break down fiber ends on the textile surface, allowing the dye to be removed during the wash cycle by mechanical abrasion [74]. Another important application example of cellulases is in bioethanol production, where they are used to convert lignocellulosic biomass into fermentable sugars [75].

Phytases (EC 3.1.3.x) catalyze the stepwise hydrolysis of phytic acid to lower inositol phosphate esters and orthophosphate [76]. This process, shown in Fig. 1.5, is crucial for improving the bioavailability of phosphorus in animal feed and reducing phosphorus pollution in animal waste [77].
First described in 1907, phytases have gained significant industrial relevance since their commercialization in 1991 [78, 79]. Crops and legumes used for animal feed typically contain 2-8 % phytic acid, which accounts for 55–90 % of their total phosphorus content [80]. However, monogastric animals, such as pigs and chickens, cannot effectively digest phytic acid [81]. This limitation necessitates the addition of phytase to animal diets to liberate inorganic phosphorus from phytic acid, thereby eliminating

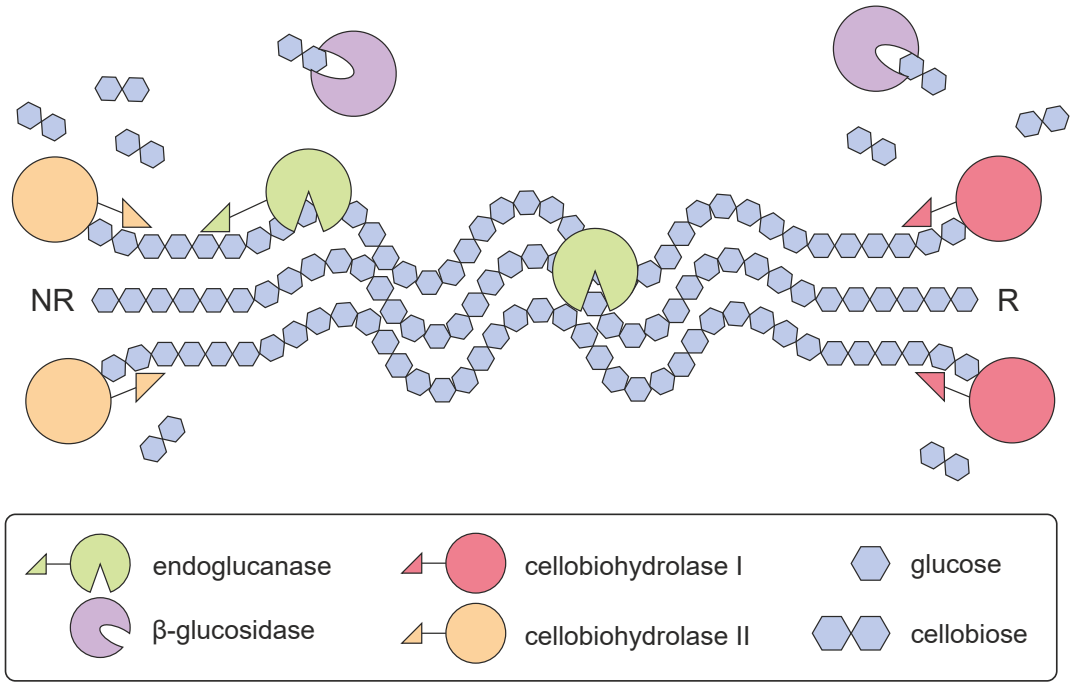

Fig. 1.4. **Mechanism of action of cellulases.** Cellulases hydrolyze cellulose to glucose through the coordinated action of EG, CBH and BGL. EG cleaves the β-1,4-glycosidic bonds to create new chain ends, CBH removes cellobiose units from these ends and BGL hydrolyzes the cellobiose units into glucose. NR = non reducing end, R = reducing end.

the need for supplemental phosphorus, an expensive and non-renewable resource [82, 83].
The addition of phytase to animal feed not only reduces the need for supplemental phosphorus, but also reduces the excretion of unused phosphate in the form of phytate, thereby reducing environmental impact [84]. Furthermore, phytic acid chelates divalent cations such as calcium, iron and zinc, making these essential nutrients unavailable [85]. By hydrolyzing phytic acid, phytase releases these chelated cations, making them available for absorption and further reducing the environmental impact.
In 2023, the global market for phytase used in animal feed was valued at more than USD 570 million and is projected to exceed USD 1 billion by 2032 [86, 87]. This substantial market growth, ongoing since the 1990s, underscores the continued importance of phytase as a biotechnological product in animal nutrition and environmental sustainability.

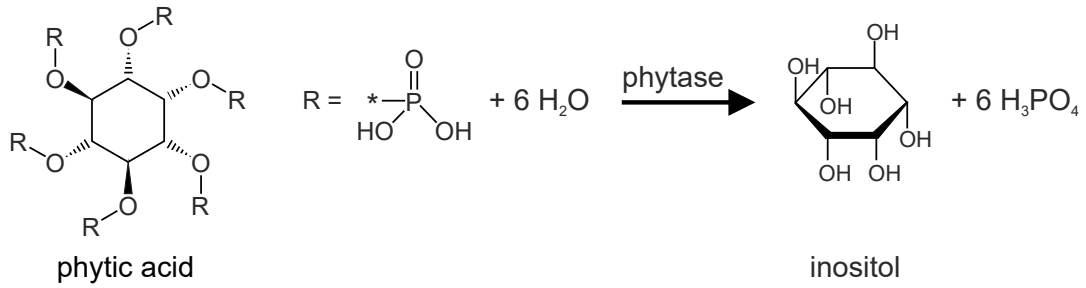

Fig. 1.5. **Reaction catalyzed by phytases.** Phytases catalyze the stepwise hydrolysis of phytic acid to lower inositol phosphate esters and orthophosphate.

1.3. Small-scale cultivation and laboratory automation

Conventional bioprocess development is divided into two main stages: strain screening followed by the development, optimization and validation of the bioprocess [88]. Strain screening is typically performed in microtiter plates (MTPs) and shake flasks, while the later stages of bioprocess development take place in increasingly larger stirred tank bioreactors [89].
This conventional approach to bioprocess development has several significant limitations. Firstly, strain screening and bioprocess development should be performed simultaneously [90]. This holds especially true for filamentous fungi, as morphology, physiology and productivity of these microorganisms are interlinked with each other and therefore should be addressed collectively [21]. Secondly, strain screening

should be conducted under conditions that closely mimic industrial production processes [91]. This is critical because the performance of different strains can vary significantly depending on the cultivation conditions [92, 93]. If these concepts are not applied, it can result in the erroneous elimination of top-performing strains or the selection of strains that perform only moderately under actual production conditions [94].
In addition, as development progresses, process knowledge increases, but the cost per experiment also increases significantly due to the increasing scale. Consequently, fewer experiments are typically performed in later stages [95]. However, poorly informed decisions based on inadequate early data can require additional experiments and iterations, ultimately increasing overall development time and cost [96]. Therefore, obtaining robust, relevant data early on is critical to streamlining later stages of the bioprocess.
In a continuous evolution since the 1990s, microbioreactors (MBRs) and laboratory automation have emerged as key technologies to address these challenges [97]. In the field of filamentous fungi, automated microscopy has additionally been introduced as a significant advance [98]. Thus, these technologies will be introduced in more detail in the following.

1.3.1. Microbioreactors

MBRs are miniaturized bioreactor systems designed for the cultivation of microorganisms at volumes ranging from microliters to milliliters [99]. These systems are intended to replace traditional MTPs, shake flasks and laboratory-scale stirred tank bioreactors in the early and mid-stages of bioprocess development, with the primary goal of accelerating bioprocess development [100]. MBRs achieve this through a high degree of parallelization, enabling high experimental throughput while providing high-resolution monitoring of key cultivation parameters such as biomass, DO and pH. In addition, MBRs allow precise control of critical cultivation parameters, including temperature and pH [100]. The successful scalability of these systems has been reported by numerous studies [101–103].
Commercial MBR systems are based on two basic principles, miniaturized stirred tank bioreactors and advanced MTP cultivation instruments [104]. Examples of commercially available MBR systems include the bioREACTOR (2mag, München, DE) for stirred MBRs, while shaken systems include the BioLector (Beckman, Brea, US),

Bioscreen C (Oy Growth Curves Ab Ltd., Helsinki, FI), Growth Profiler (EnzyScreen BV, Heemstede, NL) and SensorDish Reader (PreSens, Regensburg, DE) [105–109]. In recent years, shaken MBR systems have received considerable attention due to their versatile capabilities. Shaken MBR systems are particularly attractive for their ease of setup and ability to perform non-invasive optical biomass measurements without interference from impellers or gas bubbles [101]. In addition, some shaken systems offer advanced features such as microfluidic channel-based feeding, allowing precise control of cultivation conditions [94]. Based on these strengths, the shaken MBR BioLector Pro was selected as the primary MBR cultivation instrument at IBG-1.

The BioLector is an advanced orbital shaking MBR system designed for high-throughput (HTP) bioprocess development. One of the key features of the BioLector is its ability to perform non-invasive optical measurements with high temporal resolution, approximately every three to ten minutes, while maintaining continuous shaking [110, 111]. The system enables online monitoring of scattered light, indicative of biomass concentration, and fluorescence intensity through the transparent MTP bottom. It additionally supports monitoring of DO and pH via pre-calibrated optodes [112].
The measurement process, illustrated in Fig. 1.6 A, uses an x-y positioning device to direct an optical fiber bundle under each MTP well. The bundle emits excitation light through the transparent bottom of the well into the culture suspension or onto the optode. The returning signal is detected and the fiber bundle is moved to the next well, which is processed accordingly [113, 114].
The BioLector uses disposable MTPs, available in two different geometries, round well plates (RWPs) and FlowerPlates (FPs). The latter MTP is equipped with baffled wells to improve oxygen transfer while maintaining a stable liquid height at the well center, which is required for the optical measurements [115]. The working volumes per well range from 0.8 ml to 2.4 ml, depending on plate type and rotational frequency. The system provides volumetric oxygen transfer coefficient (k_La) values ranging from 30 to 160 h^{-1} for RWPs and 100 to 650 h^{-1} for FPs [116, 117].
Both plate types accommodate either 48 or 32 parallel cultivation wells, depending on the mode of operation (batch or fed batch/pH control). For fed batch cultivation and pH control, the BioLector supports simultaneous feeding of two different solutions, for example glucose and sodium hydroxide [118]. The feed plate layout, presented in Fig. 1.6 B, features eight columns, with each column containing two reservoir wells connected to the four cultivation wells below, resulting in a total of 16 reservoir wells

and 32 cultivation wells per plate [119, 120]. A microfluidic chip, which replaces the bottom of a conventional MTP, enables controlled dosing of nanoliter volumes of feed solution using a micropump [112].

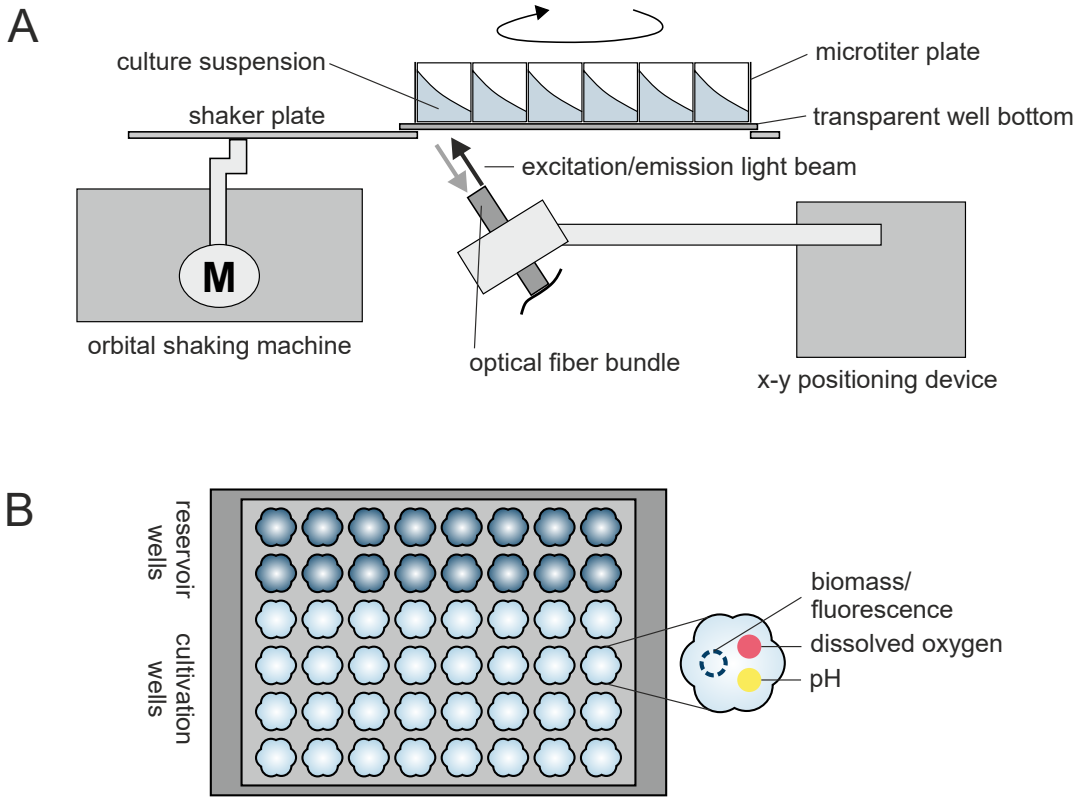

Fig. 1.6. **The BioLector MBR.** (A) Measurement process. An x-y positioning device directs an optical fiber bundle under each well of the MTP. The device emits excitation light through the transparent bottom of the wells and collects the resulting signal before moving to the next well. (B) Schematic of an FP for fed batch cultivation. The plate contains 32 cultivation wells and 16 reservoir wells, allowing two different solutions to be fed simultaneously. Optodes for non-invasive DO and pH measurements are integrated into the bottom of the plate. Subfig. A adapted from [114].

The use of MBRs is a critical first step in achieving high experimental throughput while generating robust and relevant data in the early stages of bioprocess development. However, further automation is essential to realize the full potential of HTP bioprocess development. Integrating MBR systems with laboratory automation significantly expands their applications and enables more complex workflows [121, 122]. This synergy between advanced MBR technology and automation opens new possibilities to optimize and accelerate bioprocess workflows.

1.3.2. Laboratory automation

Laboratory automation refers to the use of technology to perform tasks with minimal human intervention [123]. It includes the use of automated instruments, robotics, control systems, software and data management tools to conduct and manage experiments, processes and workflows [124]. The primary goals of laboratory automation are to increase the efficiency, precision and reproducibility of bioprocesses and bioprocess development, to minimize the potential for human error and to increase the research output per full-time equivalent [125, 126]. This allows researchers to focus on more complex, non-repetitive tasks and to work more efficiently without the interruptions typically caused by routine activities such as sampling or process monitoring [127].
This thesis focuses on laboratory automation through the use of automated instrumentation and liquid handling robotics. Commercial liquid handling robotics systems vary in complexity, ranging from simple pipetting robots to advanced systems with extensive functionalities and integrated devices.
For example, the BRAND Liquid Handling Station (BRAND, Wertheim, DE) is a basic pipetting robot designed for tasks such as preparing dilution series or dispensing liquids into MTPs, bridging the gap between manual electronic pipets and more complex robotics systems [128]. The Opentrons OT-2 Robot (Opentrons, Long Island City, US) not only provides automated pipetting capabilities, but also allows the integration of additional devices such as a heater-shaker module, which can be used for mixing and incubating biological samples, and a thermocycler for molecular biology tasks such as polymerase chain reactions [129]. At the more advanced end, the Tecan Fluent (Tecan, Männedorf, CH) is a sophisticated liquid handling workstation featuring up to three liquid handling and robotic gripping arms, enabling complex multi-step workflows. It includes a camera for remote deck inspection, allowing process monitoring from the office. The system can be further equipped with thermocyclers for molecular biology tasks, positive pressure modules for sample filtration, plate sealers for preparing MTPs for storage and microplate readers for assay applications [130]. These systems have been widely adopted in academic research laboratories, where they have greatly expanded research capabilities [131, 132].

Integrating an MBR into a robotics system greatly expands the capabilities of both technologies and several platforms combining these technologies have been reported [133–135]. At IBG-1, this integration has been realized in a customized automation

platform, forming the cornerstone of the bioprocess development strategies presented in this thesis. This automation platform is schematically shown in Fig. 1.7.
The platform is based on a Tecan Freedom EVO 200 (Tecan, Männedorf, CH) with a sterile hood. It includes a robotic manipulator for labware transfer and a liquid handler with eight steel needles for pipetting operations, both of which operate along the x-y-z-axes. Additional components include a washing station for the pipet needles, trough and plate carriers, a cryostat for cooling specific plate carriers and a plate shaker with heating capabilities for incubation and assay applications. Furthermore, a microplate reader is available for product analysis.
Microbial cultivation is conducted within a BioLector Pro MBR system with the respective control unit (Beckman Coulter, Brea, US). All instruments are interconnected and managed by a custom-designed process control system, details of which can be found in Osthege [136].
This unique combination of instruments enables the automation of diverse bioprocessing tasks. For example, the platform has been used for automated inoculation and sampling of MBR main cultures based on the scattered light online signal, a method published by Helleckes et al. [137]. Another important application example is the Adaptive Laboratory Evolution (ALE) of *Corynebacterium glutamicum*, where the platform was used for untargeted strain optimization. As presented by Radek et al. [138], this resulted in a strain variant with a significantly improved growth rate on D-xylose as the sole carbon and energy source. Additionally, the platform has enabled automated downstream processing of cell suspensions via bead mill cell disruption immediately after MBR cultivation, allowing for subsequent analysis of intracellular targets, as shown by Jansen et al. [139].

The use of advanced MBR systems and state-of-the-art robotics platforms has greatly accelerated bioprocess development and expanded the capabilities for HTP experimentation and process optimization [141]. However, when working with filamentous fungi, whose complex morphologies directly influence their productivity, additional tools are required to fully understand and optimize these processes. Microscopy is critical for capturing the intricate morphological changes in filamentous fungi that cannot be detected by standard cultivation data alone. However, manual microscopy is both time-consuming and subjective [142]. It is therefore impractical for the HTP requirements of modern bioprocessing, making automation essential.

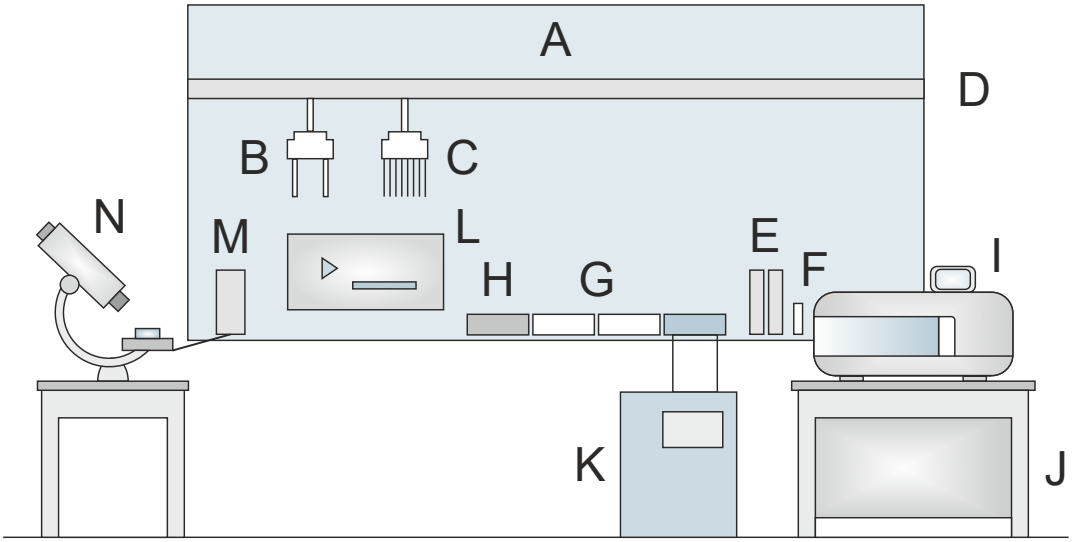

Fig. 1.7. **Schematic of the laboratory automation platform used in this work.** A Tecan Freedom EVO 200 base unit is equipped with (A) a sterile hood, (B) a robotic manipulator for labware transfer and (C) a liquid handler for pipetting operations, which can move along the (D) axis in x-y-z direction, (E) a washing station, (F) trough carriers, (G) plate carriers, (H) a plate shaker with heating capability, (I) a BioLector Pro MBR system with the corresponding (J) control unit, (K) a cryostat cooling one of the plate carriers for sample storage, (L) a microplate reader for product analysis assays and (M) an injection station allowing sample transfer to the (N) adjacent inverted light microscope. Adapted after [140].

1.3.3. Automated microscopy and image analysis

There are various commercially available solutions for automated microscopy, each with features tailored to specific research needs. For example, the Zaber Nucleus (Zaber, Vancouver, CA) offers HTP image acquisition across multiple fluorescence channels, commonly used for MTP screening purposes [143]. The Leica Mica (Leica, Wetzlar, DE) provides both widefield and confocal microscopy imaging in a controlled incubation environment, making it suitable for dynamic imaging applications [144]. The Agilent BioTek Lionheart FX (Agilent, Santa Clara, US) combines brightfield and fluorescence imaging with environmental controls such as O_2/CO_2 and humidity, and a dual reagent injector for kinetic assays [145].
Although these systems have advanced the automation of image acquisition, they are primarily designed for fundamental research and lack critical features for bioprocess development. For example, while the BioTek Lionheart FX is suitable for static cultivation in MTPs, it lacks shaking capabilities. Moreover, the unavailability of integration with MBRs further limits their applicability in bioprocess development, where online or at-line monitoring is essential [89]. Thus, customized solutions are necessary to bridge these gaps.

At IBG-1, a customized solution was developed by integrating an inverted light microscope with a laboratory automation platform (Fig. 1.7). As described by Jansen et al. [146], an injection station was incorporated into the laboratory automation platform to allow seamless sample transfer from an MBR to the adjacent light microscope for automated microscopy (Fig. 1.8). Specifically, the liquid handler transfers cultivation samples into a custom-built injection station (Fig. 1.8 A), which then fills a flow chamber mounted under the microscope (Fig. 1.8 B). The injection station and flow chamber are connected by tubing and the microscope is equipped with a camera that automatically captures images at preset intervals.
This setup enables a wide range of morphological studies. For example, Jansen et al. [146] used this system to track the pellet size of *Aspergillus carbonarius* over time at different cultivation temperatures. Similarly, Ruzaeva et al. [147] monitored the size and quantity of catalytically active inclusion bodies in *Escherichia coli* over time.
Although these studies have demonstrated the utility of the setup for certain microorganisms, challenges remain when applying it to filamentous fungi with mycelial morphologies. These fungi are much more difficult to analyze than pellet-forming organisms due to their intricate hyphal structures and overlapping growth patterns.

These complexities make it difficult to capture high-quality images that can be used for accurate morphological analysis. This underscores the ongoing challenges in adapting automated microscopy for more complex microorganisms.

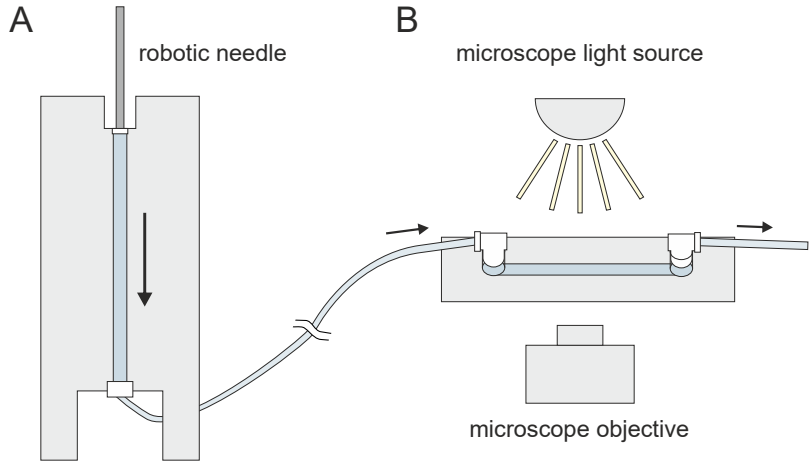

Fig. 1.8. **Schematic of the automated microscopy equipment used in this work.** (A) Custom-built injection station, (B) flow chamber mounted under an inverted light microscope. The liquid handler loads cultivation samples into the injection station, filling the flow chamber, which is connected by tubing. The arrows indicate the flow direction of cultivation samples.

When combined with MBRs and laboratory automation, automated microscopy enables HTP image acquisition for the at-line monitoring of cell growth, morphology and other critical parameters. However, the large datasets generated by this approach require automated extraction of cellular features for quantitative analysis or risk becoming a new bottleneck in the workflow [148]. Although recent advances in image analysis techniques, particularly those using deep learning, have significantly improved automated feature extraction, these methods rely on the availability of large, well-annotated datasets [149–151]. To address this need, Seiffarth et al. [152] developed an annotation platform that provides a robust workflow for annotating and segmenting microorganisms in time-lapse images. However, this platform has primarily been applied to bacteria, because the complex and variable morphology of filamentous fungi makes it difficult to generate suitable datasets. Consequently, there remains a pressing need for the generation and annotation of high-quality fungal datasets to enable accurate image analysis of these more complex organisms.

1.4. Aim and outline of this thesis

The primary objective of this thesis is to advance bioprocess development for filamentous fungi by developing and optimizing efficient small-scale cultivation protocols. This is achieved through the use of MBR systems, laboratory automation and automated microscopy. In addition, this thesis aims to deepen the understanding of filamentous fungi, with a particular focus on *T. reesei*, *A. niger* and *T. thermophilus*. These fungi are important industrial producers, but their complex morphology and the influence of environmental factors on their productivity present significant challenges. These challenges are addressed by the following objectives:

I. **Optimization of MBR cultivation strategies.**
Chapter 2 focuses on the optimization of small-scale cultivation protocols in batch and fed batch mode, specifically tailored to cellulase-producing *T. reesei* strains. The aim is to develop MBR strategies that closely mimic industrial production conditions on a smaller scale. This involves a systematic evaluation of key cultivation parameters such as plate geometry, rotational frequency and feeding strategies to improve fungal growth and productivity.

II. **Automating MBR workflows.**
The objective of Chapter 3 is to implement and evaluate automated workflows for the cultivation of *A. niger*. This chapter leverages the potential of automation to streamline the cultivation process by automating inoculation. The integration of laboratory automation systems with the MBR setup is expected to significantly enhance experimental throughput, reproducibility and efficiency.

III. **Elucidating the morphology-productivity relationship.**
Chapter 4 aims to unravel the complex relationship between fungal morphology and productivity, focusing on a phytase-producing strain of *T. thermophilus*. The goal is to understand how different cultivation conditions, including pH and feeding rates, affect the morphology of *T. thermophilus* and its subsequent impact on enzyme production. To achieve this, this work employs an advanced workflow that integrates MBR cultivation, liquid handling robotics and automated microscopy with image analysis. In addition, this work aims to provide a valuable tool for further research in this field by developing a methodology that can be applied to similar studies. Ultimately, this will allow the association of

specific morphological characteristics with productivity and the optimization of bioprocesses for maximum efficiency.

The research presented in this thesis is expected to have a substantial impact on the field of industrial biotechnology by identifying and optimizing key parameters for efficient bioprocess development for filamentous fungi. While the strategies outlined in objectives I-III target important aspects of fungal cultivation that are relevant to all filamentous fungi, specific examples are provided through studies on *T. reesei*, *A. niger* and *T. thermophilus*. Although the insights and tools developed in this thesis are tailored to these particular fungi, the methods and workflows established can serve as a basis for further research on other fungi.

2. Optimizing microbioreactor cultivation strategies for *T. reesei*

Parts of this chapter have been previously published in publication I, conference posters I-III and conference talk I. This chapter is partly based on data collected during student project II. K. Rohr is the author of this chapter, had the scientific lead on this project, conceptualized and supervised student project II and analyzed and visualized all data. L. Gremm conducted all BioLector experiments, established the cellulase assay on the robotics platform and developed the adapted medium. E. Jourdier and F. Ben Chaabane provided the strains.

In modern bioprocess development, the optimization of small-scale cultivation strategies is critical to establishing efficient workflows that can meet the demands of HTP experimentation while closely mimicking industrial production conditions. MBRs play an essential role in this process by providing high experimental throughput along with comprehensive bioprocess monitoring and control. The advantages of MBRs are particularly important for complex microorganisms such as filamentous fungi. The morphology of these microorganisms is highly sensitive to environmental conditions and their productivity is directly influenced by their morphology. Therefore, optimizing their cultivation parameters is crucial to maximizing their industrial potential.
This chapter focuses on optimizing MBR-based cultivation strategies for *T. reesei*, an important industrial cellulase-producer. This involves a systematic investigation of several critical parameters, including plate geometry, rotational frequency and feeding strategies, all aimed at enhancing fungal growth and maximizing productivity. By optimizing these conditions, this chapter lays the groundwork for workflows that streamline fungal bioprocess development and thus accelerate development cycles. Furthermore, the methods and results presented in this chapter lay the foundation for the implementation of more advanced techniques, such as the automation of cultivation workflows and microscopy. These will be discussed in subsequent chapters.

2.1. Development of batch cultivation protocols

2.1.1. Plate geometry

In the development of MBR batch cultivation protocols for three cellulase producing *T. reesei* strains, two types of BioLector plates, FPs and RWPs were investigated. These two plate types offer different well geometries. BioLector FPs offer a three to four times higher k_La than RWPs due to their baffled structure, with k_La values ranging from 100 to 650 h^{-1} for FPs and 30 to 160 h^{-1} for RWPs [116, 117]. In order to introduce sufficient oxygen for fungi growing with a microfilamentous morphology, a high k_La is required. Therefore, an FP was tested first in the development of a milliliter-scale cultivation workflow.

Fig. 2.1 displays cultivation results of the strains WT, RutC30 and RutC30 TR3158 at a rotational frequency of 1200 rpm and a cultivation volume of 1 ml. For each strain, six biological replicates were run with sampling of three replicates each. The reproducibility of the biomass growth profile, measured by scattered light, was low for the WT and RutC30 TR3158, but high for RutC30. A more detailed examination revealed that only two replicates of the WT showed biomass growth measurable by an increase in scattered light. In contrast, an increase in scattered light was visible for all replicates of RutC30 and RutC30 TR3158.
These observations can most likely be attributed to the strong wall growth observed for all strains (Fig. 2.1, right side). While the WT and RutC30 adhered to the wall of the well above the culture suspension, RutC30 TR3158 formed a thick rim at the bottom of the well. The preferential growth of WT biomass along the edge of the well rather than in suspension elucidates the absence of a notable increase in scattered light for most replicates.

Due to the extensive wall growth and the partly missing growth in suspension, the FP was considered unsuitable for a reproducible cultivation workflow. Different cultivation vessel geometries exert different levels of shear stress on the microorganisms in a culture suspension [154]. As shear stress has an important influence on fungal morphology [28, 155, 156], this could also affect the wall growth behaviour. Therefore, following cultivations were conducted in RWPs.
RWPs yield a lower k_La than FPs at the same rotational frequency and filling volume [116, 117]. However, the maximum rotational frequency, which is recommended by the manufacturer for RWPs with a filling volume of 1 ml, is 1000 rpm. Therefore,

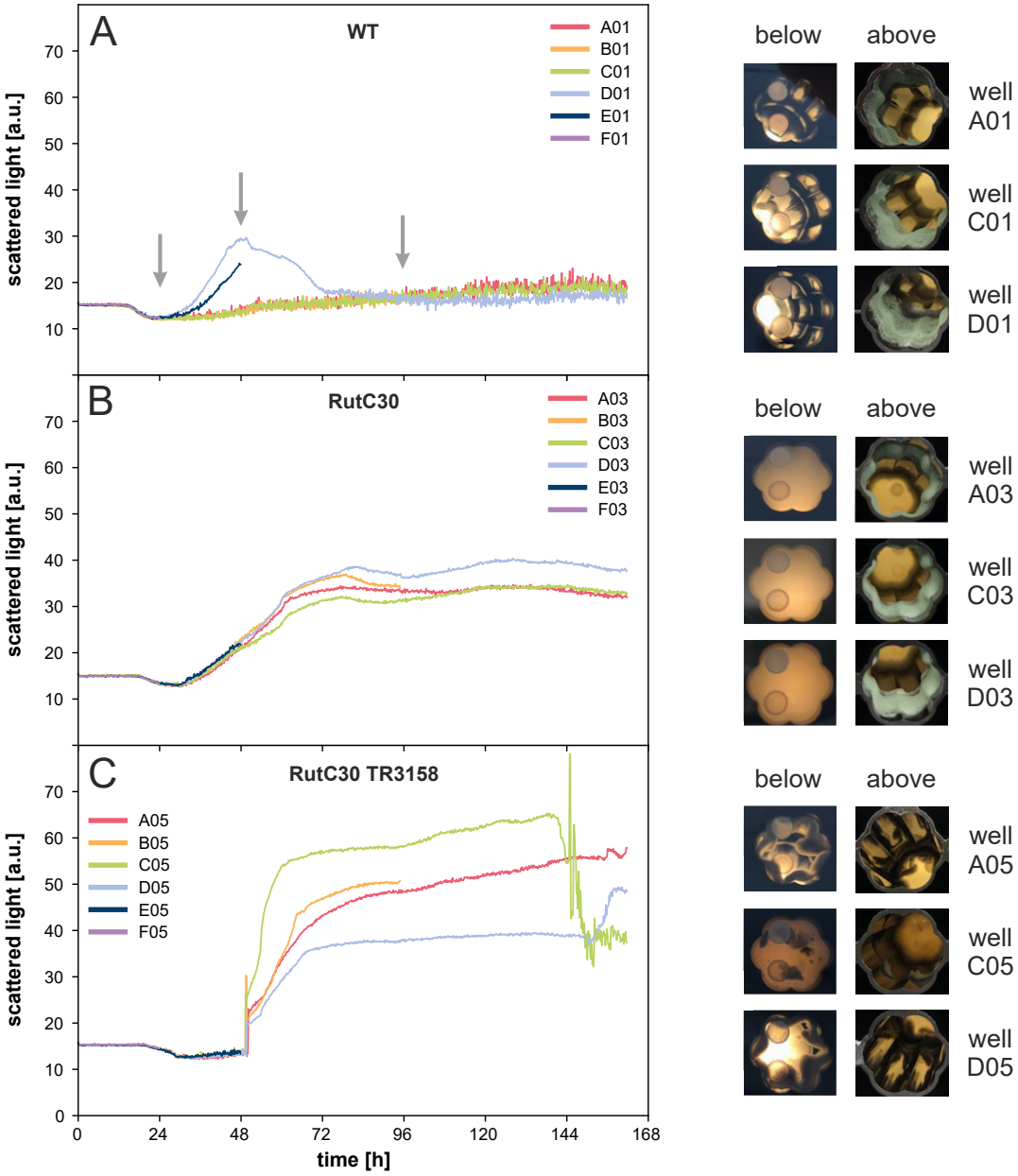

Fig. 2.1. **Batch cultivation of *T. reesei* in an FP.** Scattered light over time and pictures taken from the bottom and top of the cultivation plate at the end of cultivation for (A) WT, (B) RutC30 and (C) RutC30 TR3158. Reproducibility of the scattered light was low for the WT and RutC30 TR3158, but high for RutC30. All strains exhibited strong wall growth. Due to this extensive wall growth, the FP was considered unsuitable for a reproducible cultivation workflow. Cultivation conditions: FP, n = 1200 rpm, d_0 = 3 mm, V_W = 3.2 ml, V_L = 1 ml, T = 30 °C, Jourdier Medium with 20 g·l^{-1} glucose, inoculum = 10^5 spores·ml^{-1}, n_{bio} = 6 with sampling of 3 replicates indicated by a gray arrow. [153]

in order to avoid contact between the culture suspension and the sealing foil, the rotational frequency was reduced to 1000 rpm in subsequent cultivations to remain within the manufacturer's specifications.

Fig. 2.2 shows the results of all three strains cultivated in an RWP at 1000 rpm with six biological replicates each. It illustrates the high reproducibility of the time course of scattered light and DO. This can be exemplified by the mean value and standard deviation of the time at which the DO minimum was reached (data not shown). The DO minimum was reached at t_{WT} = 36.0$\pm$0.5 h, t_{RutC30} = 49.5$\pm$1.4 h and $t_{RutC30\ TR3158}$ = 51.4$\pm$0.9 h (Fig. 2.2 A-C). This shows very similar growth profiles between replicates for all three strains based on scattered light and DO signal.
Compared to the previous cultivations, wall growth was considerably reduced (compare Figs. 2.1 and 2.2, both right side) and contact between culture suspension and sealing foil was successfully prevented. However, for WT and RutC30, the DO signal decreased to approximately 10 %, possibly resulting in short-term oxygen limitation in these cultures (Fig. 2.2 A and B). This was not observed in previous cultivations using an FP at 1200 rpm or an RWP at 1200 rpm (data not shown). In contrast, the DO of RutC30 TR3158 only decreased to approximately 90 %.
According to the findings of Giese et al. [29], the maximum oxygen transfer capacity in shake flasks decreases when the viscosity exceeds approximately 80 mPa·s. Given that MTPs are similar to shake flasks in terms of the geometry of the surface aeration mechanism, it is likely that higher viscosities also result in lower maximum oxygen transfer capacities. RutC30 TR3158 is a spontaneous mutant derived from RutC30 that results in a lower viscosity of the culture suspension [46]. It is therefore highly likely, that the lower viscosity of the RutC30 TR3158 cultures provided a higher oxygen transfer capacity, thereby avoiding oxygen limitations.

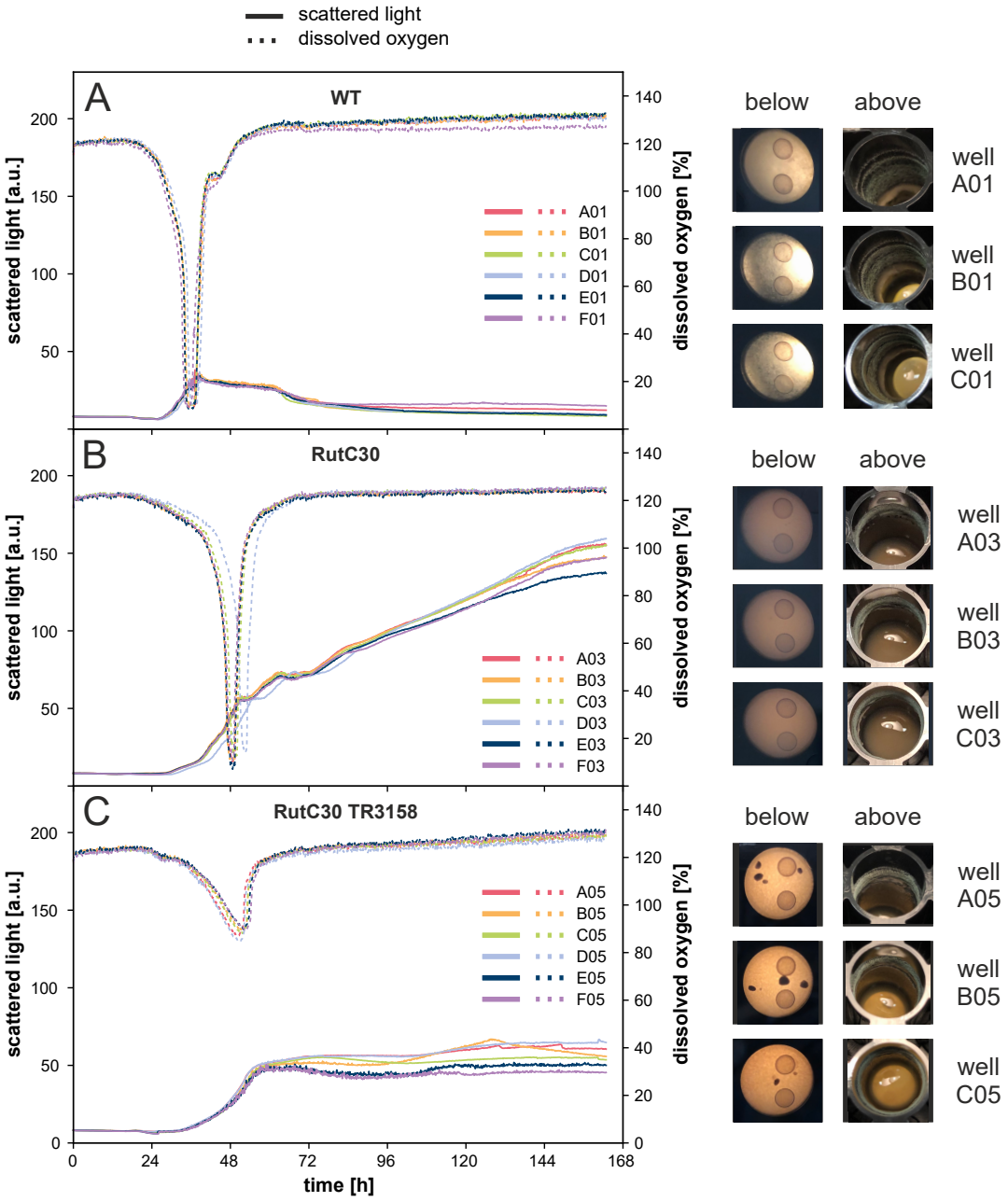

Fig. 2.2. **Batch cultivation of *T. reesei* in an RWP at 1000 rpm.** Scattered light and DO over time as well as pictures taken from the bottom and top of the cultivation plate at the end of cultivation for (A) WT, (B) RutC30 and (C) RutC30 TR3158. Scattered light and DO showed high reproducibility between biological replicates for all strains. Compared to the previous cultivations, wall growth was drastically reduced and contact between culture suspension and sealing foil was successfully prevented. Cultivation conditions: RWP, n = 1000 rpm, d_0 = 3 mm, V_W = 3.4 ml, V_L = 1 ml, humidity $\geq$85 %, O_2 = 21 %, T = 30 °C, Jourdier Medium with 20 g·l^{-1} glucose, inoculum = 10^5 spores·ml^{-1}, n_{bio} = 6. [153]

2.1.2. Cultivation medium

A medium adaptation can potentially increase the maximum oxygen transfer capacity by producing morphologies that lead to a lower viscosity [22]. Moreover, a medium adaptation was required to provide more flexibility in medium preparation and to reduce complex and undefined side reactions during autoclaving. Thus, the medium was adapted for subsequent cultivations as described in Subsection 6.3.1.
In the cultivation experiments shown so far, the Jourdier Medium was used, which is a complex medium consisting of mineral salts, buffer, trace elements, 1.5 $g \cdot l^{-1}$ cornsteep solids and glucose [157]. As described in the literature, the medium including all components is finally autoclaved, which allows the components to react with each other. To avoid this and to increase flexibility, medium preparation was changed to individual stock solutions. These stocks were autoclaved separately and combined immediately before an experiment to form the complete medium used for subsequent cultivations. This medium was labelled "adapted medium".

Fig. 2.3 depicts cultivations with adapted medium for all three strains. As before, the reproducibility of scattered light and DO can be exemplified by the mean and standard deviation of the time the DO minimum was reached (data not shown). The DO minimum was reached at t_{WT} = 33.9$\pm$0.6 h (Fig. 2.3 A), t_{RutC30} = 52.5$\pm$0.6 h (Fig. 2.3 B) and $t_{RutC30\ TR3158}$ = 53.9$\pm$0.9 h (Fig. 2.3 C). This low standard deviation of $\sigma \leq 0.9$ h demonstrates an even higher reproducibility of biological replicates in the adapted medium than in the Jourdier Medium (compare Figs. 2.2 and 2.3). This higher reproducibility most likely results from the prevention of complex and undefined side reactions during autoclaving.
As in the previous cultivation, wall growth in the form of biomass formation at the upper well wall above the culture suspension was low (compare Figs. 2.2 and 2.3, both right side). No biomass aggregation was observed at the bottom border of any of the wells. The growth profile of the biomass, given by the scattered light, was very comparable between the two media.

The DO profiles of RutC30 and RutC30 TR3158 were also very comparable between Jourdier Medium and adapted medium (compare 2.2 B and C with Fig. 2.3 B and C). However, the profile of the WT exhibited significant changes (compare Fig. 2.2 A and Fig. 2.3 A). Most prominently, the DO went down to approximately 70 % only, indicating a much lower oxygen demand of the fungi or an improved maximum oxygen transfer capacity in the adapted medium. As stated before, according to the findings

of Giese et al. [29], the maximum oxygen transfer capacity in shake flasks decreases when the viscosity exceeds approximately 80 mPa·s. This suggests that adapted medium may result in growth of the WT with altered morphological characteristics, such as shorter hyphal length or reduced branching and thus reduced viscosity.
Strikingly, no similar effect of altered DO profile was observed for RutC30 and RutC30 TR3158. Since RutC30 was derived from the WT by three rounds of random mutagenesis [45], it is genetically different from the WT. This offers a possible explanation as to why no changes in the DO limitation were observed in RutC30. Our hypothesis proposes that, due to the genetic differences, the changes made to the medium do not effect this strain in the same way as the WT. As previously stated, RutC30 TR3158 is a spontaneous mutant derived from RutC30, yielding a lower viscosity of the culture suspension. This property of lower viscosity appears to be present in both the Jourdier Medium and the adapted medium, resulting in a lower DO decrease under both conditions.

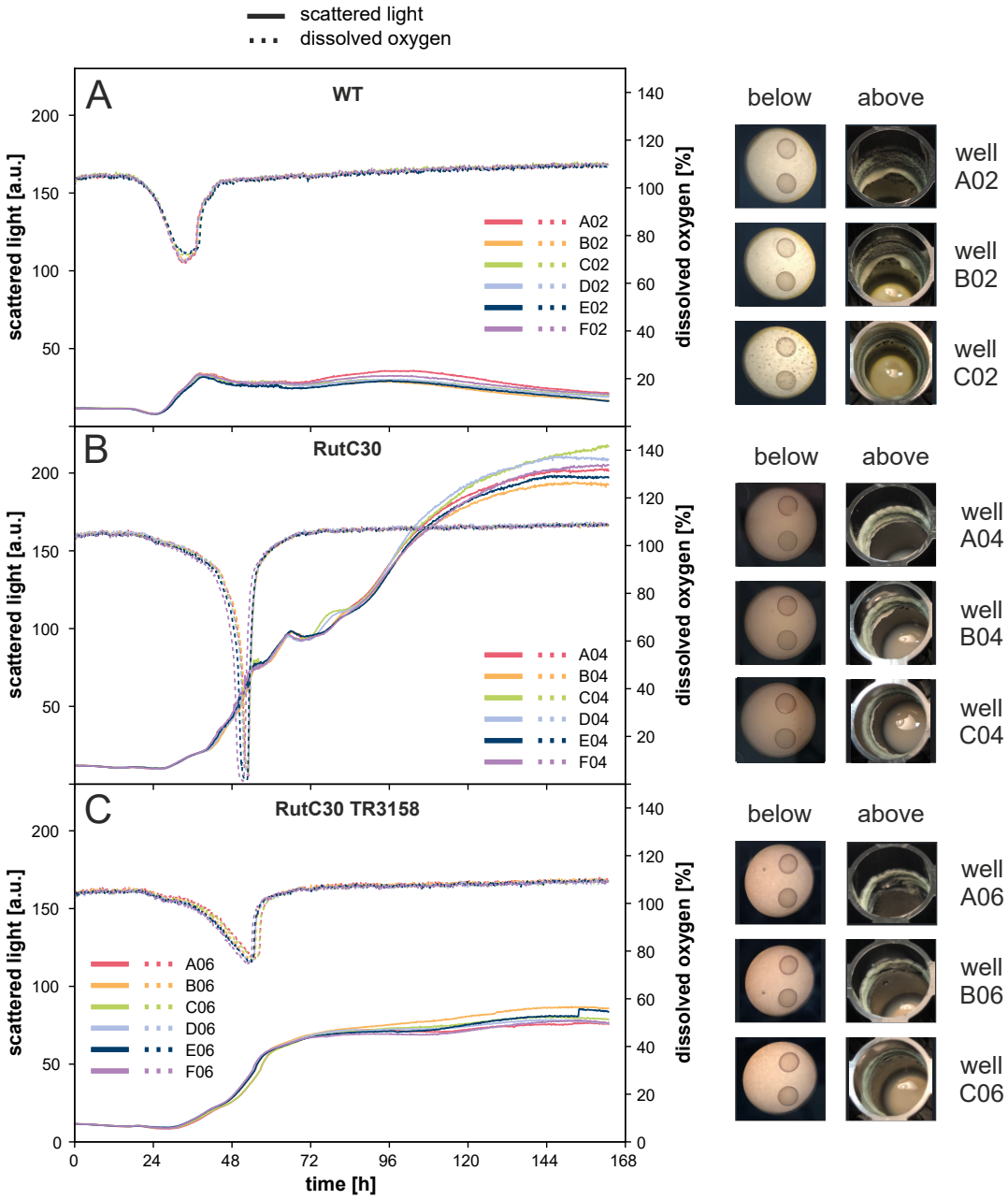

Fig. 2.3. **Batch cultivation of *T. reesei* with adapted medium.** Scattered light and DO over time as well as pictures taken from the bottom and top of the cultivation plate at the end of cultivation for (A) WT, (B) RutC30 and (C) RutC30 TR3158. Reproducibility of scattered light and DO for biological replicates was high for all strains in both media. However, cultures with adapted medium showed even higher reproducibility between biological replicates. Wall growth was comparably low for both media. Cultivation conditions: RWP, n = 1000 rpm, d_0 = 3 mm, V_W = 3.4 ml, V_L = 1 ml, humidity $\geq$85 %, O_2 = 21 %, T = 30 °C, adapted medium with 20 g·l^{-1} glucose, inoculum = 10^5 spores·ml^{-1}, n_{bio} = 6. [153]

2.1.3. Correlation of scattered light and cell dry weight

The reliable determination of biomass concentration is important to characterize the cultivation process, e.g. to derive biomass-specific performance indicators. So far, the scattered light of the BioLector online measurement has been used as a representative proxy for biomass concentration. Since scattered light is a complex optical signal, it can be affected by morphological changes during cultivation. Therefore, due to the complex nature of fungal morphology, a linear correlation between scattered light and cell dry weight (CDW), as often observed for unicellular microbial systems, cannot necessarily be expected [27].

Fig. 2.4 shows the correlation between scattered light and CDW for all three strains resulting from cultivations using the developed batch cultivation protocol with adapted medium. CDW sampling points were chosen throughout the steep increase of scattered light. The application of linear regression analysis revealed a strong correlation between scattered light and CDW with high coefficients of determination of R^2_{WT} = 0.97, R^2_{RutC30} = 0.90 and $R^2_{RutC30\ TR3158}$ = 0.96. These results show that the scattered light accurately tracks biomass formation for all three strains during the phase of steep scattered light increase when the developed batch cultivation protocol is applied.
In addition, the derived linear equations can be used as a calibration function for future cultivations, allowing scattered light measurements to be converted directly into CDW values. This significantly reduces the need for offline analysis, as wells no longer need to be sacrificed to measure CDW. As a result, the number of available replicates is increased and the additional hands-on time for offline analysis is eliminated.

The linear correlations for all three *T. reesei* strains underscore the adaptability and effectiveness of the batch protocol to accommodate different genetic backgrounds. Moreover, these results highlight scattered light measurement as a non-invasive real-time monitoring technique for *T. reesei* WT, RutC30 and RutC30 TR3158.

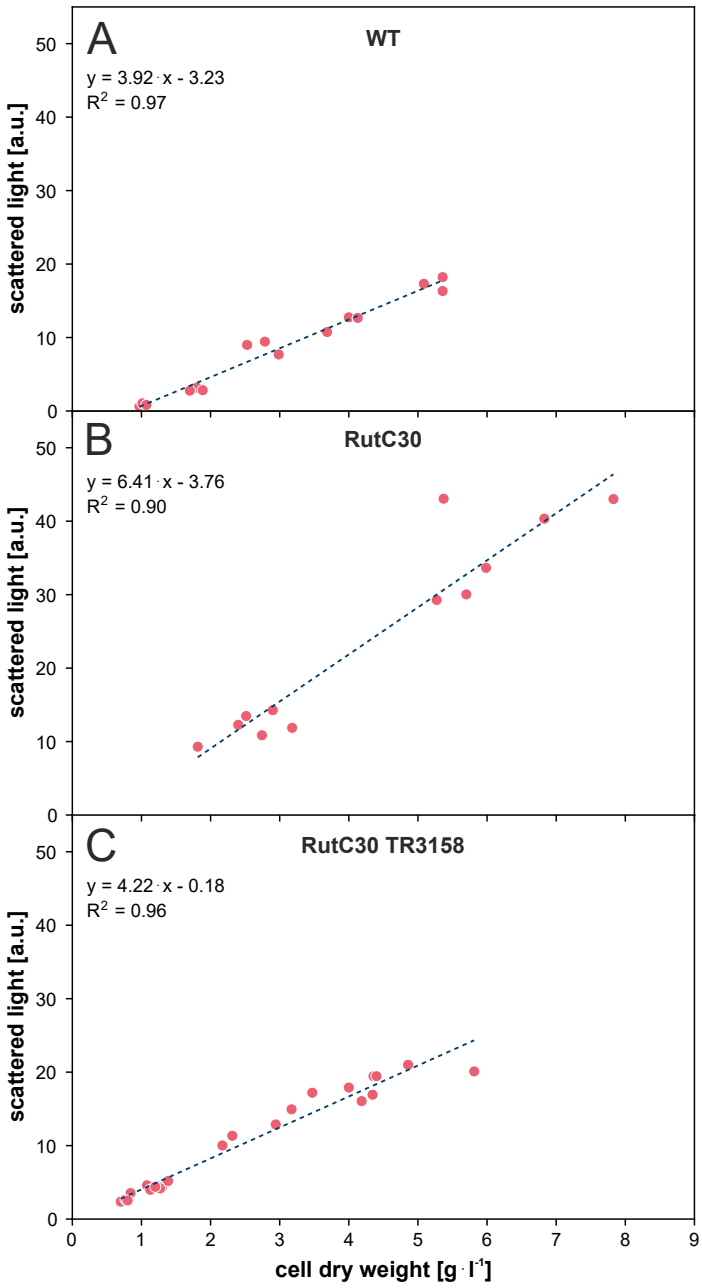

Fig. 2.4. **Correlation between scattered light and CDW for *T. reesei* using linear regression.** (A) WT, (B) RutC30 and (C) RutC30 TR3158. Linear regression analysis shows a strong correlation between scattered light and CDW for all three strains, with coefficients of determination of $R^2_{WT} = 0.97$, $R^2_{RutC30} = 0.90$ and $R^2_{RutC30\ TR3158} = 0.96$. These results shows that scattered light accurately tracks biomass formation during the phase of steep scattered light increase. Cultivation conditions: RWP, n = 1000 rpm, d_0 = 3 mm, V_W = 3.4 ml, V_L = 1 ml, humidity $\geq$85 %, O_2 = 35 %, T = 30 °C, adapted medium with 20 g·l^{-1} glucose, inoculum = 10^5 spores·ml^{-1}. [153]

2.2. Applying industrially relevant conditions: fed batch cultivation

The developed cultivation protocol can be used for the screening of new *T. reesei* strain constructs. However, as stated by several authors [92, 94], it is crucial to closely match the screening conditions to industrial production conditions to ensure the selection of the most promising candidates. In order to produce cellulases, *T. reesei* requires an inducer of the cellulolytic system, with cellulose being a natural inducer that leads to good production levels [157]. However, the insolubility of cellulose makes it difficult to handle on an industrial scale. Therefore, lactose, a soluble disaccharide, is the most commonly used alternative inducer and carbon source [157].
Nonetheless, cellulase production remains very low in the presence of excess readily metabolized sugars, even in catabolite-derepressed strains such as RutC30. Therefore, soluble inducing carbon sources, such as lactose, must be fed in a carbon-limited manner, either in fed batch or continuous mode. Since cellulase production processes using *T. reesei* are typically run in fed batch mode [158], the suitability of a microfluidic fed batch approach was evaluated.

2.2.1. Ratio of batch to fed batch substrate

The fed batch process was designed using glucose for cell growth in the batch phase and lactose to induce cellulase production in the fed batch phase. However, prior to the fed batch cultivation, the appropriate ratio of batch to fed batch substrate, i.e. glucose to lactose, needs to be determined.
This was achieved by conducting batch cultivation experiments with varying glucose to lactose ratios. The aim was to identify the combination that yields the highest cellulase activities. This data can then be used to examine whether these activities can be further improved using the same amount of glucose and lactose, but in a fed batch mode, to allow a fair comparison of the two process modes. The total carbon source was maintained at an equimolar equivalent of $20\,g{\cdot}l^{-1}$ glucose, in alignment with previous batch cultivations.

Fig. 2.5 shows the volumetric activity of two cellulases, CBH and BGL, produced by RutC30, which play a crucial role in cellulose hydrolysis (refer to Subsection 1.2.4 for further information). Surprisingly, a non-linear relation between the activity of

cellulases and the quantity of lactose added was observed. The experiment with 0 g·l^{-1} lactose and 20 g·l^{-1} glucose resulted in the lowest CBH and BGL activities, measuring at 120$\pm$6 U·l^{-1} and 106$\pm$4 U·l^{-1}, respectively. With increasing lactose concentrations of 4.7 and 7.1 g·l^{-1}, an increase in cellulase activities was observed. These results were in line with expectations, since lactose acts as an inducer of cellulase production, whereas glucose acts as a repressor [157, 158]. Interestingly, this trend does not continue, but a decrease in cellulase activities was observed at lactose concentrations of 9.5 g·l^{-1} and 11.9 g·l^{-1}. Nevertheless, the highest cellulase activities of 400$\pm$14 U·l^{-1} (CBH) and 311$\pm$43 U·l^{-1} (BGL) were achieved when lactose was used as the sole carbon source. This represents a 3-fold increase in activity compared to the standard batch approach using glucose as the sole carbon source.

Importantly, in all cases, complete uptake of glucose and lactose was confirmed by a characteristic increase in DO, shown in Fig. 2.6. In order to facilitate a cell growth phase in the fed batch cultivation, a configuration of 2.5 g·l^{-1} glucose followed by 17 g·l^{-1} lactose was selected for the fed batch process, as this resulted in considerable activities for CBH and BGL as well.

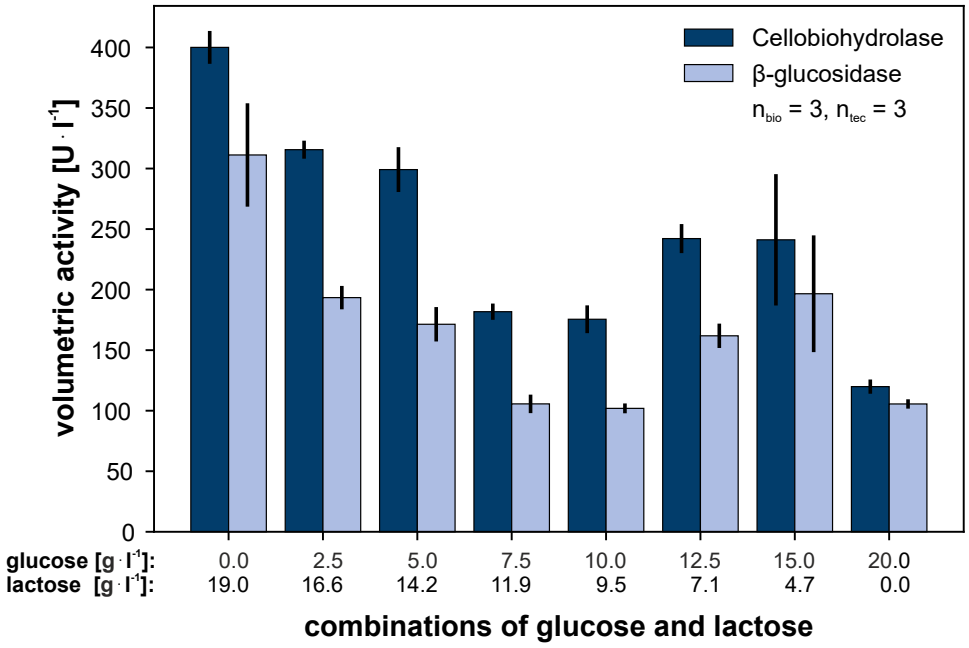

Fig. 2.5. **Volumetric activity of CBH and BGL for different combinations of glucose and lactose in batch cultivation.** The experiment with 0 g·l^{-1} lactose and 20 g·l^{-1} glucose resulted in the lowest CBH and BGL activities, while he highest activities were observed when lactose was used as the sole carbon source. Cultivation conditions: *T. reesei* RutC30, RWP, n = 1000 rpm, d_0 = 3 mm, V_W = 3.4 ml, V_L = 1 ml, humidity $\geq$85 %, O_2 = 35 %, T = 30 °C, adapted medium with 20 g·l^{-1} glucose, inoculum = 10^5 spores·ml^{-1}. [153]

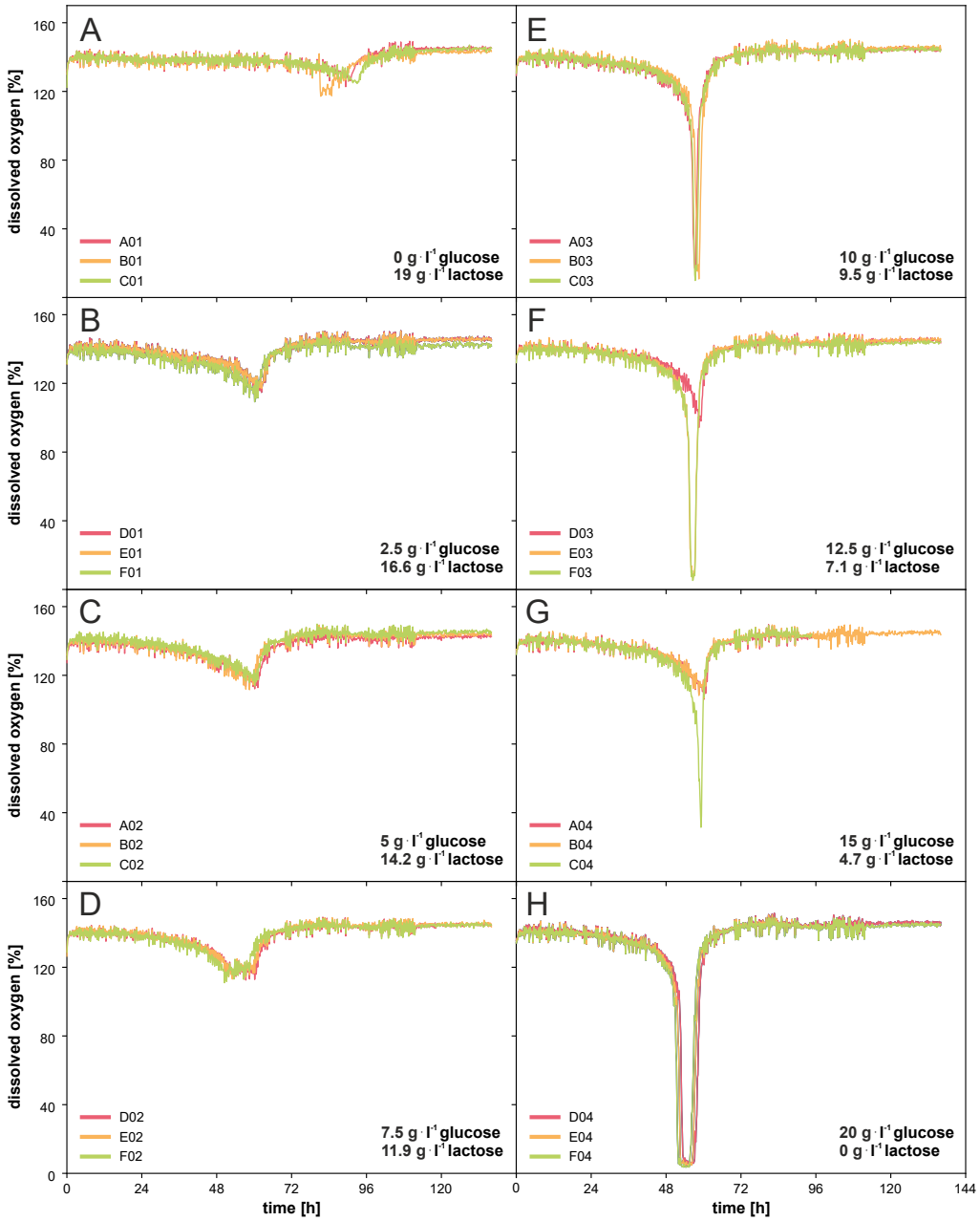

Fig. 2.6. **DO of *T. reesei* batch cultivations with glucose and lactose.** Glucose and lactose concentrations: (A) $0\,g{\cdot}l^{-1}/19\,g{\cdot}l^{-1}$, (B) $2.5\,g{\cdot}l^{-1}/16.6\,g{\cdot}l^{-1}$, (C) $5\,g{\cdot}l^{-1}/14.2\,g{\cdot}l^{-1}$, (D) $7.5\,g{\cdot}l^{-1}/11.9\,g{\cdot}l^{-1}$, (E) $10\,g{\cdot}l^{-1}/9.5\,g{\cdot}l^{-1}$, (F) $12.5\,g{\cdot}l^{-1}/7.1\,g{\cdot}l^{-1}$, (G) $15\,g{\cdot}l^{-1}/4.7\,g{\cdot}l^{-1}$, (H) $20\,g{\cdot}l^{-1}/0\,g{\cdot}l^{-1}$. All cultures showed a distinct increase in DO, indicating the full consumption of the primary carbon sources, glucose and lactose. Cultivation conditions: *T. reesei* RutC30, RWP, n = 1000 rpm, d_0 = 3 mm, V_W = 3.4 ml, V_L = 1 ml, humidity $\geq$85 %, O_2 = 35 %, T = 30 °C, adapted medium with glucose and lactose concentrations as declared in the subplots, inoculum = 10^5 spores·ml^{-1}, n_{bio} = 3.

2.2.2. Fed batch cultivation

Fig. 2.7 presents the results of a fed batch cultivation using 2.5 g·l^{-1} glucose in the batch phase and 17 g·l^{-1} lactose as a feed. The experiment investigated the influence of four different constant feeding rates on the metabolic activity and cellulase activity of RutC30. The start time for feeding was determined using glucose consumption data from preliminary experiments. These experiments revealed that an increase in DO occurs after approximately 40 h in a batch experiment that uses 2.5 g·l^{-1} glucose (data not shown). The feeding rates were estimated based on the glucose and lactose consumption rates from the batch experiment that used 2.5 g·l^{-1} glucose (data not shown) and from the batch cultivation shown in Fig. 2.6 that used 2.5 g·l^{-1} glucose and 17 g·l^{-1} lactose. The goal was to target a balance between carbon limitation and overfeeding.

During the initial batch phase of all 14 cultures, the signals of scattered light and DO were very similar between replicates, demonstrating very good comparability (Fig. 2.7 A and B). After approximately 40 h, the DO signal indicated the depletion of the glucose batch substrate and the fed batch phase was started.
In the first 75 h of cultivation, there was minimal influence of the different feeding rates on scattered light measurements. However, the observation of DO clearly showed that the feeding rates were appropriately selected to cover the range from limiting to high substrate feeding. The two lowest feeding rates, 0.3 g·(l·h)$^{-1}$ and 0.45 g·(l·h)$^{-1}$, had no effect on the DO levels, indicating a strong carbon limitation. The feeding rate of 0.6 g·(l·h)$^{-1}$ led to a moderate decrease in DO. However, when the feeding stopped, there was a sudden increase in DO, clearly indicating a carbon limiting feed profile. The highest feeding rate, 0.75 g·(l·h)$^{-1}$, resulted in a strong decrease in the DO after feed start. Even after the feeding stopped, the DO signal continued to decrease, suggesting a state of strong overfeeding.

Comparing Fig. 2.3 and Fig. 2.7 C, a noticeable morphological change from pure microfilamentous structures in the batch cultivation to a combination of microfilamentous structures and pellets in the fed batch cultivation was observed. This change could be caused by the use of lactose in addition to glucose as a carbon source. Another possible explanation is the influence of a short starvation phase prior to the initiation of lactose feeding. The activation of the feed occurred approximately 2 h after the initial rise in DO, as shown in the DO signal Fig. 2.7 B.

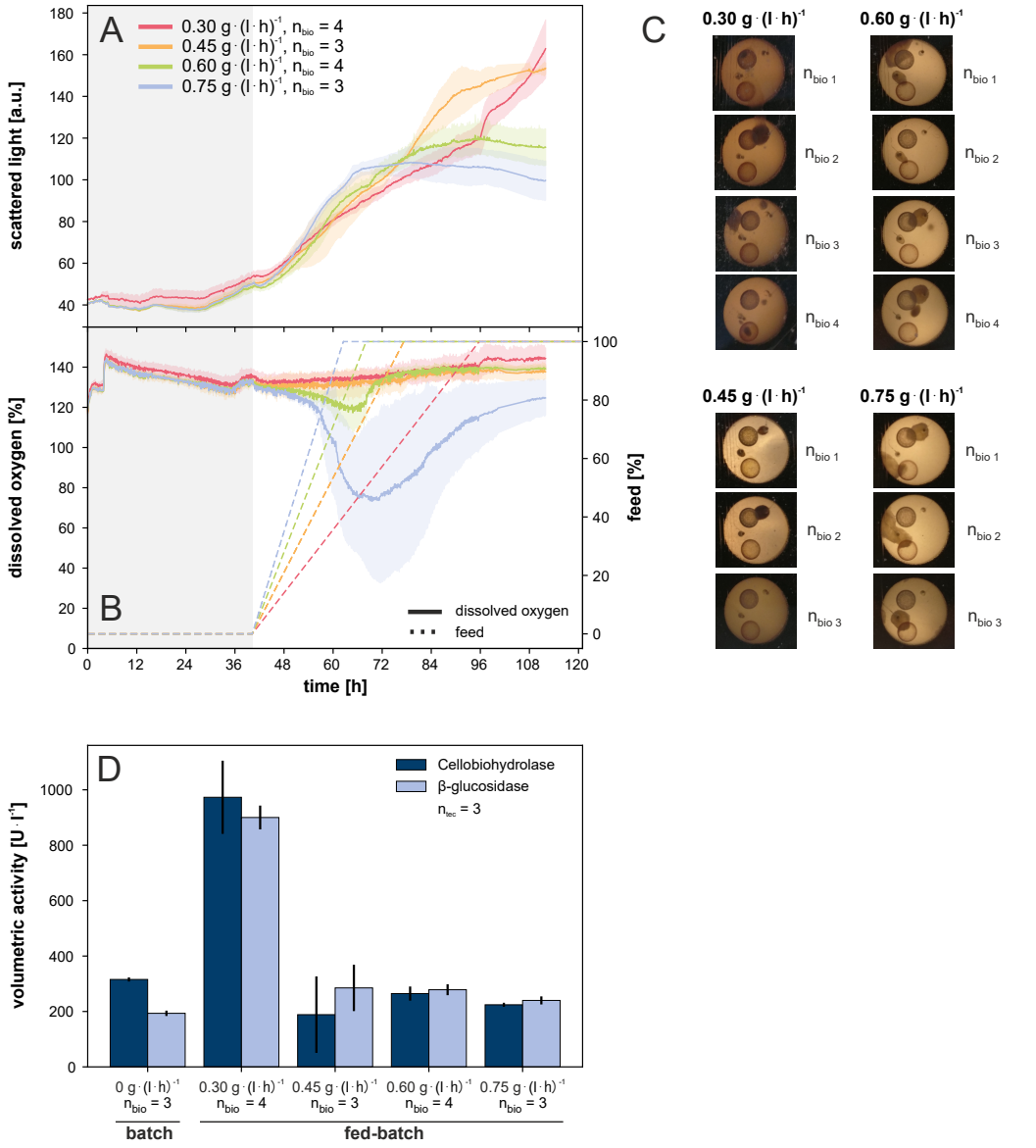

Fig. 2.7. **Fed batch cultivation of *T. reesei* RutC30.** (A) Scattered light, (B) DO and feed over time, with the line graph showing the mean and colored areas representing the standard deviation. (C) Pictures taken from the bottom of the cultivation plate at the end of cultivation. (D) Volumetric activity of CBH and BGL for batch and fed batch cultivations, both with 2.5 g·l^{-1} glucose and 16.6 g·l^{-1} lactose. The DO indicates that appropriate feeding rates were chosen, from limiting to high substrate feeding. The lowest feeding rate of 0.3 g·(l·h)$^{-1}$ revealed a 3-fold increase in CBH and a 5-fold increase in BGL activity compared to the batch conditions. A morphological change to a combination of microfilamentous structures and pellets cultivation was observed for all feeding rates. Cultivation conditions: *T. reesei* RutC30, microfluidic RWP, n = 1000 rpm, d_0 = 3 mm, V_W = 3.4 ml, V_L = 1 ml, humidity ≥85 %, O_2 = 35 %, T = 30 °C, adapted medium with 2.5 g·l^{-1} glucose (batch) and 16.6 g·l^{-1} lactose as constant feed with a rate of 0.30, 0.45, 0.60 or 0.75 g·(l·h)$^{-1}$, inoculum = 10^5 spores·ml^{-1}. [153]

The offline measurement of cellulase activities produced surprising results, elucidating the benefits of the optimized fed batch over the batch process (Fig. 2.7 D). As expected, the highest feeding rate of 0.75 g·(l·h)$^{-1}$, which was too high for carbon-limited conditions based on the DO signal, resulted in low cellulase activities. These activities were similar to batch cultivations with identical glucose and lactose concentrations.
In contrast, at feeding rates of 0.3 g·(l·h)$^{-1}$, 0.45 g·(l·h)$^{-1}$ and 0.6 g·(l·h)$^{-1}$, which were all assumed to be carbon limiting, only the lowest feeding rate of 0.3 g·(l·h)$^{-1}$ revealed a significant increase in cellulase activities compared to the other conditions. Specifically, there was a 3-fold increase in CBH and a 5-fold increase in BGL activity compared to the batch conditions with identical concentrations of glucose and lactose.
These findings strongly suggest that cellulase production is significantly affected not only by the transition to substrate-limiting conditions but also by the degree of carbon limitation. This influence likely operates through the genetic regulation of cellulase production. Remarkably, the lowest feeding rate led to the highest level of enzyme activity. These observations underscore the promise of MBR systems in enhancing enzyme production optimization.

2.3. Conclusion Chapter 2

This chapter systematically developed and validated a robust MBR batch cultivation protocol for *T. reesei* WT, RutC30 and RutC30 TR3158. Optimization of the protocol was achieved by implementing an RWP, an adapted medium and a rotational frequency of 1000 rpm. A strong correlation between scattered light intensity and CDW during the growth phase was observed, underscoring the reliability of scattered light measurements in accurately reflecting the biomass formation process. This is particularly noteworthy given the complex morphology of filamentous fungi compared to unicellular microbial systems.
Based on the batch cultivation results, a fed batch cultivation strategy was established for *T. reesei* RutC30 using glucose during the batch phase and lactose as a dual-purpose feed during the fed batch phase. This approach, designed to prevent carbon catabolite repression while inducing cellulase production, showed that the lowest feeding rate of 0.3 g·(l·h)$^{-1}$ resulted in a significant increase in cellulase activities,

specifically a 3-fold increase in CBH and a 5-fold increase in BGL compared to the batch process.

These results highlight the effectiveness of MBR workflows for optimizing cellulase production using *T. reesei*. The developed workflows provide a valuable tool for efficient strain screening and in-depth investigation of critical parameters such as feeding rates. However, the study also underlines the challenges associated with filamentous morphologies in small-scale cultivation devices, in particular highlighting that these protocols may not be directly transferable to other strains or filamentous fungi. Nonetheless, the insights gained from optimizing these workflows provide a solid foundation for more efficient adaptation of protocols to other biological systems by helping to anticipate and address potential pitfalls.
In the broader context of this thesis, the development of these MBR cultivation strategies represents a critical step in the advancement of bioprocess development for filamentous fungi. The established protocols serve as a basis for the automation of small-scale cultivation workflows, which will be explored in the following chapter. This integration of optimized protocols with automation technologies is expected to further increase efficiency and reliability of bioprocess development.

Looking forward, future research should focus on refining and extending MBR protocols for different *T. reesei* strains. Moreover, systematically varying cultivation conditions such as pH, temperature or nutrient composition to assess their impact on both scattered light measurements and product formation would provide valuable insights. This ongoing research is key to realizing the full potential of MBR systems, paving the way for improved biotechnological applications and industrial processes.

3. Automating microbioreactor workflows for *A. niger*

This chapter is partly based on data collected during student project I. K. Rohr is the author of this chapter, had the scientific lead on this project, conceptualized and supervised student project I and analyzed and visualized all data. L. Gremm conducted the first three presented BioLector experiments and implemented the adapted liquid class for handling *A. niger* culture suspension with the liquid handling robotics system equipped with standard tips. K. Rohr conduced all other BioLector experiments and implemented the remaining liquid classes on the liquid handling robotics system. A. Spieß and M. Papenfuß provided the strain.

Building on the optimized MBR cultivation protocols developed in the previous chapter, this chapter shifts the focus to the automation of these processes and introduces *A. niger* as a new biological system. The focus is on automating the critical task of inoculation using liquid handling robotics systems and evaluating the effect on the cultivation of *A. niger*.

Automation is a cornerstone of modern bioprocess development, essential for establishing reproducible workflows that can meet the demands of HTP experimentation. For filamentous fungi in particular, automation provides an efficient solution to the challenge of testing the numerous environmental factors that influence both morphology and productivity.

The advances discussed in this chapter are key to overcoming the limitations of manual methods by reducing variability and accelerating the pace of bioprocess development. In addition to improving cultivation processes, these automated workflows provide a robust foundation for the application of automated microscopy and image analysis techniques, which will be discussed in the following chapter.

3.1. Applying state-of-the-art methods: microbioreactor cultivation workflow for *A. niger*

In 2021, Jansen et al. [56] introduced a protocol for the MBR cultivation of *A. niger* ANIp7-MCS-gfp2, which is schematically shown in Fig. 3.1. In the manual workflow, a pre-culture master mix is distributed into eight FP wells and incubated in the BioLector for 44 h (Fig. 3.1 A). Subsequently, the pre-culture is harvested, pooled and used to inoculate the main culture medium. After inoculation, the main culture master mix is distributed to the remaining 42 FP wells (Fig. 3.1 B). Then, the main culture is incubated in the BioLector under selected conditions (Fig. 3.1 C).
While this manual protocol provides a solid foundation for preliminary studies, the fixed 44 h pre-culture duration requires precise timing to ensure consistent inoculation conditions. Since inoculation is critical to subsequent cultivation, it should be standardized through automation to ensure main culture reproducibility, particularly when screening strain libraries. In such cases, automation is also essential to enable strain-dependent, flexible inoculation times for individual wells. In addition, transitioning to automated inoculation could significantly enhance MBR time utilization by reducing dependency on staff availability and minimizing idle time.
However, implementing automated inoculation requires modifications to various steps of the workflow, as illustrated by the schematic robotics system in Fig. 3.1. To achieve a fully automated inoculation process, it is necessary to automate both the harvesting of the pre-culture and the subsequent inoculation and distribution of the main culture master mix (Fig. 3.1 B).

Before adapting the workflow, it is essential to conduct a reference cultivation. This preliminary step enables subsequent comparisons to identify any deviations resulting from changes to the protocol. Fig. 3.2 illustrates the results of a reference cultivation run performed according to the established manual protocol.
The scattered light was largely reproducible between the 42 biological replicates (Fig. 3.2 A). An initial increase in scattered light was observed after 6 h of cultivation. During the phase characterized by a sharp increase in scattered light, from 10 h to 15 h, a temporal deviation of up to 2 h was observed between biological replicates. From 15 h onwards, in the phase of less pronounced increase in scattered light, sporadic peaks were evident.
After 25 h of cultivation, the macroscopic morphology was predominantly microfilamentous, with some small pellets and aggregates (Fig. 3.2 B). The size of these

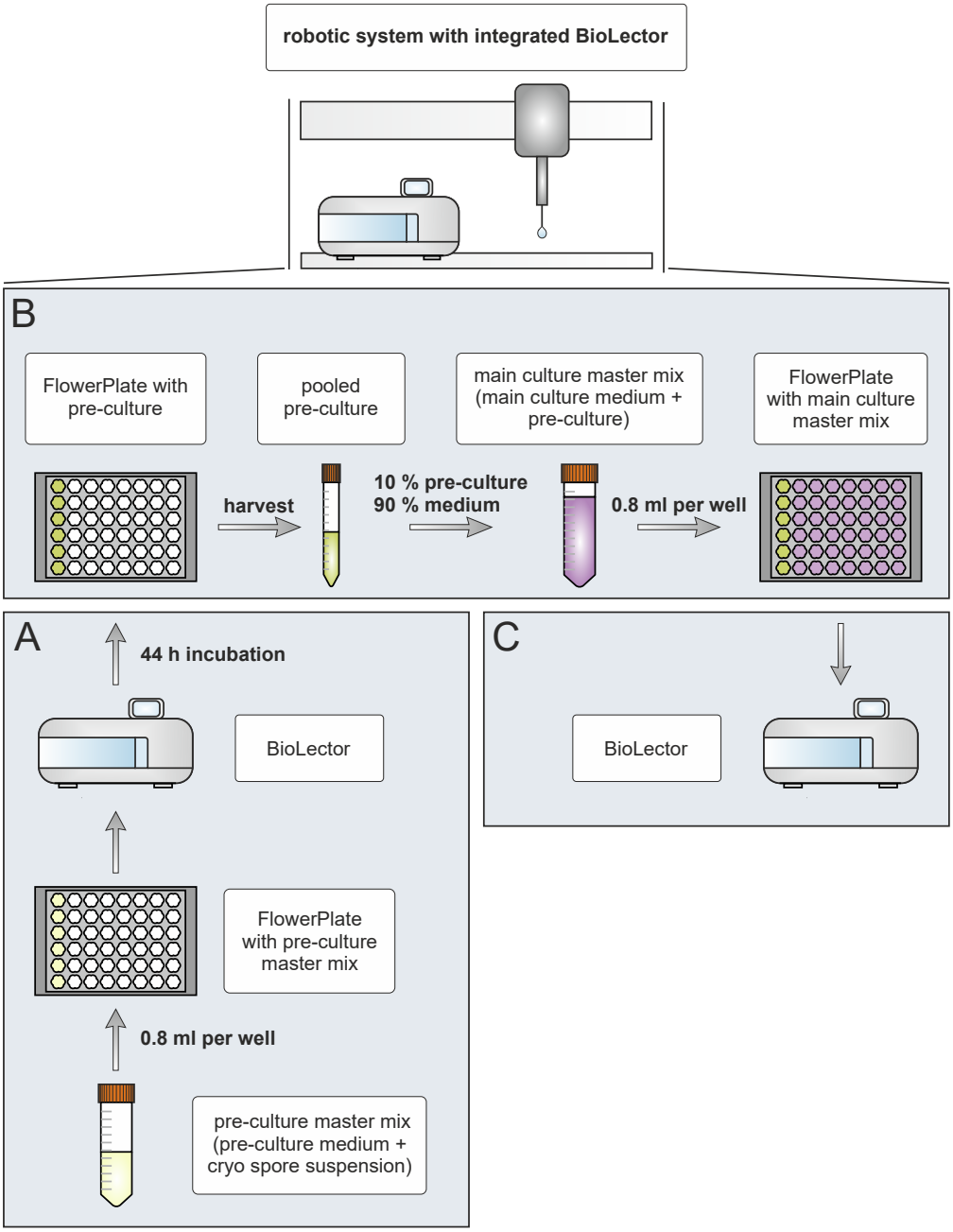

Fig. 3.1. **Schematic of the cultivation workflow for *A. niger* ANlp7-MCS-gfp2 and required adjustments for automation.** (A) Pre-culture preparation and cultivation. A pre-culture master mix is distributed into different FP wells and incubated in the BioLector for 44 h. (B) Pre-culture harvest and main culture preparation. The pre-culture is manually harvested, pooled and used to inoculate the main culture medium. After inoculation, the main culture master mix is distributed to the remaining FP wells. (C) Main culture cultivation. The main culture is incubated in the BioLector at the selected conditions. For a fully autonomous inoculation, it is necessary to automate all steps of pre-culture harvest and main culture inoculation (B).

spherical pellets and amorphous aggregates varied, with diameters and lengths ranging from 0.7 mm (pellets) to 2.2 mm (aggregates). The sporadic peaks observed during the phase of less pronounced scattered light increase were likely caused by these pellets. When a pellet is positioned at the measurement point during the scattered light recording, it produces a higher signal compared to the presence of mycelial structures. These findings provide a reference for subsequent cultivation experiments.

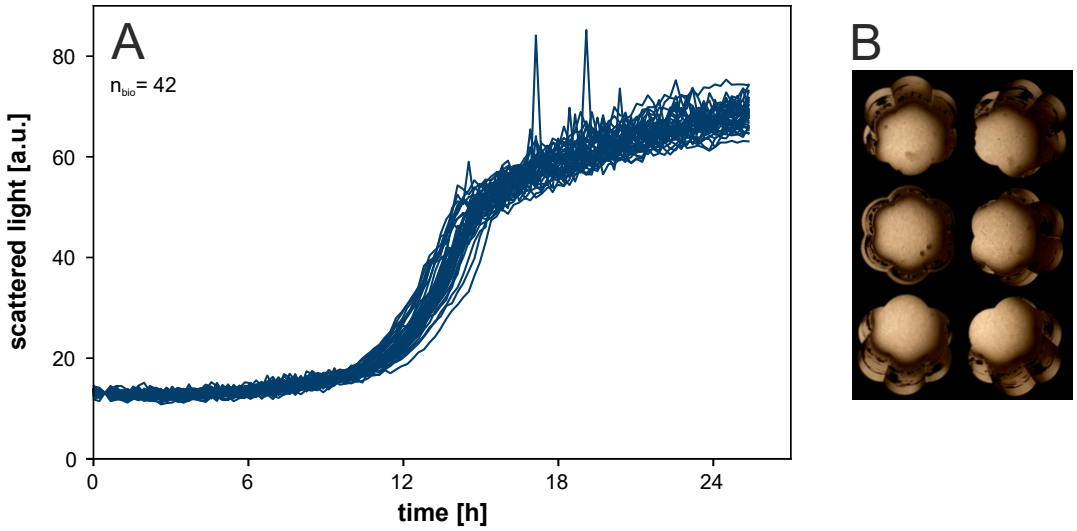

Fig. 3.2. **Manual reference cultivation of *A. niger*.** (A) Scattered light and (B) pictures taken from the top of the cultivation plate at the end of cultivation, showing the macroscopic morphology of exemplary wells. The scattered light was largely reproducible between the 42 biological replicates, despite temporal variations of up to 2 h and occasional peaks. The macroscopic morphology was predominantly microfilamentous, with the presence of some small pellets and aggregates. Cultivation conditions: *A. niger*, FP, n = 1400 rpm, d_0 = 3 mm, V_W = 3.2 ml, V_L = 0.8 ml, humidity $\geq$85 %, O_2 = 35 %, T = 37 °C, Vogel medium with 20 g·l^{-1} maltose, inoculum = 10 %, n_{bio} = 42.

3.2. Automated liquid handling of *A. niger*

The pursuit of automated main culture inoculation required the creation of a liquid class with tailored liquid handling parameters for managing *A. niger* culture suspension. This customization was necessary because the physical properties of *A. niger* culture suspension differ significantly from the standard liquid class optimized for water. For example, *A. niger* culture suspension has distinct characteristics such as particle suspension, altered rheology and viscosity.

Liquid handling parameters refer to the specific settings of the robotic pipetting system to account for these unique physical and chemical characteristics. These settings are essential to ensure that the pipetting process is accurate, reproducible and efficient. Adjustable specifications include, for example, fluid aspiration and dispense speeds, the delay after aspiration and dispense as well as the speed at which the last drop breaks off the needle. Tab. 3.1 compares the standard settings, designed for pipetting water, with the customized settings for handling *A. niger*.

Tab. 3.1. Comparison of the liquid class for pipetting water with the liquid handling robotics system and the adapted liquid class for *A. niger* culture suspension.

Specification	**Water liquid class**	***A. niger* liquid class**
Aspiration speed [µl·s^{-1}]	150	40
Delay after aspiration [ms]	200	500
Dispense speed [µl·s^{-1}]	600	250
Breakoff speed [µl·s^{-1}]	150	250

The adapted settings are tailored to accommodate the unique characteristics of *A. niger* culture suspension as observed in the reference cultivation. The reference cultivation had a predominantly microfilamentous morphology, indicating a higher viscosity of the culture suspension compared to water (Fig. 3.2) [159]. To account for this difference, the aspiration speed was reduced by a factor of 3.8 from 150 µl·s^{-1} to 40 µl·s^{-1} and the dispense speed by a factor of 2.4 from 600 µl·s^{-1} to 250 µl·s^{-1}. These adjustments give the viscous liquid sufficient time to rise in the pipet during aspiration and prevent the retention of liquid inside the robotic needle during dispense [160].
In addition, the pause after aspiration was increased by a factor of 2.5, from 200 ms to 500 ms, also to give the viscous liquid sufficient time to rise in the pipet. Furthermore, the breakoff speed was increased by a factor of 1.7, from 150 µl·s^{-1} to 250 µl·s^{-1}, to avoid a drop remaining on the needle due to high viscosity.

3.3. Simplifying the inoculation procedure for efficient robotic implementation

The adjustment of liquid handling parameters enabled the first attempt at automated inoculation of the main culture. In this initial automated run, the adapted liquid class

for *A. niger* was used to automatically harvest and pool the pre-culture from the first row of an FP (8 wells) after a cultivation period of 44 h. The remaining 42 FP wells were then filled with the main culture medium and inoculated individually.
This procedure deviated from the reference workflow shown in Fig. 3.1, which used a master mix for inoculation. This adjustment was made to simplify the procedure on the robotics platform by eliminating the need for a master mix preparation step. Using a master mix inoculation would require a beaker with a magnetic stirrer to maintain a homogeneous cell suspension, as fungi sediment faster than most bacteria. By inoculating wells individually, this added complexity was avoided, streamlining the process for efficient robotic implementation.

The results of the cultivation run are shown in Fig. 3.3. During the first 16 h, no variation in scattered light was observed across all 18 biological replicates (Fig. 3.3 A). Thereafter, the scattered light began to increase slowly but with a jagged profile. This is in sharp contrast to the reference cultivation, where the scattered light began to increase after only 6 h of cultivation, following a comparatively smooth curve (Fig. 3.2 A).
This jagged scattered light profile correlated with the observed macroscopic morphology, which consisted entirely of pellets without microfilamentous growth (Fig. 3.3 B). As described in Section 3.1, the presence of a pellet at the measurement point generates a higher scattered light signal compared to mycelial structures. Therefore, in cultures dominated by a pelletous morphology, the scattered light signal typically fluctuates within certain bounds rather than forming a smooth curve, with the amplitude of these fluctuations increasing as the pellet size increases.
The observed elliptical pellets were mostly uniform, ranging from 2.1 mm to 2.6 mm in width and 1.3 mm to 1.6 mm in height. These findings differ substantially from the reference cultivation, which showed a predominantly microfilamentous morphology with some smaller pellets and aggregates (Fig. 3.2 B). Overall, these differences demonstrate that the applied cultivation process yields results that are not comparable to the manual reference procedure and leads to a fundamentally different morphology of *A. niger*.

A clear difference between the manual inoculation procedure of the reference process and the applied automated inoculation procedure is that in the manual process, the main culture medium is inoculated as a master mix prior to dispersion into the FP wells. In the automated process, individual wells already containing the main culture medium were inoculated. This difference led to a substantial impact on the duration

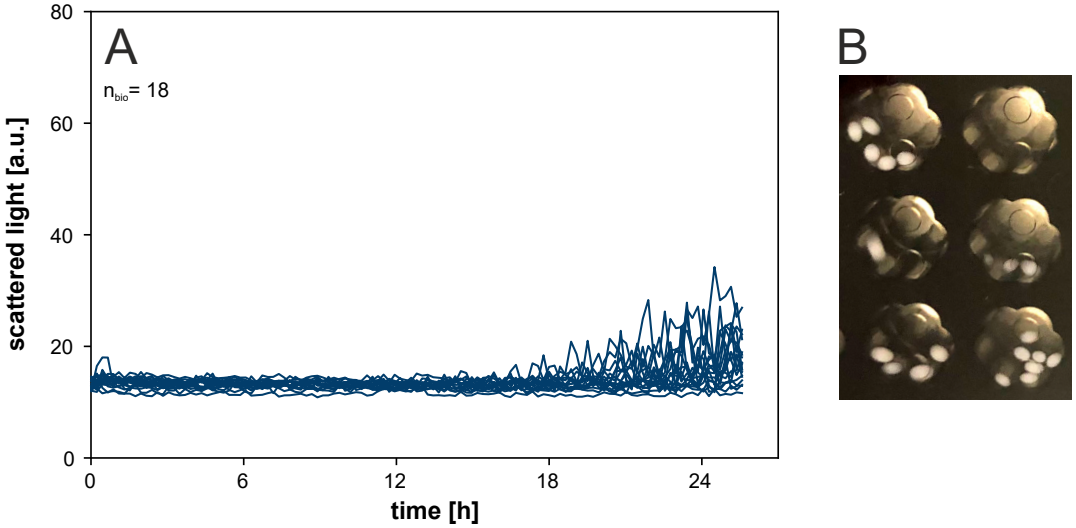

Fig. 3.3. **Cultivation of *A. niger* with automated inoculation of individual wells.** (A) Scattered light and (B) pictures taken from the bottom of the cultivation plate at the end of cultivation, showing the macroscopic morphology of exemplary wells. The scattered light only increased after 16 h of cultivation and showed a jagged progression. The macroscopic morphology consisted exclusively of mostly uniform elliptical pellets. Cultivation conditions: *A. niger*, FP, n = 1400 rpm, d_0 = 3 mm, V_W = 3.2 ml, V_L = 0.8 ml, humidity $\geq$85 %, O_2 = 35 %, T = 37 °C, Vogel medium with 20 g·l^{-1} maltose, inoculum = 10 %, n_{bio} = 18.

of the entire inoculation process. Specifically, the inoculation process extended from 39 to 52 minutes. This 1.3-fold increase in duration is attributable to the method used to process the pre-culture. The pre-culture is pooled in a narrow 15 ml centrifugal tube to minimize the required excess volume. However, due to the small diameter of the tube, only one robotic needle can enter the tube at a time. As a result, both pre-culture harvest and main culture medium inoculation can only be performed one well at a time.

This methodological bottleneck introduces a longer processing period for the fungal cells. During this time, the culture remains unshaken, likely resulting in oxygen limitation and an uneven distribution of nutrients and pH. Such conditions could inflict long-term damage, potentially manifesting in the pelletous morphology of the main culture. Moreover, since the pre-culture is not shaken during processing, the fungi sediment, resulting in close cell contact. This condition could also favor pellet formation, as pellets can be formed through the agglomeration of hyphal elements [21].

3.4. Reducing processing time of the pre-culture

In order to avoid a prolonged processing period for the fungi, the automated cultivation workflow was adjusted to enable a master mix inoculation, i. a. resulting in a shorter process time. As before, the inoculation process used the adapted liquid class for *A. niger* (Tab. 3.1) to automatically harvest and pool the pre-culture in a 15 ml centrifugal tube after a cultivation period of 44 h.
Then, in contrast to the previous protocol, a beaker containing the main culture medium was inoculated to form the main culture master mix. This master mix was continually stirred using a magnetic stirrer integrated into the robotic deck. The size of the beaker was chosen to allow simultaneous access by four robotic needles, reducing the time required to distribute the inoculated master mix to the FP. These modifications reduced the inoculation time 1.5-fold, from the previous 52 minutes to 34 minutes, thereby even surpassing the efficiency of the manual process, which took 39 minutes.

Fig. 3.4 presents the results of a cultivation run using automated inoculation of a master mix. Similarly to the previous cultivation run using individual well inoculation, no increase in scattered light was observed across all 36 biological replicates during the first 18 h of cultivation (Fig. 3.4 A). In addition, the subsequent increase in scattered light showed jagged curves for all replicates.
As described in Section 3.3, this jagged scattered light profile was most likely caused by the macroscopic morphology characterized by the presence of pellets and aggregates with minimal to no microfilamentous growth (Fig. 3.4 B). Moreover, in contrast to the previous cultivation process, the round pellets and amorphous aggregates had a wide range of sizes and shapes. Pellet sizes ranged from 1.1 mm to 6.3 mm in width and 0.9 mm to 2.9 mm in height, while aggregates up to 5.9 mm in length were present. This length of aggregate spans almost half of the well, which measures 12.4 mm at its widest point.
These results demonstrate that the adapted cultivation process still differs significantly from the manual reference process. Furthermore, the experiment reveals that the morphological differences between the manual reference cultivation and the automated process are not attributable to cellular damage or hyphal aggregation caused by an extended process duration. An additional influence of the magnetic stirrer was excluded by a separate manual cultivation run (results not shown).

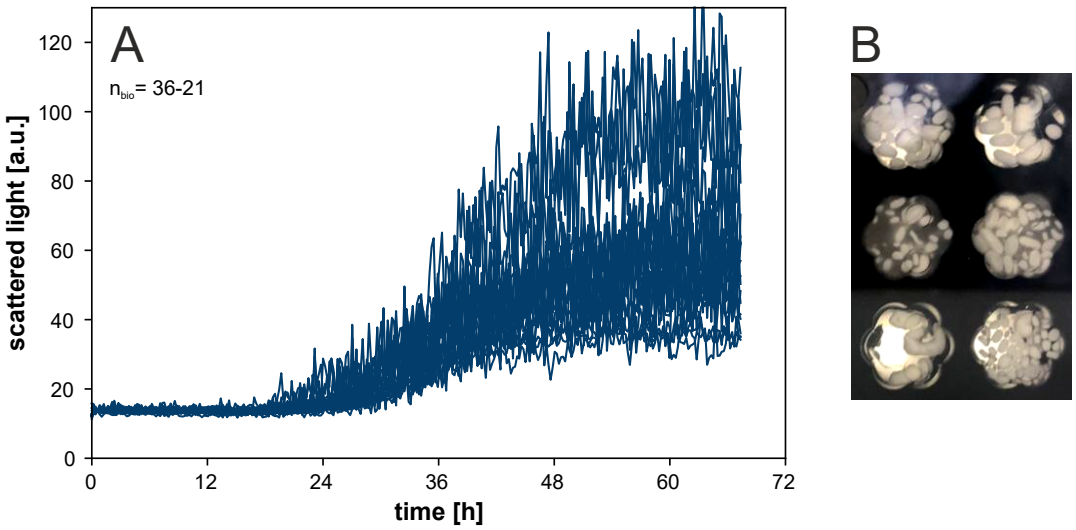

Fig. 3.4. **Cultivation of *A. niger* with automated master mix inoculation.** (A) Scattered light and (B) pictures taken from the bottom of the cultivation plate at the end of cultivation, showing the macroscopic morphology of exemplary wells. Scattered light increased only after 18 h of cultivation and showed a jagged progression. The macroscopic morphology consisted of pellets and aggregates with a wide range of sizes and shapes, with almost no microfilamentous growth. Cultivation conditions: *A. niger*, FP, n = 1400 rpm, d_0 = 3 mm, V_W = 3.2 ml, V_L = 0.8 ml, humidity $\geq$85 %, O_2 = 35 %, T = 37 °C, Vogel medium with 20 g·l^{-1} maltose, inoculum = 10 %, n_{bio} = 36 with sampling of 15.

Although the master mix inoculation process is more similar to the manual reference process than the individual well inoculation, a significant difference remains. The robotic tips have an outlet diameter of 0.5 mm as opposed to the 0.8 mm outlet diameter of the standard 1 ml pipet tip used for manual inoculation.
This difference led to several theories as to how it might cause the morphological discrepancies observed. Firstly, it was hypothesized that the smaller robotic pipet tip could be clogged by pre-culture pellets, thereby reducing the inoculum volume and changing the process conditions. Secondly, the narrower opening of the robotic tip could act as a selective barrier, potentially filtering out larger pre-culture pellets, thus affecting which pre-culture morphologies are able to pass through. Numerous studies have shown that both, variations in inoculum volume or inoculum type, can influence the predominant main culture morphology [161–163].
Moreover, differences in mechanical stress during inoculation could also contribute to the observed morphological variation [164]. By identifying the factors leading to the morphological discrepancies, adjustments can be made to the automated system to ensure it replicates the manual inoculation process as closely as possible. Therefore, the hypotheses were systematically analyzed.

3.5. Evaluating the influence of the reduced robotic pipet tip size

In order to explore the first hypothesis regarding reduced inoculum volume, a manual cultivation run was performed using inoculum volumes of 7.5 %, 5 % and 1 %. For direct comparability, a reference cultivation was carried out within the same run, using the standard inoculum volume of 10 %. Fig. 3.5 shows a comparison of cultures with reduced inocula and the reference cultures with the standard inoculum volume.

The patterns of scattered light were generally similar across all conditions, each exhibiting an initial lag phase, followed by a sharp increase in scattered light, a phase of less pronounced increase and finally a stationary phase of minimal change in scattered light. The onset of the sharp increase in scattered light was delayed with decreasing inoculum volumes (Fig. 3.5 A-C). Specifically, the delay was 1.4 h for 7.5 % inoculum, 2.7 h for 5 % inoculum and 8.5 h for 1 % inoculum compared to the reference. In the phase of a less pronounced increase in scattered light, both reference cultures and cultures with reduced inocula showed distinct peaks.
The macroscopic morphology was microfilamentous under all conditions (Fig. 3.5 D-F). Only cultures with 1 % inoculum additionally contained very small spherical pellets, approximately 0.4 mm in diameter. This morphology contrasts sharply with the large pellets and aggregates observed in previous automated cultivation runs (Fig. 3.3 B, Fig. 3.4 B). Therefore, this manual cultivation run refutes the hypothesis that the altered morphology in automated runs was caused by a reduction in inoculum due to a clogged robotic pipet tip.

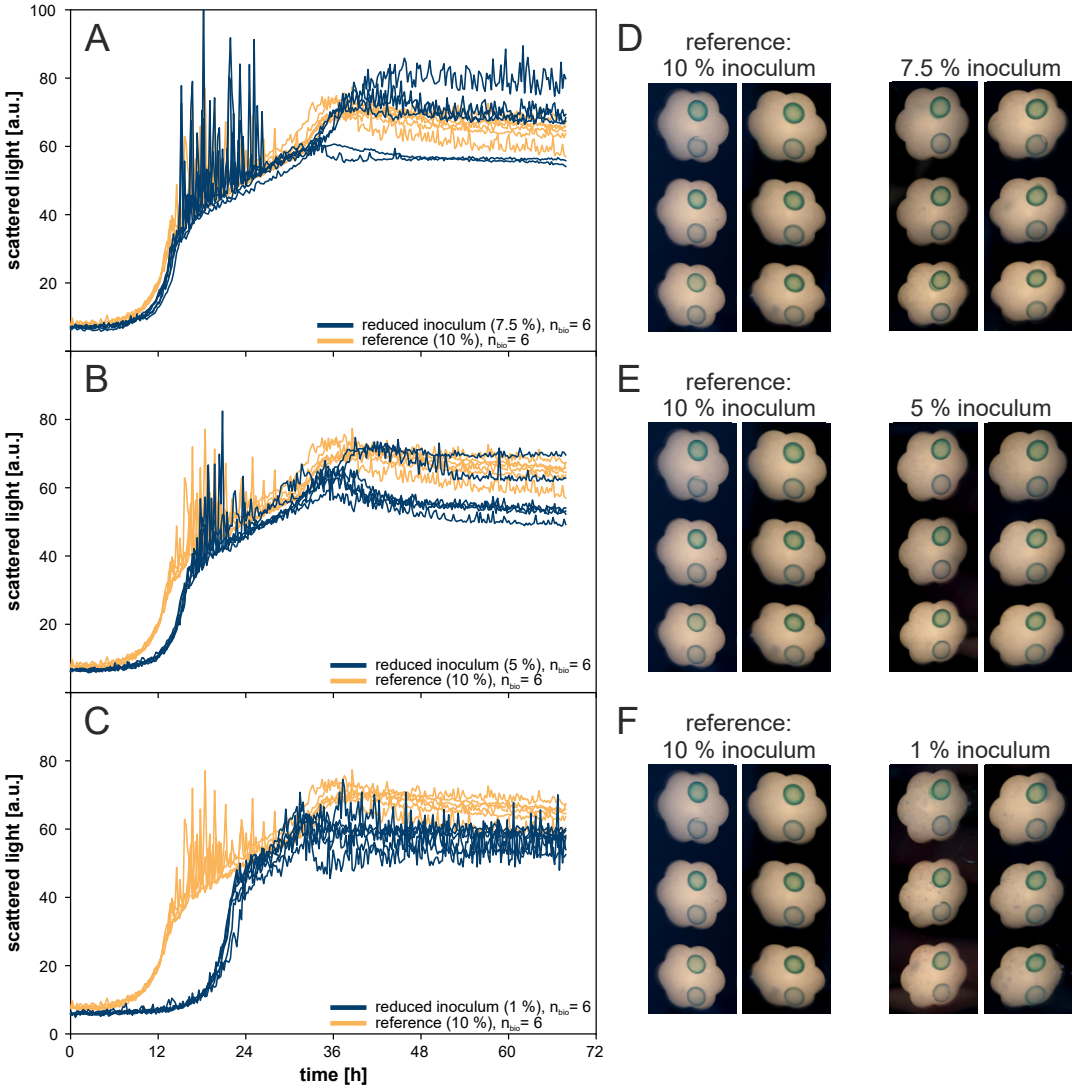

Fig. 3.5. **Manual cultivation of *A. niger* with reduced inoculum.** (A), (B), (C) Scattered light of the reference cultures with 10 % inoculum (yellow) and cultures with reduced inoculum volumes of 7.5 %, 5 % and 1 % (blue). (D), (E), (F) Pictures taken from the bottom of the cultivation plate at the end of cultivation, showing the macroscopic morphology of exemplary wells. The onset of the sharp increase in scattered light was delayed with decreasing inoculum volumes. The macroscopic morphology was microfilamentous under all conditions, only cultures with 1 % inoculum additionally contained very small spherical pellets. Cultivation conditions: *A. niger*, FP, n = 1400 rpm, d_0 = 3 mm, V_W = 3.2 ml, V_L = 0.8 ml, humidity $\geq$85 %, O_2 = 35 %, T = 37 °C, Vogel medium with 20 g·l^{-1} maltose, inoculum = 1-10 %, n_{bio} = 6.

3.6. Applying wide bore robotic pipet tips

Having rejected the first hypothesis, the focus shifted to the second hypothesis, which suggested a possible size selection effect of the inoculum due to the narrower opening of the robotic pipet tips. To investigate this possibility, the standard robotic tips were replaced with wide outlet robotic tips, which have the same outlet diameter as the pipet tips used in manual procedures. Accordingly, the liquid handling parameters of the robotics system were adjusted to accommodate the larger tip diameter (see Appendix Tab. A.1).
Subsequently, two independent cultivation rounds were conducted using two separate MBR devices of the same model (BioLector II). Each round directly compared six biological replicates of the manual inoculation process with six biological replicates of the automated inoculation process using the wide outlet robotic tips. The results are presented in Fig. 3.6.

Strikingly, the macroscopic morphology was exclusively microfilamentous under all conditions in both cultivation rounds (Fig. 3.6 C and D). This is in sharp contrast to previous cultivation runs using automated inoculation with standard robotic tips, which produced large pellets (Fig. 3.3 B, Fig. 3.4 B).
This finding strongly supports the hypothesis that the morphological changes observed in previous automated inoculation runs were caused by an inoculum size selection effect due to the smaller opening of the robotic tip. An alternative explanation could be variations in mechanical stress under the different pipetting conditions. However, quantifying these mechanical stresses is challenging due to significant differences between the pipetting systems. For example, manual pipet tips widen towards the top, whereas robotic pipet tips consist of two connected cylinders: a narrower cylinder at the opening and a wider cylinder at the top, connected to the rest of the robotics system. In addition, the pipetting speed in the manual workflow is operator dependent and can vary significantly.

The scattered light of all cultures in both cultivation rounds showed an initial lag phase, followed by a rapid increase in scattered light, a phase of less pronounced increase and finally a stationary phase of minimal change (Fig. 3.6 A and B). In the first round of cultivations, the scattered light of the automatically inoculated wells closely matched that of the reference cultures (Fig. 3.6 A). Similarly, in the second round, the scattered light of four out of six automatically inoculated wells was very comparable to the reference cultures (Fig. 3.6 B). The remaining two replicates showed a delay

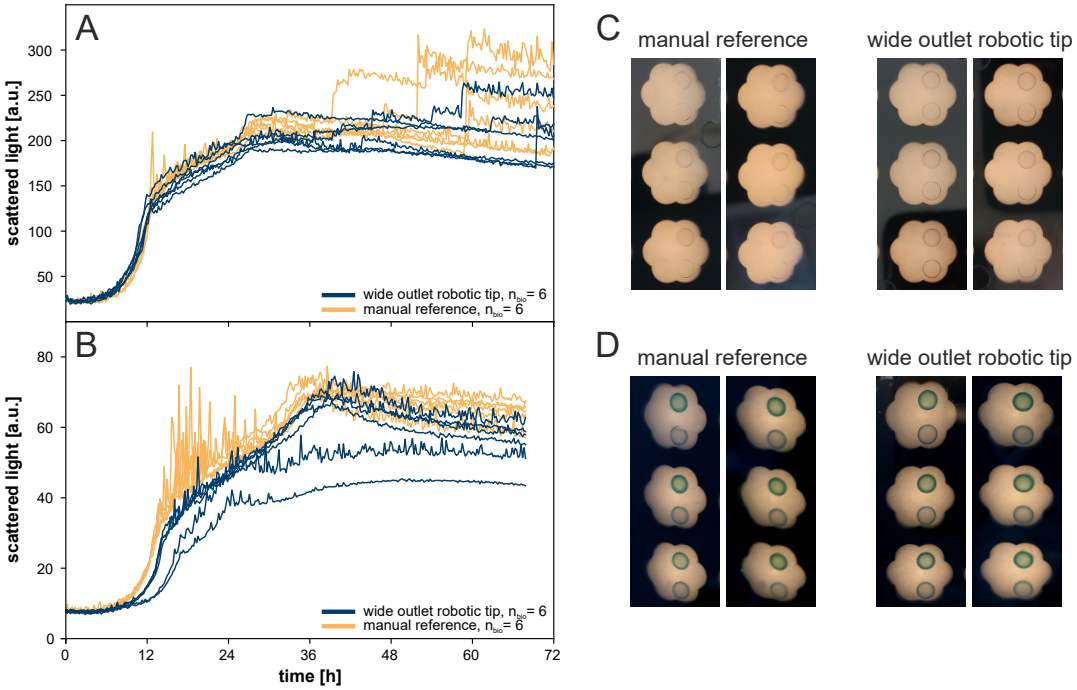

Fig. 3.6. **Cultivation of *A. niger* with automated inoculation using wide outlet robotic tips.** (A), (B) Scattered light from manual reference cultures (yellow) and cultures automatically inoculated with wide outlet robotic tips (blue) from two independent cultivation rounds. (C), (D) Pictures taken from the bottom of the cultivation plate at the end of cultivation, showing the macroscopic morphology of exemplary wells. The scattered light from automatically inoculated wells was consistent with reference cultures in the first round, but two replicates showed delays and reduced intensity in the second round. Nonetheless, a consistent microfilamentous morphology was found for all conditions in both rounds. Cultivation conditions: *A. niger*, FP, n = 1400 rpm, d_0 = 3 mm, V_W = 3.2 ml, V_L = 0.8 ml, humidity $\geq$85 %, O_2 = 35 %, T = 37 °C, Vogel medium with 20 g·l^{-1} maltose, inoculum = 10 %, n_{bio} = 6.

of approximately 3 h at the time of the transition from rapid to moderate increase in scattered light, although their macroscopic morphology was comparable to the reference. In addition, the scattered light intensity of the latter two replicates reached only 40 a.u. and 50 a.u., respectively, at the transition from moderate increase to stationary phase. In comparison, the reference and other automatically inoculated replicates reached approximately 70 a.u.

Such variations within one cultivation run can indicate issues such as media inconsistencies, reproducibility problems of the pre-culture or inaccuracies of the liquid handling system. However, it is highly unlikely that media or pre-culture inconsistencies were the cause of these discrepancies, since the same medium master mix was used for all cultivation wells. A more likely explanation for the observed variability is pipetting inaccuracies of the liquid handling system.

Several factors may contribute to pipetting inaccuracies of the robotic liquid handling system. Despite the use of wider tips, the potential for a size selection effect on the pre-culture pellets remains. Larger pellets may still be excluded or unevenly aspirated, resulting in an altered inoculum volume. Unlike manual pipetting, where a human operator can visually detect blockages and adjust accordingly, the automated system lacks the ability to detect and correct such issues. The high negative pressure applied during pipetting can further exacerbate the situation: a pellet can either be completely pulled into the pipet, subjecting it to excessive shear forces, or it can become stuck, altering the flow dynamics. If the pellet is stuck, the rest of the culture suspension flows past it, potentially causing variations in shear forces and affecting the reproducibility of the inoculation process.

However, it is also possible that these deviations are not (solely) caused by pipetting inaccuracies. Other, as yet unidentified, factors may be contributing to the differences of the cultivation results. Such factors could potentially affect both the automated inoculation and the manual workflow. To address this uncertainty, a detailed study of the variance of manual replicates is essential. This comparison will help to clarify whether the inconsistencies observed in the automated system are specific to the automation process or reflect broader variability inherent to the biological cultivation process itself.

3.7. Analyzing the variance of manual biological replicates

A total of 222 biological replicates of manual reference cultures, cultivated in seven separate rounds using three different MBR instruments of the same model, provide a robust dataset for assessing the variability inherent to the biological cultivation process. For direct visualization of this variability, the data from these replicates is collectively shown in Fig. 3.7, which focuses exclusively on manual inoculation. All presented cultures had a microfilamentous morphology with some small pellets, comparable to the replicates shown in Fig. 3.2.
A direct comparison between the 222 manual reference cultures (Fig. 3.7) and those inoculated automatically using wide outlet robotic tips (Fig. 3.6 A and B, both blue), is provided in the appendix Fig. A.1. This overlay highlights the differences in variability between these two methods.

Fig. 3.7 reveals a temporal deviation between the manual replicates of approximately 3 h at the transition from rapid to moderate increase in scattered light. Considering that this data is derived from seven independent rounds of cultivation on multiple instruments and no adjustments were made to the time-axis for the overlay, this demonstrates a good reproducibility during the lag phase and the phase of rapid increase in scattered light.
However, as the cultivation progresses beyond the rapid increase phase, the variability between replicates becomes more pronounced. These larger deviations are particularly evident in two areas. First, the slopes during the moderate increase in scattered light show significant differences. Second, there are significant differences in the absolute values of scattered light during the minimal change phase, even among replicates cultivated within the same MBR instrument. For example, the range of absolute scattered light values among replicates from the same MBR instrument can reach up to 60 % of the maximum scattered light value recorded for those replicates in this phase.
In contrast to these observations, the two deviating automatically inoculated replicates (Fig. 3.6 B) show clear differences from the start. These findings suggest that the deviations are not inherent to the cultivation process itself, but specific to the automated process. While pipetting inaccuracies of the liquid handling system seem plausible, the exact cause remains unknown.

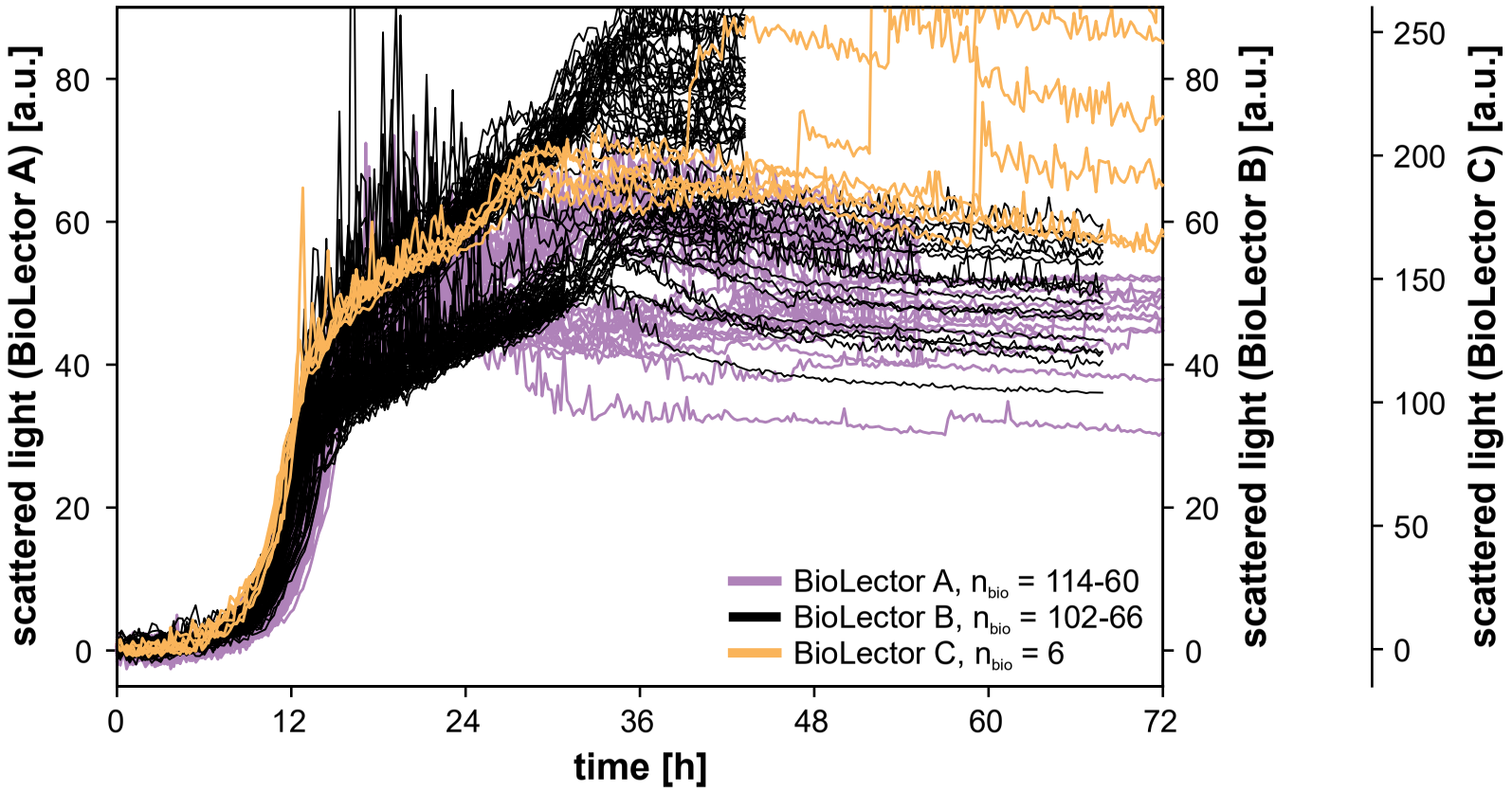

Fig. 3.7. **Comparison of 222 biological replicates of manual reference cultures of *A. niger*.** The dataset encompasses seven separate cultivation rounds using three different MBR instruments. The results show high reproducibility during the lag phase and the phase of rapid increase in scattered light. However, notable differences are observed in the slope during the moderate increase in scattered light and in the phase of minimal change. Cultivation conditions: *A. niger*, FP, n = 1400 rpm, d_0 = 3 mm, V_W = 3.2 ml, V_L = 0.8 ml, humidity ≥85 %, O_2 = 35 %, T = 37 °C, Vogel medium with 20 g·l^{-1} maltose, inoculum = 10 %, $n_{bio\ total}$ = 222 with sampling of 90.

3.8. Weighing the risks and rewards of automation

The results presented in Section 3.6 demonstrate that, despite the presence of outliers, the robotics system, equipped with wide outlet tips, is suitable for handling *A. niger* ANIp7-MCS-gfp2 cultures and achieving the desired microfilamentous morphology. This capability enables a fully automated inoculation workflow, including automated harvest of pre-cultures as well as inoculation and distribution of the main culture master mix (compare Fig. 3.1).

However, integrating automation into the inoculation process presents both significant advantages and potential new sources of error. A critical evaluation of the cultivation results is required after every run to identify any discrepancies that may occur. In some cases, it may be necessary to repeat experiments or specific culture conditions. However, this is also required in the manual process due to the potential for human error. Importantly, the incidence of inconsistencies in the automated runs was relatively low, with only two out of twelve replicates affected in one of the two independent cultivation rounds. This suggests that while errors can occur, they are rare, further supporting the potential of automation. Nonetheless, automation requires more rigorous monitoring than manual processes, as manual processes benefit from the observation of experienced operators. To fully harness the advantages of automation, this gap must be bridged through robust online monitoring systems to detect and address any deviations in real time.
Despite these challenges, the benefits of automation can potentially outweigh these drawbacks through higher throughput. As shown in Fig. 3.8, transitioning to automated inoculation significantly improves MBR time utilization. The manual workflow (Fig. 3.8 A) requires staff availability for pre-culture inoculation, pre-culture harvesting and processing as well as main culture inoculation. Thus, these process steps can only be performed during business hours (non-hatched area). Consequently, only two cultivations can be run in two weeks, resulting in 136 h of MBR downtime. Conversely, the automated workflow (Fig. 3.8 B) requires staff presence only for pre-culture inoculation. This allows for three cultivations within the same time period, reducing MBR idle time to 36 h, a nearly 4-fold improvement (Fig. 3.8 C). Moreover, automation increases throughput 1.5-fold and eliminates the need for staff to perform the main culture inoculation, significantly reducing the hands-on time.

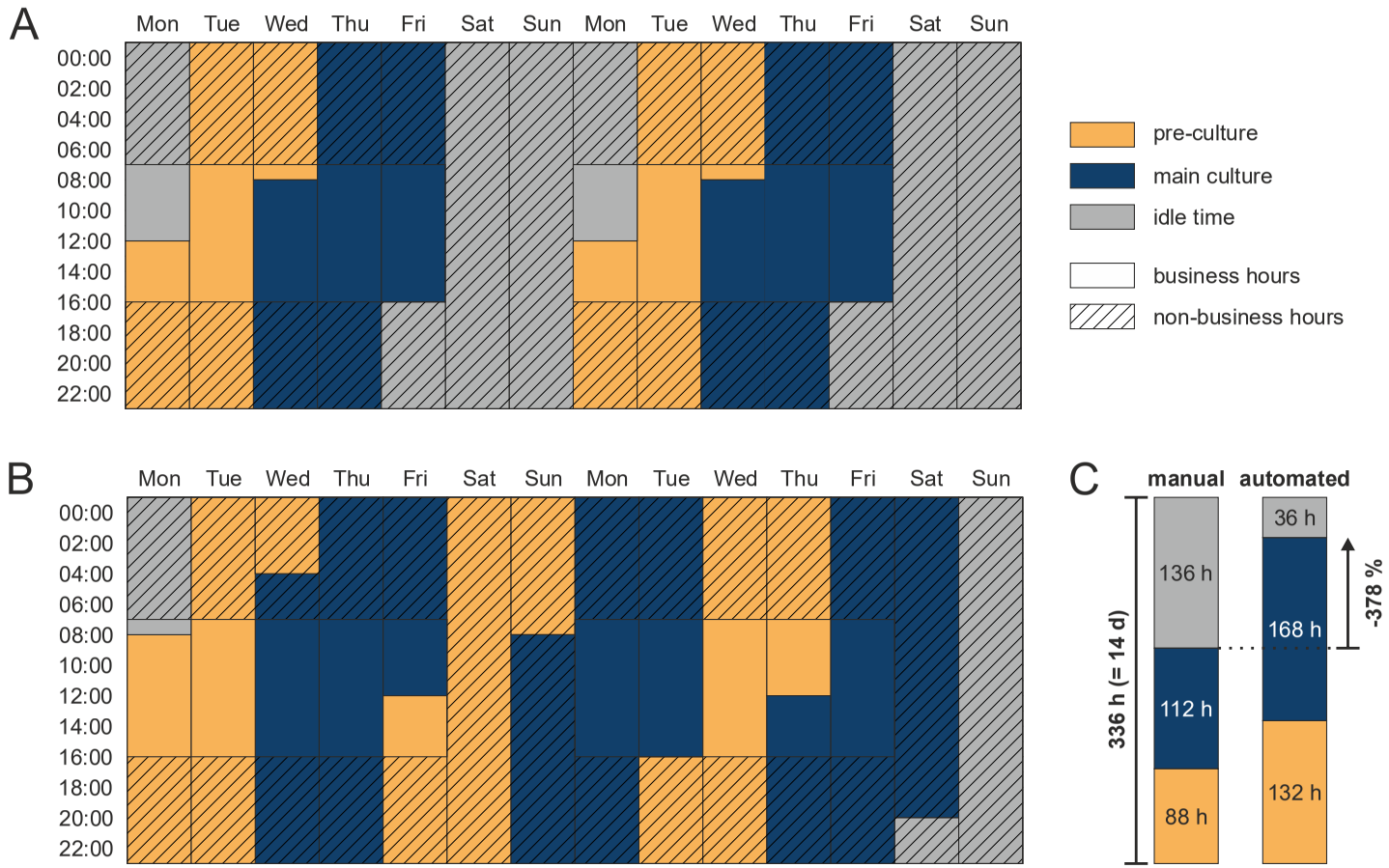

Fig. 3.8. **Two-week schedules for *A. niger* cultivation procedures.** (A) The manual workflow schedule allows only two cultivation cycles within two weeks due to the need for staff presence to harvest and process the pre-culture and inoculate the main culture. (B) In contrast, the automated workflow schedule allows three cultivations within the same time frame, increasing throughput by a factor of 1.5. (C) The automated workflow also significantly reduces MBR downtime from 136 h to 36 h, an almost 4-fold improvement.

3.9. Conclusion Chapter 3

This chapter contributes to the goal of reaching a fully automated MBR screening workflow for the phenotyping of *A. niger* ANIp7-MCS-gfp2. The introduction of automated inoculation significantly optimized the workflow, reducing MBR downtime and increasing cultivation throughput by a factor of 4 and 1.5, respectively. These advances foster extensive strain library screening and detailed analysis of process conditions.

Overall, this chapter provides important insights into the complex relationship between inoculation procedures and fungal morphology. It highlights the sensitivity of filamentous fungi such as *A. niger* to changes in environmental conditions and workflow modifications, particularly inoculum handling. The challenges encountered underscore the importance of carefully weighing the risks and benefits when automating cultivation processes. While the increase in throughput is a significant benefit, it must be balanced against potential challenges, such as pipetting inaccuracies that may require the repetition of experiments.
This work also emphasizes the critical importance of using a large number of biological replicates and conducting several independent cultivation rounds to ensure reliable and reproducible results. Conventional methods, which often rely on limited replicates, are prone to miss critical deviations or to prematurely discard promising strains. This was clearly demonstrated by the two cultivation rounds with automated inoculation using wide bore robotic tips (Section 3.6). If only the first round of cultivations had been performed, the process would have been considered fully validated, with no indication of underlying issues. Only by using a larger number of replicates and performing a second, independent cultivation run were the deviations identified and the underlying complexities of the automated and biological systems revealed.
In the broader context of this thesis, the development of this automated MBR workflow represents a significant advancement towards the overall goal of optimizing industrial bioprocesses for filamentous fungi. The successful implementation of automation in the cultivation process sets the stage for the integration of at-line morphology monitoring, which will be discussed in Chapter 4. This addition allows for real-time observation and analysis of fungal morphology, further improving the understanding and control of the cultivation process.

Looking ahead, future research should focus on further streamlining the automation protocols, in particular by automating pre-culture inoculation to enable a fully au-

tonomous cultivation workflow. This step is critical to further reduce MBR downtime and increase cultivation throughput, unlocking the full potential of MBR systems in combination with laboratory automation.

4. Unraveling the morphology-productivity relationship of *T. thermophilus*

Parts of this chapter have been previously published in publication II, conference poster IV and talk II. The work presented was performed in collaboration with BASF SE and is partly based on data collected during student project III. K. Rohr is the author of this chapter, had the scientific lead on this project, conceptualized and supervised student project III, conducted all BioLector experiments, established and conducted the phytase assay on the robotics platform, conducted the study to establish appropriate microscopy settings, annotated all microscopy images and analyzed and visualized all data. J. Seiffarth set up the annotation platform, selected and adapted the algorithm for biomass segmentation and assisted with the automated extraction of morphological features from microscopy images. L. van Balen supported the establishment of the phytase assay. M. Moch partly handled medium preparation and pre-culture inoculation. A. Anbarani and S. Bernauer provided the strain (both BASF SE).

Building on the advances in MBR cultivation and automation discussed in the previous chapters, this chapter shifts the focus to examining the relationship between the fungal morphology and productivity of *T. thermophilus*. Understanding the morphology-productivity relationship is critical because the physical structure of filamentous fungi can directly influence the efficiency of product formation.
Therefore, the aim of this chapter is to investigate how different cultivation conditions, such as pH and feeding rates, affect the morphology of *T. thermophilus* and its subsequent phytase production. By implementing an advanced workflow that integrates MBR cultivation with automated microscopy and image analysis, this chapter not only aims to elucidate the intricate morphology-productivity relationship, but also to establish a robust methodology that can be used for further research with *T. thermophilus*. Thus, this chapter will provide critical insights into the optimization of bioprocesses for filamentous fungi and contribute to the broader goal of enhancing the industrial application of these microorganisms.

4.1. Cultivation and analysis workflow

An overview of the workflow established to study the effects of different cultivation conditions on the morphology and product formation of *T. thermophilus* is illustrated in Fig. 4.1. During MBR cultivation, a liquid handling robotics system automatically collects samples at pre-determined time points. These samples are then processed on the laboratory automation platform. Half of each sample is diluted with 0.9 % NaCl to prepare it for automated at-line microscopy. The other half is stored on a cooling carrier for later product analysis.
After cultivation, the stored samples are analyzed regarding phytase activity, while the microscopy images are used for automated morphology analysis (both performed offline). Further details on the configuration of the laboratory automation platform can be found in Subsection 1.3.2. For a comprehensive description of the automated microscopy workflow, please refer to Subsection 1.3.3.

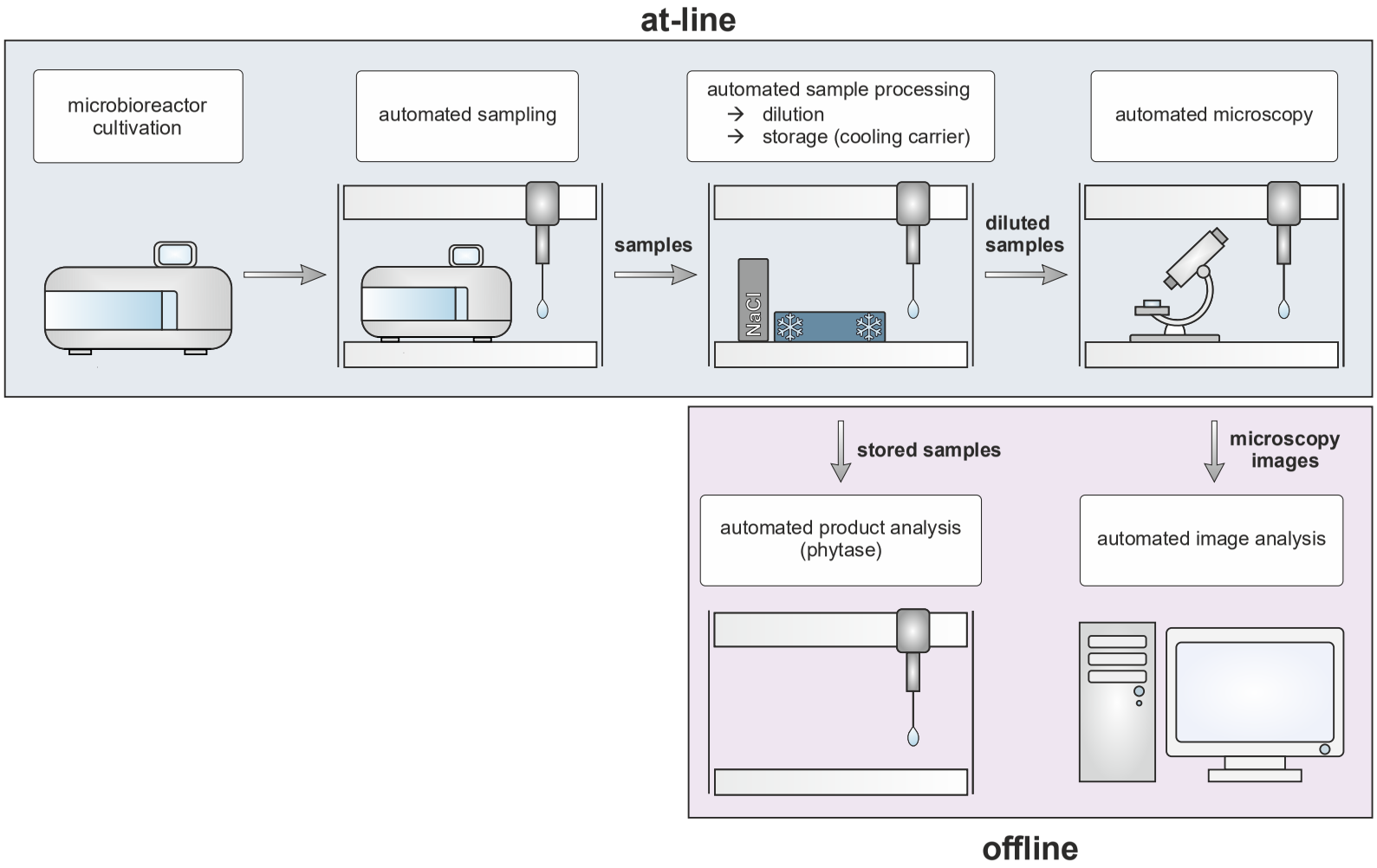

Fig. 4.1. **Schematic of the cultivation and analysis workflow for *T. thermophilus*.** During MBR cultivation, samples are automatically collected using a liquid handling robotics system. Each sample is split, with half diluted in 0.9 % NaCl for automated at-line microscopy and the other half stored on a cooling carrier for subsequent product analysis. After cultivation, the stored samples are analyzed regarding phytase activity and the obtained microscopy images are used for automated morphology analysis (both offline).

4.2. Microscopy settings

The first step in establishing the cultivation and analysis workflow described in Section 4.1 was to select appropriate microscopy settings. The goal was to ensure that both mycelial aggregates and the intricate details of freely dispersed hyphae are clearly visible. Achieving this would enable automated analysis to detect and quantify the fungal area, which in this context refers to the imaged surface area of individual fungal structures. Monitoring this fungal area is essential as it allows to track the development and changes in size and complexity of fungal structures throughout the cultivation process. In addition to tracking the fungal area, the chosen microscopy settings, which capture the fine details of freely dispersed hyphae, could also enable automated analysis to count hyphal tips - a key morphological feature for characterizing processes involving filamentous fungi [34].
In order to determine suitable microscopy settings, an MBR cultivation was conducted, with automated sampling between 12 h and 23 h. The specific cultivation conditions are detailed in Section 6.5. Samples were automatically diluted with 0.9 % NaCl. Subsequently, the diluted samples were manually transferred to the flow chamber for microscopic analysis. Fig. 4.2 shows exemplary microscopy images of a sample taken after 12 h of cultivation.

Fig. 4.2 A compares different sample dilutions and microscopy magnifications. It demonstrates that while biomass aggregates and larger structures are well visualized at 40-fold magnification, individual hyphae cannot be distinguished. Conversely, 150-fold magnification provides the resolution necessary to clearly visualize details such as individual fungal tips. In addition, this magnification is also suitable for imaging fungal aggregates, as shown in Fig. 4.2 B. Consequently, 150-fold magnification was chosen for use in subsequent microscopy experiments.
Regarding dilution, a superposition of different fungal structures was observed at low dilutions in later samples. However, at high dilutions during earlier sampling times, only a small amount of fungal biomass was captured per image. Therefore, a dynamic dilution strategy was chosen for subsequent cultivation runs. The dilution was adjusted according to the cultivation time, ranging from 4-fold dilution at 2 h of cultivation to 70-fold dilution from 22 h onwards.

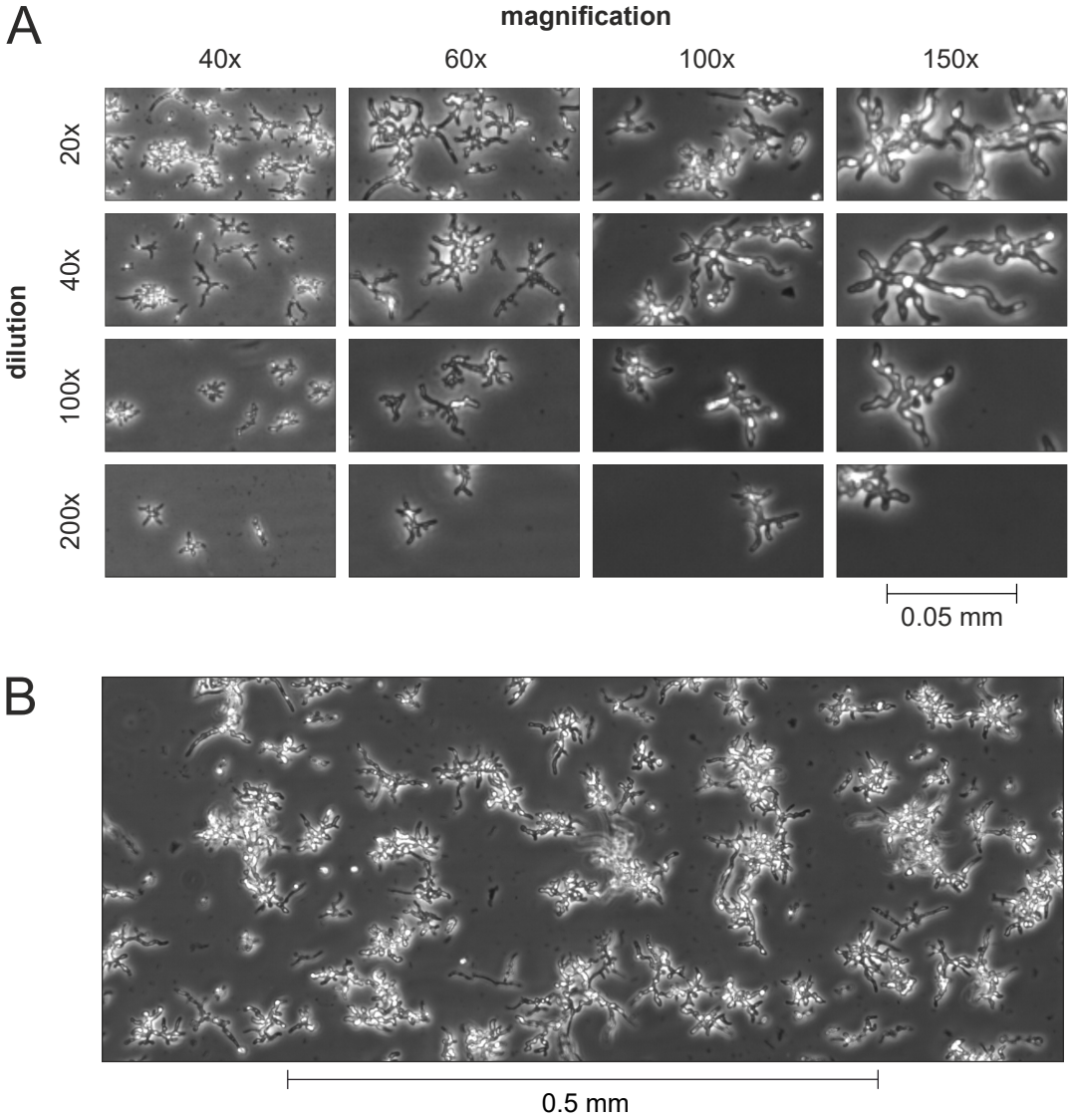

Fig. 4.2. **Comparison of microscopy settings for a *T. thermophilus* sample after 12 h of cultivation.** (A) Sections of microscopy images using different dilutions and magnifications. Each section represents 0.7 % of the full microscopy image to highlight the level of detail. (B) A section of a microscopy image using a 20-fold dilution and 150-fold magnification. The section represents 50 % of the full microscopy image to provide an overview of the imaged biomass. A 150-fold magnification was selected for subsequent experiments, as it allowed for clear visualization of both detailed structures and aggregates. Additionally, a dynamic dilution strategy was implemented, ranging from 4-fold dilution at 2 h to a 70-fold dilution from 22 h onwards.

4.3. Batch cultivation

After choosing appropriate microscopy settings, the next step was setting up a batch cultivation. With the aim of providing conditions that mimic those found in industrial settings, this cultivation was conducted using pH control. During cultivation, the impact of two different pH-setpoints, pH 5.5 and 6.5, on fungal growth and phytase activity were assessed. These pH-setpoints were chosen as they are within the optimal growth range of *T. thermophilus* (pH 4.5 to 7.0) and are representative of conditions found in industrial applications [70]. The results are presented in Fig. 4.3. See appendix Fig. A.2 for an enlarged version of the microscopic images.

The online measurement of scattered light initially showed a similar progression for cultures at both pH-setpoints (Fig. 4.3 A). However, over the course of cultivation, the fungi cultivated at pH 5.5 showed slightly faster growth than those at pH 6.5, as indicated by reaching the initial maximum of scattered light approximately 0.8 h earlier. This faster growth at pH 5.5 was also evident by an earlier increase in pH, also by approximately 0.8 h at around 10 h process time (Fig. 4.3 B). An increase in pH, as observed in these cultivations, is typically found after the depletion of glucose, as only one-sided pH control with base (3 M KOH) was applied. One-sided pH control has been deliberately chosen for the batch mode to match the MBR fed batch conditions. In fed batch mode, the BioLector Pro, which is capable of feeding two solutions simultaneously, allows the application of a (glucose) feed in combination with one-sided pH control (refer to Subsection 1.3.1 for further details).
Phytase activity was similar for both pH conditions during the first 18 h of cultivation (Fig. 4.3 C). However, towards the end of cultivation, from 22 h onwards, up to 2-fold higher enzyme activity was observed at pH 5.5. At the end of cultivation at 26 h, cultures at pH 5.5 had a 1.5-fold higher phytase activity than those at pH 6.5. These results clearly demonstrate that the applied pH-setpoints are well-suited to achieve productivity variations in *T. thermophilus*.

Morphology analysis was performed by qualitative manual evaluation of 15 different microscopy images per sampling point and condition. Each image was assessed for the presence of morphological structures in five size categories: very large, large, medium, medium-small and small. For each sampling point and condition, the identified categories were recorded. If multiple size groups (e.g. large and medium) were observed, all applicable groups were noted. This evaluation was repeated in two independent rounds.

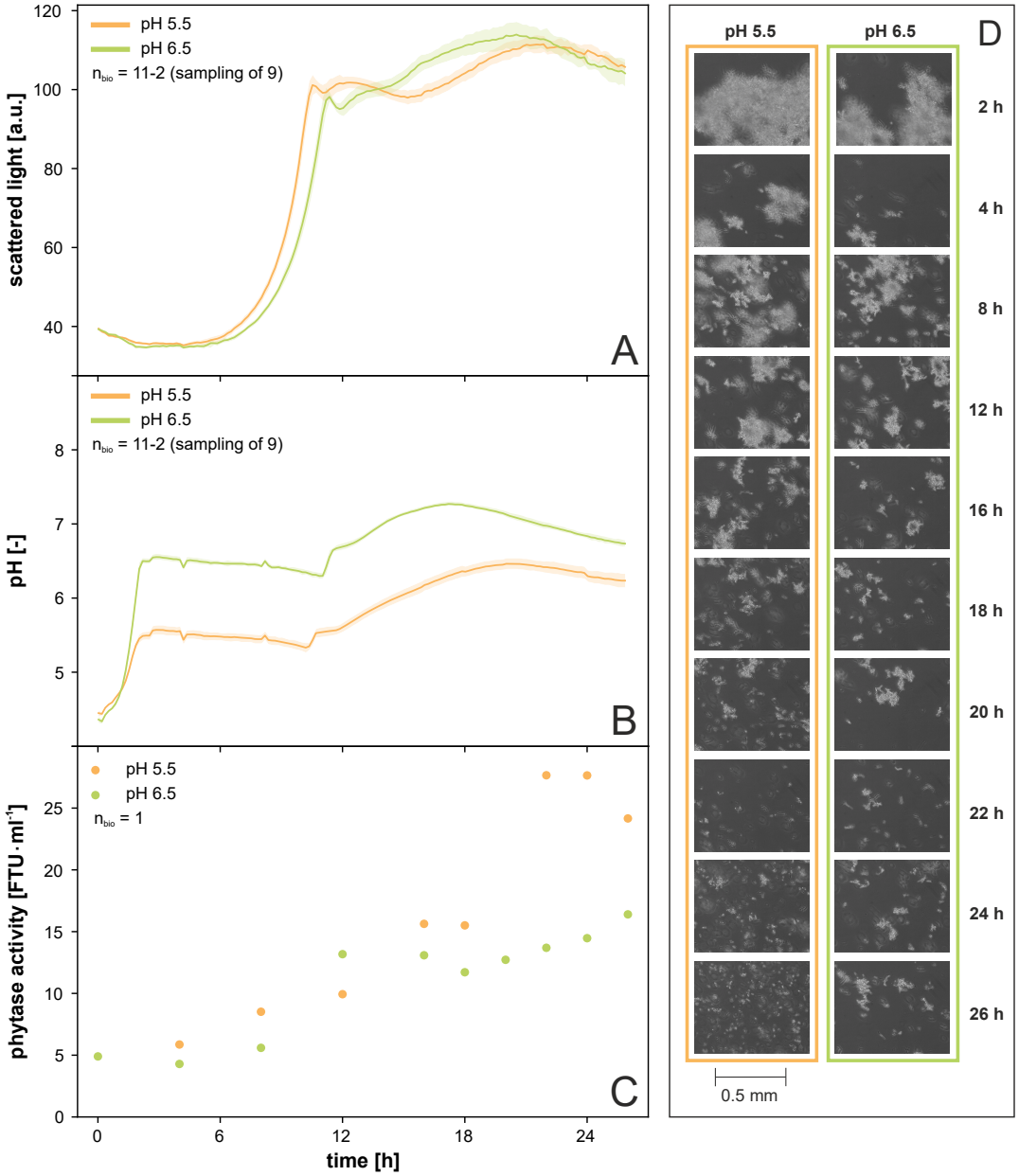

Fig. 4.3. **Batch cultivation of *T. thermophilus* with microfluidic pH control.** (A) Scattered light, (B) pH and (C) phytase activity over time. (D) Exemplary microscopic images taken fully automatically during cultivation. Phytase activity was similar for both pH-setpoints during the first 18 h of cultivation. However, from 22 h onwards, enzyme activity was up to 2-fold higher at pH 5.5. This higher enzyme activity coincided with significant morphological differences, showing much smaller fragments at pH 5.5 than at pH 6.5. Cultivation conditions: *T. thermophilus*, microfluidic FP, n = 1400 rpm, d_0 = 3 mm, V_W = 3.2 ml, V_L = 0.8 ml, humidity $\geq$85 %, O_2 = 35 %, T = 37 °C, 20 g·l^{-1} glucose, n_{bio} = 11 with sampling of 9. [165]

The analysis revealed the presence of very large to medium-sized structures in both conditions during the first 8 h of cultivation (Fig. 4.3 D). A notable morphological change occurred between 8 h and 12 h, marked by the breakdown of larger structures into predominantly medium-sized aggregates. This shift coincided with the depletion of the primary carbon source, as indicated by a peak in the scattered light signal and the increase in pH. It is therefore very likely that the observed breakdown of larger structures was caused by sugar depletion.
From 22 h onwards, there was a clear morphological difference between the cultures. At pH 5.5, significantly smaller fragments were present, which were not observed at pH 6.5. This morphological variation coincided with the up to 2-fold higher phytase activities at pH 5.5. It is widely recognized that the morphology of filamentous fungi has a strong influence on their productivity [20, 34]. The results of this cultivation run thus suggest that smaller fragments of *T. thermophilus* can lead to higher productivity and therefore phytase activity under the given batch conditions. Alternatively, it is possible that larger aggregates show significant productivity and the degradation of these aggregates at pH 5.5 promotes the release of previously synthesized phytase, thereby increasing the enzyme activity in the supernatant.
It should be noted that despite the differences in morphology, the progression of scattered light at this time was very comparable between the two pHs. This underlines the importance of using several complementary measurement techniques for screening and process development with filamentous fungi, as such important relationships may otherwise go undetected.

4.4. Bridging laboratory screening and industrial production: applying fed batch conditions

After establishing the batch cultivation protocols with two different pH-setpoints, the next step was to apply a microfluidic fed batch with pH control to even more closely mimic industrial conditions. During cultivation, the effect of the previously tested pH-setpoints (pH 5.5 and 6.5) in combination with two feeding rates on fungal growth, phytase activity and morphology was assessed.
In the present gene cassette, phytase production is regulated by the glaA promoter derived from *A. niger*. While Ganzlin and Rinas [166] report that glucose acts as an inducer rather than a repressor of the glaA promoter in *A. niger*, the observations

from the previous batch cultivations at pH 5.5 revealed a more than 2-fold increase in phytase activity after depletion of the primary carbon source until the end of cultivation (Fig. 4.3 C). Thus, the fed batch process was tailored to provide glucose for cell growth in the batch phase and to facilitate phytase production in the fed batch phase by avoiding the drawbacks associated with a potential carbon catabolite repression. The glucose feeding rates, 1 and 2 g·(l·h)$^{-1}$, were chosen to target carbon limitation. These rates were determined based on glucose consumption rates from previous experiments (data not shown). The results of the fed batch cultivations are presented in Fig. 4.4. See appendix Fig. A.3 for an enlarged version of the microscopic images.

Scattered light at the end of the batch phase showed a steeper increase for cultures at pH 5.5 compared to pH 6.5, indicating faster growth (Fig. 4.4 A). This observation is additionally supported by the earlier increase of DO, indicating an earlier carbon depletion (Fig. 4.4 B). These results are consistent with observations from the previous batch experiment (Fig. 4.3 A).
During the fed batch phase, cultures fed at 2 g·(l·h)$^{-1}$ had a very similar progression of scattered light for both pHs. In contrast, cultures fed at 1 g·(l·h)$^{-1}$ showed a slightly faster increase of scattered light at pH 5.5 than cultures with the same feeding rate at pH 6.5. Comparing the two feeding rates, the faster feeding rate, 2 g·(l·h)$^{-1}$, resulted in faster growth at both pHs, which is the expected result in a carbon-limited fed batch cultivation. Nevertheless, similar final scattered light values were reached for all conditions, ranging only within 10 a.u. of each other.
In contrast to the batch cultivations, the pH-setpoints 5.5 and 6.5 were very well-matched throughout the cultivation, even though one-sided pH control was applied (compare Fig. 4.3 B and Fig. 4.4 C). This is most likely an effect of the switch to fed batch cultivation.

Samples for phytase measurements were taken at the beginning and end of batch and after the addition of 50 % and 100 % feed volume. As the same total amount of glucose was fed at both feeding rates, end point samples were taken at 15 h and 22 h respectively.
At the end of cultivation, very similar phytase activities were detected for cultures at pH 5.5 and 6.5, which were both fed with 2 g·(l·h)$^{-1}$ (Fig. 4.4 D, yellow and blue). Their final activities were 20$\pm$2 and 20$\pm$5 FTU·ml^{-1} (n_{bio}=3, n_{tec}=1). In contrast to these results, a clear difference in phytase activity was observed between cultures at pH 5.5 and 6.5, which were both fed with 1 g·(l·h)$^{-1}$ (Fig. 4.4 D, red and green). With

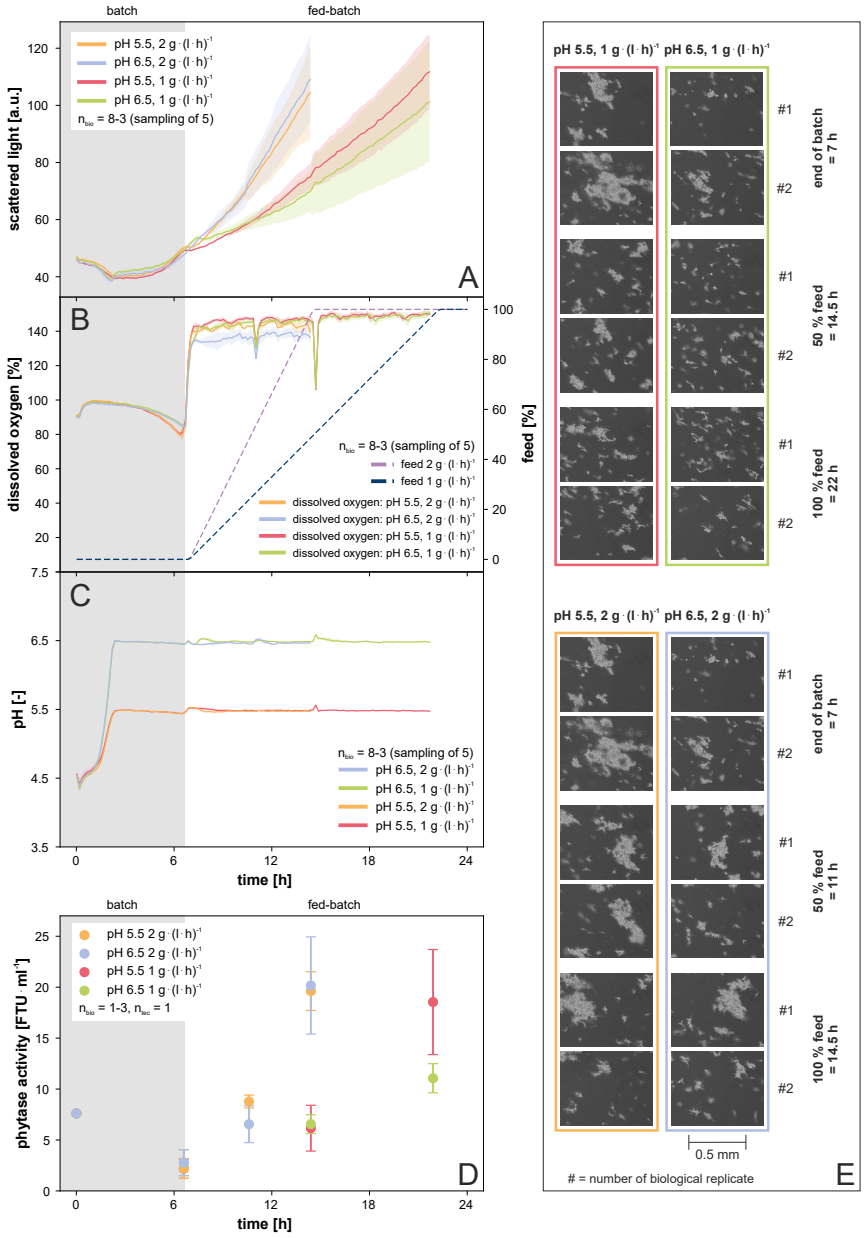

Fig. 4.4. **Fed batch cultivation of *T. thermophilus* with microfluidic pH control.** (A) Scattered light, (B) DO and feed, (C) pH and (D) phytase activity over time. (E) Exemplary microscopic images taken fully automatically during cultivation. In cultures fed with 2 g·(l·h)$^{-1}$, medium to large aggregates were present and high final phytase activities were yielded, regardless of pH. In cultures fed with 1 g·(l·h)$^{-1}$, medium-sized aggregates were seen at pH 5.5, while only small pieces were present at pH 6.5. Phytase activity at pH 5.5 was comparable to that of cultures fed with 2 g·(l·h)$^{-1}$, but activity at pH 6.5 was 1.6-fold lower. Cultivation conditions: *T. thermophilus*, microfluidic FP, n = 1400 rpm, d_0 = 3 mm, V_W = 3.2 ml, V_L = 0.8 ml, humidity ≥85 %, T = 37 °C. Batch: 5 g·l^{-1} glucose, O_2 = 21 %; fed batch: 15 g·l^{-1} glucose as a constant feed with a rate of 1 or 2 g·(l·h)$^{-1}$, O_2 = 35 %; n_{bio} = 8 with sampling of 5. [165]

final activities of 18±5 and 11±1 FTU·ml^{-1} (n_{bio}=3, n_{tec}=1), the activities at pH 5.5 were 1.6-fold higher than those at pH 6.5. Yet, compared to the faster feeding rate of 2 g·(l·h)$^{-1}$, the activity at pH 5.5 was very similar. A direct comparison of the final phytase activities is given in Tab. 4.1.

It is important to not only consider the total enzyme activity but also the space-time yield (STY). The STY in the fed batch phase was calculated by dividing the difference in activity between the end of feed and the end of batch by the time elapsed between these two points, as detailed in Eq. 6.4. It was 1.1 FTU·(ml·h)$^{-1}$ for cultures at pH 5.5 fed with 1 g·(l·h)$^{-1}$, but 2.2 FTU·(ml·h)$^{-1}$ for all cultures that were fed with 2 g·(l·h)$^{-1}$. This represents a 2-fold improvement in this important key performance indicator. Moreover, the STY of cultures at pH 6.5 fed with 1 g·(l·h)$^{-1}$ was only 0.5 FTU·(ml·h)$^{-1}$. Compared to these results, the adjustment of pH and/or feeding rate achieves a 2-fold and 4-fold increase in the STY. A direct comparison of the STYs is given in Tab. 4.1. These results clearly demonstrate that the workflow is well-suited to induce a variation in productivity through the applied pH and feed conditions.

Morphology analysis was performed by qualitative manual evaluation of 100 different microscopy images per sampling point, condition and biological replicate. Two biological replicates were sampled at the end of batch for each condition, while three were sampled at each sampling point during the feeding phase, resulting in a total of 200-300 different images per sampling point and condition. As in the batch process, each image was assessed for the presence of morphological structures in five size categories: very large, large, medium, medium-small and small. For each sampling point, condition and biological replicate, the identified categories were recorded. If multiple size groups were observed, all applicable groups were noted. This evaluation was repeated in two independent rounds.
In cultures fed with 2 g·(l·h)$^{-1}$, medium to large aggregates were present after the addition of 50 % and 100 % feed, irrespective of pH (Fig. 4.4 E, yellow and blue). Conversely, no large aggregates were present in cultures fed with 1 g·(l·h)$^{-1}$. However, medium-sized aggregates were observed at pH 5.5, whereas only small pieces were present at pH 6.5 (Fig. 4.4 E, red and green). The cause of these differences between the two feeding rates is likely the stronger carbon limitation of the slower feeding rate. As can be seen in Fig. 4.4 B, no decrease in DO is observed during feeding. Thus, both feeds represent C-limited conditions. It is therefore clear that the slower feeding rate results in higher stress and a stronger carbon limitation for the cells than the faster feeding rate. This reduced availability of glucose could lead to the breakdown

of larger fungal aggregates, analogous to the observations in the batch experiments after carbon depletion (Fig. 4.3 D).

The more pronounced carbon limitation of the slower feeding rate also offers an explanation for the differences observed in morphology and phytase activity between the cultures at pH 5.5 and those at pH 6.5 (Fig. 4.4 D and E, red and green). In this particular case, at a feeding rate of 1 g·(l·h)$^{-1}$, pH 6.5 led to a morphology of predominantly small fragments and a 1.6-fold lower phytase activity, while no similar effect of pH on morphology and phytase activity was observed at a feeding rate of 2 g·(l·h)$^{-1}$. One possible explanation is that the cells are more susceptible to the effects of pH on morphology and productivity due to the higher environmental stress.

Tab. 4.1. Comparison of key performance indicators for a fed batch cultivation of *T. thermophilus* with microfluidic pH control. Phytase activity given is the activity at the end of cultivation. The STY was calculated for the fed batch phase according to Subsection 6.7.4. Morphology describes the predominant aggregate sizes in the fed batch phase. All data was obtained with n_{bio}=3 and n_{tec}=1. Adapted from [165].

Condition	**Activity [FTU·ml^{-1}]**	**Space-time yield [FTU·(ml·h)$^{-1}$]**	**Morphology (aggregate size)**
pH 5.5, 1 g·(l·h)$^{-1}$	18±5	1.1	Medium
pH 6.5, 1 g·(l·h)$^{-1}$	11±1	0.5	Small
pH 5.5, 2 g·(l·h)$^{-1}$	20±2	2.2	Medium to large
pH 6.5, 2 g·(l·h)$^{-1}$	20±5	2.2	Medium to large

Based on these observations, the appearance of small fungal fragments in a fed batch cultivation of *T. thermophilus* may indicate suboptimal environmental conditions, such as an insufficient feeding rate and suboptimal pH, which can result in lower product formation. As product analysis in cultivation processes is usually performed offline, the presented at-line morphology analysis could be used in the running process to adjust the conditions, e.g. to increase the current feeding rate, in order to improve product formation and thus STY.

4.5. Evaluating workflow insights: a side-by-side comparison of batch and fed batch results

A comparative analysis of batch and fed batch cultivation results yields several key insights. In batch experiments, similar morphologies and phytase activities were observed between pH 5.5 and 6.5, as long as glucose was present. After depletion of the primary carbon source, a breakdown of aggregates into small fragments was observed at pH 5.5. Simultaneously, phytase activity continued to increase more than 2-fold until the end of cultivation. Based on these results, two hypotheses were put forward:

I. Small fungal fragments of *T. thermophilus* lead to high productivity.

II. Large aggregates yield high productivity, but the breakdown of these aggregates effectively releases previously produced phytase, increasing enzyme activity in the supernatant.

In fed batch experiments, small fungal fragments combined with low phytase activities were observed at pH 6.5 and a feeding rate of 1 g·(l·h). These results clearly contradict the first hypothesis that small fungal fragments lead to high productivity. Since larger fungal aggregates and a 1.6-fold to 1.8-fold higher phytase activity were observed in all other conditions, the second hypothesis is likely to apply. However, no breakdown of the aggregates was detected. Therefore the second part of this hypothesis can neither be rejected nor confirmed.

Even after extensive analysis, the similar morphology at different pH values between batch and fed batch cultivations cannot be conclusively explained. It remains unclear, why a breakdown of large aggregates into small fragments was observed in batch cultivations at pH 5.5, whereas exclusively small fragments were observed during the feeding period of fed batch experiments at pH 6.5 (1 g·(l·h)$^{-1}$). Obviously, batch cultivations and carbon-limited fed batch cultivations provide fundamentally different environmental conditions. This could be a factor in the similar morphology at different pH values, however further investigations are required.
Nevertheless, these results clearly show that the workflow is well-suited to apply different environmental conditions to a large number of biological replicates in order to induce changes in productivity and morphology of *T. thermophilus*. The insights

gained demonstrate the significant value of this workflow in investigating the important morphology-productivity relationship.

4.6. Automated image analysis

The presented workflow offers substantial advantages for analyzing the morphology-productivity relationship. With 32 parallel cultivation wells, each providing 100 images per sampling, this approach allows for precise analysis. However, it also requires considerable effort due to the extensive image analysis involved. The resulting 3200 images per cultivation run must be manually reviewed and analyzed, highlighting the need for automated image analysis. Although powerful image analysis methods based on deep learning have been developed, they must be adapted for the analysis of fungal morphologies in the flow chamber setup and trained on annotated data sets [148, 152].

4.6.1. Training and validation of the algorithm

Based on a preliminary literature review, an adapted OMNIPOSE algorithm [151] was selected for automated image analysis. This algorithm was chosen because, unlike methods using bounding boxes, it provides pixel-precise segmentation, which is essential for accurate mapping of fungal structures. After selecting the algorithm, the microscopy image dataset obtained from the cultivation described in Section 4.2 was manually annotated to serve as training data for the algorithm.
The training process involved two rounds on the same dataset. In the first round, 20 full microscopy images were annotated. In the second round, 20 crops (sections) of microscopy images were annotated to increase annotation efficiency. Annotating whole images is time consuming, while cropping allows more image and cell features to be covered in the same annotation time, resulting in a more diverse training set. The crops were generated using the method described by Scherr et al. [167], extracting random sections from non-overlapping regions of each image.
As shown in Fig. 4.2 B, the morphology consisted mainly of freely dispersed mycelium with no larger aggregates. However, when the fungus is out of the focal plane of the microscope, the boundaries of the hyphae are unclear, making it difficult to accurately determine where the fungal structures start or end. In such cases, annotation of

these regions could lead to misleading results. Therefore, out-of-focus areas were deliberately not annotated to ensure the reliability of the annotation.

After training, the performance of the algorithm was evaluated by reapplying it to the training dataset and comparing its segmentation with the manual annotations. The results of this procedure are presented in Fig. 4.5. Fig. 4.5 A and B show both an overview and enlarged sections of an exemplary microscopy image, in its original form (left) and with manual annotations (right). As illustrated in Fig. 4.5 B (right), the hyphal structure of each fungus was carefully traced. The automatic segmentation, shown in Fig. 4.5 C and D (right), closely matched the manual annotations (left) after these two training rounds.

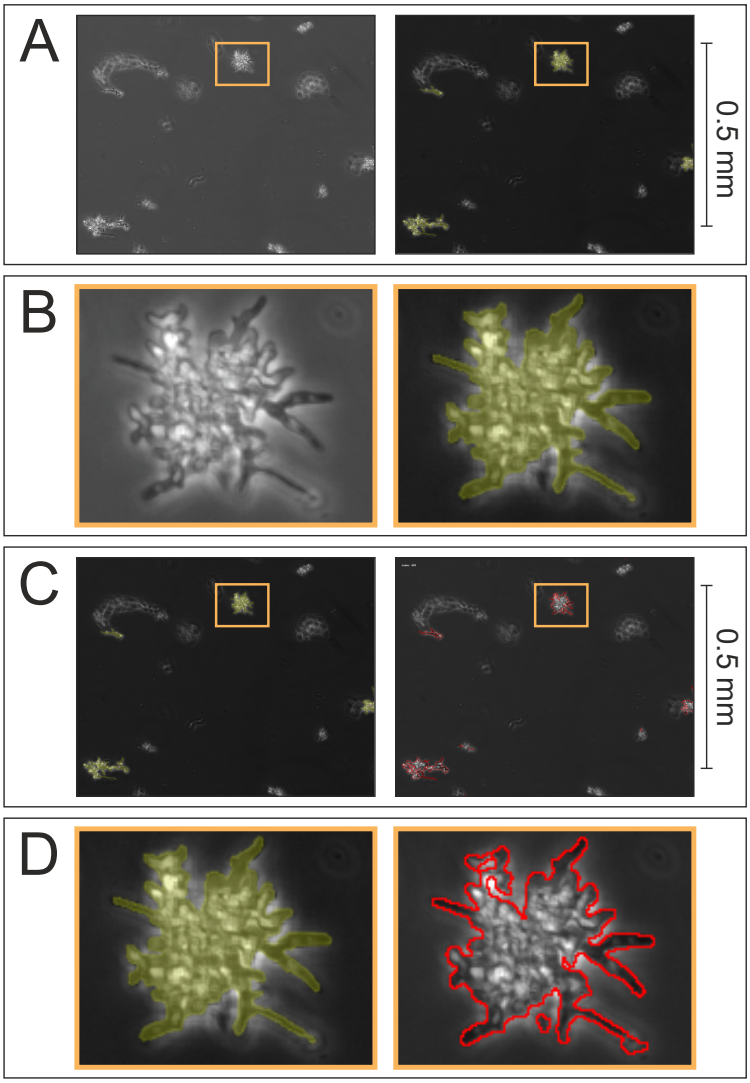

Fig. 4.5. **Training and validation of the algorithm for segmentation of *T. thermophilus* biomass.** (A) Overview and (B) enlarged sections of an original microscopy image (left) and the manually annotated image (right). (C) Overview and (D) enlarged sections of the same manually annotated image (left) and the segmentation after reapplication of the trained algorithm to the training dataset (right). After two training rounds, the segmentation of *T. thermophilus* biomass closely matched the manual annotations.

4.6.2. Application and analysis of cultivation data

Following training and validation, the algorithm was applied to the cultivation datasets obtained from the batch cultivations described in Section 4.3 and illustrated in Fig. 4.3. This allowed the automatic extraction of morphological metrics. The results are shown in Fig. 4.6. In addition, histograms showing the distribution of the detected fungal size are provided in the appendix Figs. A.4 and A.5.

Fig. 4.6 A depicts the number of detected fungi over the cultivation period. Each enclosed area is counted as a fungus, regardless of its size. Therefore, the number of detected fungi does not necessarily correlate with the fungal area, shown in Fig. 4.6 B. Nonetheless, the graphs indicate that both the number of fungi and the fungal area increased throughout the cultivation period for cultures at pH 5.5. In contrast, cultures at pH 6.5 reached a plateau between 12 h and 22 h of cultivation.
These automatically derived metrics differ significantly from the scattered light data presented in Fig. 4.3. The scattered light measurements show no further increase in biomass after 12 h of cultivation. Furthermore, as discussed in Section 4.3, the scattered light shows a similar growth trajectory for both pH-setpoints, with only slightly faster growth observed at pH 5.5.

The violin plots in Fig. 4.6 C and D illustrate the distribution of the detected fungal size for cultures cultivated at pH 5.5 and pH 6.5, respectively. Both plots show similar results regarding the 25^{th} percentiles and medians. The 25^{th} percentiles suggest a consistent size for the smallest fungi throughout the cultivation process. Similarly, the median indicates only small changes. This is likely due to the high number of very small detected fungal structures, as evidenced by the large width of the violin plots for these smaller sizes. For more details on the distribution of detected fungal sizes, please refer to the histograms in the appendix Figs. A.4 and A.5.
In contrast, the 75^{th} percentile profiles differ considerably between the two pH-setpoints. For cultures at pH 5.5, the size of the largest detected fungal structures increases until 20 h of cultivation, then decreases to approximately its original size by 26 h. For cultures at pH 6.5, the largest detected fungal structures gradually increase in size until 24 h of cultivation.
However, a comparison with manual morphology analysis reveals significant discrepancies (see also Section 4.3 and Fig. 4.3 D). For example, the 25^{th} percentiles from the automated analysis suggest a consistent size for the smallest fungi throughout the cultivation. This clearly contrasts with the manual analysis, which showed no small

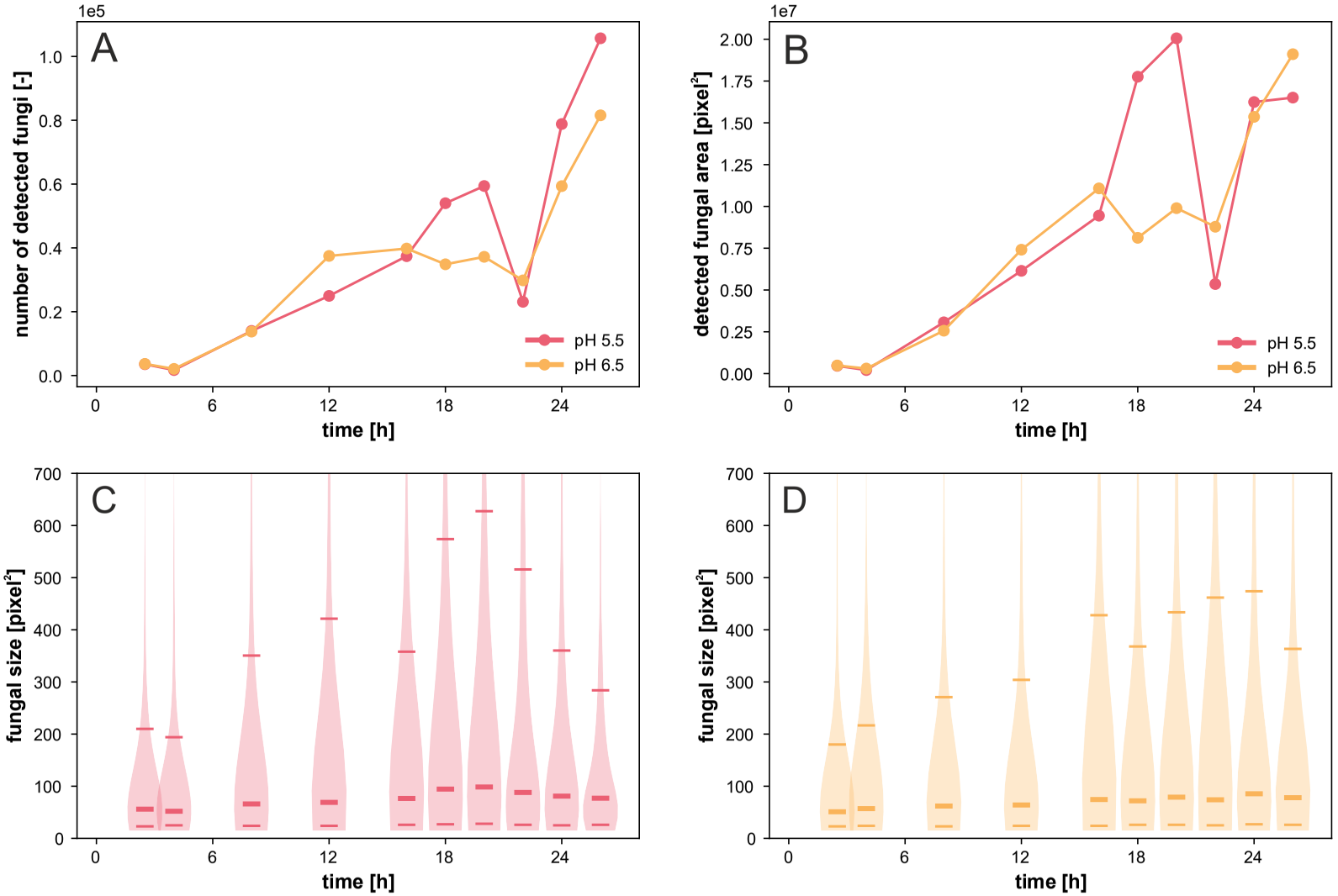

Fig. 4.6. **Automatically extracted morphological metrics of an MBR batch cultivation of *T. thermophilus*.** (A) Number of detected fungi over time, (B) detected fungal area over time. (C), (D) Violin plots showing the distribution of the detected fungal size for cultures cultivated at pH 5.5 and pH 6.5, respectively. The violin plots include markers for the median and the 25th and 75th percentiles. All plots account for sample dilution by multiplying the metric by the corresponding dilution factor at each given time. For cultures at pH 5.5, both the number of detected fungi and the fungal size increase throughout the cultivation period. At pH 6.5, these metrics plateau between 12 h and 22 h. As indicated by the violin plots, the largest fungi at pH 5.5 increase until 20 h, then revert to their original size by 26 h. At pH 6.5, the largest fungi steadily increase until 24 h.

fungal structures at the beginning of the cultivation. Small fungal structures did not appear until about 8 h of cultivation. Moreover, at the end of cultivation, aggregates at pH 5.5 were observed to be significantly smaller than those at pH 6.5. This direct comparison demonstrates that the automated analysis erroneously detected small fungal structures at the beginning of the cultivation and failed to capture the smaller aggregate size at pH 5.5 compared to pH 6.5 at the end of cultivation.
For the 75^{th} percentiles, the automated analysis showed an increase in the size of the largest fungal structures up to 20 h for cultures at pH 5.5 and up to 24 h for those at pH 6.5. In contrast, manual analysis showed the presence of very large structures within the first 8 h for both pH values, followed by a breakdown of these larger structures into medium-sized aggregates between 8 h and 12 h. After this breakdown, no large structures were observed for the remainder of the cultivation at either of the pH values. Thus, not only did the automated system fail to detect the breakdown of large structures, but it also incorrectly detected an increase in size when in fact the aggregate sizes were decreasing. These results clearly show that the automated extraction of morphological metrics did not provide reliable results.

In order to identify the underlying causes, the automatic segmentation of the microscopy images must be analyzed. Fig. 4.7 presents exemplary microscopy images from the batch cultivation at pH 5.5 (compare Section 4.3 and Fig. 4.3). Fig. 4.7 A shows the original microscopy image and Fig. 4.7 B the segmentation performed by the trained algorithm. Fig. 4.7 C details selected sections from the segmented images.
The enlarged image sections demonstrate that the algorithm performs very well. According to the annotation, fungal structures in the focal plane are segmented in full detail, while blurred areas are excluded. However, the dataset contains a wide range of morphologies, from small fragments to large aggregates. Since only a small fraction of large structures is in the focal plane, only small sections of these large structures are mapped. In contrast, small fragments can be fully imaged. This leads to a misrepresentation of the fungal morphology present.
These results explain the discrepancies observed between the automatically extracted morphological metrics, the scattered light data and the results of the manual morphology analysis. They highlight the necessity of improving the segmentation to account for the entire structure, regardless of its size, for accurate morphological analysis.

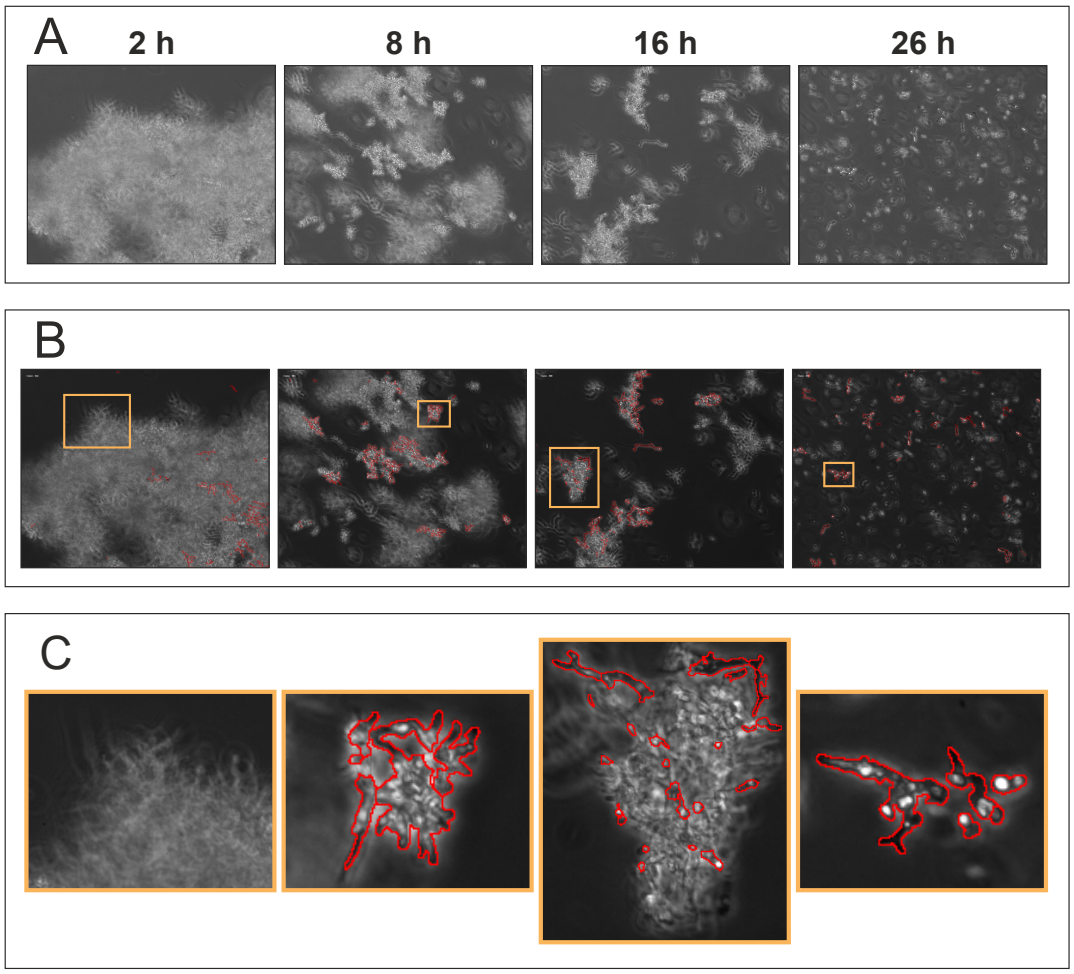

Fig. 4.7. **Automatically segmented microscopy images of an MBR batch cultivation of *T. thermophilus*.** (A) Original microscopy image, (B) automatic segmentation performed by the trained algorithm, (C) enlarged section of the segmented microscopy image. The algorithm performs as trained, segmenting fungi in focus while excluding blurred areas. However, this results in only partial mapping of large structures, leading to misrepresentation of the fungal morphology present.

4.7. Conclusion Chapter 4

This chapter investigated the morphology-productivity relationship of *T. thermophilus* using an advanced workflow integrating MBR cultivation, automated liquid handling and automated microscopy. The selected microscopy settings, specifically a 150-fold magnification combined with a dynamic dilution strategy, successfully captured mycelial aggregates and the intricate details of freely dispersed hyphae. Batch cultivation experiments showed that maintaining the pH at 5.5 results in a 2-fold increase in phytase activity and smaller fungal fragments at the end of cultivation compared to a pH of 6.5. Similarly, fed batch cultivations demonstrated that a feeding rate of $1\,\mathrm{g}\cdot(\mathrm{l}\cdot\mathrm{h})^{-1}$ at pH 5.5 leads to a 1.6-fold higher phytase activity compared to pH 6.5, accompanied by larger fungal aggregates throughout the feeding phase. These results highlight the significant impact of pH and feeding rate on *T. thermophilus* morphology and productivity.

In the broader context of this work, the integration of automated microscopy into the MBR workflow represents a major advance in optimizing bioprocess development for filamentous fungi. This combination of state-of-the-art monitoring techniques provides critical insights into the complex relationship between environmental conditions, fungal morphology and productivity that traditional cultivation methods cannot provide. These insights are critical for refining bioprocess parameters early in the development cycle. In addition, this work lays the foundation for future studies aimed at refining these methodologies and applying them to other industrially relevant organisms.
However, the study also faced limitations, particularly in the automatic segmentation of microscopy images. While the OMNIPOSE algorithm effectively identified fungi that were in focus, it did not accurately represent the full structure of larger aggregates. This was due to the deliberate decision not to annotate out-of-focus areas to ensure the reliability of the annotations. As a result, the morphological metrics automatically extracted from the images were unreliable in accurately capturing size distributions and structural transitions over time. For example, the automated metrics incorrectly detected smaller fragments as present in early cultivation, failed to capture the breakdown of larger structures between 8 h and 12 h and incorrectly indicated an increase in the size of aggregates in later stages of the process.

Future research should focus on improving the automated image analysis process, with a particular emphasis on improving the segmentation of different fungal structures. At the same time, advances in the imaging setup are required. Both com-

ponents need to be developed simultaneously, as the quality of microscopy image acquisition and the reliability of image analysis are inherently interdependent. In addition, further exploration of other environmental variables, such as temperature and nutrient concentration, could provide deeper insights into the morphology-productivity relationship of *T. thermophilus*. These advances will be key to achieving the full potential of MBR systems in combination with laboratory automation.

5. Conclusion and outlook

This thesis has successfully addressed key challenges in the field of bioprocess development for filamentous fungi, by developing and optimizing efficient small-scale cultivation protocols for *T. reesei*, *A. niger* and *T. thermophilus*. Through systematic optimization of MBR cultivation strategies, integration of laboratory automation and exploration of the intricate relationship between fungal morphology and productivity, this work presents significant advances.

Chapter 2 focused on the development and validation of robust MBR cultivation strategies for *T. reesei*. The optimized protocols included the use of an RWP, an adapted medium and a high rotational frequency of 1000 rpm. This approach demonstrated a strong correlation between scattered light intensity and biomass formation, providing a reliable tool for monitoring growth. Furthermore, the implementation of a fed batch strategy using lactose as a feed resulted in a 3-fold increase in CBH and a 5-fold increase in BGL compared to batch cultivation. These results highlight the potential of MBR workflows for efficient strain screening and early optimization of critical parameters, such as feeding rates, to improve cellulase production.
Chapter 3 extended this foundation by introducing automation into the MBR workflows for *A. niger*. Automation of the inoculation process reduced MBR downtime from 136 h to 36 h per two-week cultivation cycle, an almost 4-fold improvement, and increased cultivation throughput by 1.5-fold. These advances make the workflow more suitable for extensive strain library screening and detailed process analysis. However, the challenges encountered, such as pipetting inaccuracies and the sensitivity of *A. niger* to environmental changes underscore the importance of careful risk-benefit assessments when automating processes. Despite these challenges, the overall improvements in efficiency and reproducibility strongly support the continued integration of automation into bioprocess development.
Chapter 4 explored the complex relationship between fungal morphology and productivity for *T. thermophilus* using an advanced workflow integrating MBR cultivation with automated microscopy and image analysis. Batch cultivation experiments showed that maintaining pH 5.5 results in a 2-fold increase in phytase activity and smaller

fungal fragments at the end of cultivation compared to pH 6.5. Similarly, fed batch cultivations demonstrated that a feeding rate of 1 g·(l·h)$^{-1}$ at pH 5.5 leads to a 1.6-fold higher phytase activity compared to pH 6.5, but is accompanied by larger fungal aggregates throughout the feeding phase. These results highlight the significant influence of pH and feeding rates on morphology and enzyme production and underscore the value of integrated workflows to optimize fungal cultivation. However, this chapter has also revealed the limitations of automated image analysis in accurately capturing the structure of larger fungal aggregates, emphasizing the need for improved segmentation methods to enhance the reliability of morphological metrics.

By refining small-scale cultivation strategies and integrating automation, this work presents new opportunities for HTP screening and bioprocess optimization for filamentous fungi. The insights gained from this research, particularly regarding the relationship between morphology and productivity, underscore the critical importance of understanding and controlling morphology to optimize production processes. These findings provide a solid foundation for the development of more targeted and efficient strategies in enzyme production, which are vital to many industries.

Despite the significant contributions of this research, several limitations should be acknowledged. First, while the optimized MBR strategies and automated workflows have been shown to be effective, their application is currently limited to the specific fungi studied in this thesis. Further research is needed to determine how these methods can be adapted to other fungal species or different bioprocesses.
Moreover, while this work has provided valuable tools for optimizing bioprocesses at a small scale, it is crucial to validate these findings through successful scale-up. Small-scale conditions can mimic industrial environments, but do not fully capture the complexities of larger systems. While the scalability of MBR systems has been successfully demonstrated in numerous studies, the scalability of the specific workflows developed in this thesis has yet to be demonstrated. Challenges such as maintaining homogeneity, consistent oxygen transfer and managing shear forces must be addressed to ensure that the optimized processes work effectively at industrial scale.
In addition, although the automated workflow for *A. niger* successfully increased throughput, the environmental sensitivity of the fungus highlighted operational challenges that must be carefully managed in future automation efforts. These findings emphasize the complexity of working with *A. niger*, but also demonstrate the potential of automation to effectively address such difficulties. Moving forward, it will be crucial to critically evaluate how these challenges can be addressed in order to refine

the workflow to ensure that it is both robust and user-friendly. Ultimately, this work highlights the specific requirements of automating processes for *A. niger* and opens up new possibilities for further optimizing automation in similar cases.
This work is an important first step in understanding the relationship between fungal morphology and productivity. However, this area remains complex and largely unexplored and future research is needed to develop a more comprehensive understanding of these dynamics.
Furthermore, the work presented in Chapter 4 encountered limitations in the automatic segmentation of microscopy images. Although the algorithm was effective at segmenting fungi that were in focus, it failed to accurately represent the full structure of larger aggregates. This was due to the deliberate decision not to annotate out-of-focus areas. As a result, the morphological metrics automatically extracted from these images were unreliable, highlighting the need for improved image processing techniques to achieve more accurate and consistent analysis.

The foundation laid by this thesis opens several promising avenues for future research in the field of bioprocess development for filamentous fungi:

I. **Exploration of additional environmental variables.**
   This work has focused primarily on the effects of pH and feeding rates on fungal morphology and productivity. However, other environmental factors such as temperature, DO and nutrient composition also play an important role in fungal growth and product formation. Future studies should systematically investigate these variables to develop a more comprehensive understanding of how they interact in influencing fungal responses.

II. **Expansion to other fungal species and strains.**
   The presented research focused on *T. reesei*, *A. niger* and *T. thermophilus*. However, the developed methods could be applied to a wider range of filamentous fungi. Extending this research to other industrially relevant fungi, such as *Aspergillus terreus* or *Penicillium chrysogenum*, could provide further insights into the generalizability of the findings and help to optimize bioprocesses for these and other species.

III. **Refinement of automated image analysis.**
   The automated image analysis workflow presented in this thesis has provided valuable insights into fungal morphology. However, several challenges remain, particularly in accurately representing the complete structure of larger fungal

aggregates. Future research should aim to refine the annotation process to better capture the complexity of filamentous fungal structures.
One approach could involve creating distinct annotation labels for different aspects of the fungal biomass. For example, one annotation label could be dedicated to meticulously tracking hyphal structures of in-focus regions, ensuring accurate representation of fine details. At the same time, a second annotation label could be used for larger fungal biomass structures, whether in or out of focus, to capture the entire fungal surface. By combining these annotation labels, the workflow could address a wide range of applications. For example, it would allow the size of fungal structures to be accurately tracked, while also allowing hyphal tips to be counted over time, a critical parameter in assessing fungal morphology. Overall, improving the accuracy and reliability of these image analysis tools will enable more precise monitoring and control of fungal morphology, which is essential for optimizing productivity in industrial bioprocesses.

Beyond these specific research directions, future efforts should focus on integrating advanced computational methods and the Design-Build-Test-Learn (DBTL) principle into fungal bioprocess development. As bioprocesses become more complex and data-rich, there is a growing need and opportunity for advanced computational models that can simulate and predict fungal behaviour under different conditions. These models will help to guide experimental design, reduce the need for extensive trial-and-error testing and to identify optimal process conditions and high-performing strains more efficiently. By refining small-scale cultivation and laboratory automation techniques, this work plays a critical role in bridging the gap to ensure that these advanced computational methods and autonomous DBTL workflows can be effectively applied to fungal systems.

In conclusion, this research has highlighted the immense potential of applying advanced MBR cultivation strategies and integrating automation and morphology analysis into bioprocess development for filamentous fungi. This work has provided valuable insights and practical tools that will aid in the further optimization of bioprocesses while deepening our understanding of the morphology-productivity relationship.
The findings presented in this thesis not only enhance our ability to leverage fungal systems for enzyme production, but also open new avenues for innovation in various industries that rely on these versatile microorganisms. While the opportunities ahead are both promising and complex, the knowledge and tools gained from this thesis

will be instrumental in advancing the application of filamentous fungi in industrial bioprocesses.

6. Material and methods

6.1. Devices, software and consumables

Tab. 6.1 lists the specific hardware used for this study. Common equipment for which the model is not relevant is not listed. The software used for experiments and data analysis is listed in Tab. 6.2 and consumables in Tab. 6.3.

Tab. 6.1. List of devices used

Device	Specification	Manufacturer
Camera	DCC1545M-GL	Thorlabs, Newton, US
Microbioreactor	BioLector II	Beckman Coulter, Brea, US
	BioLector Pro	Beckman Coulter, Brea, US
Microplate reader	Infinite 200 PRO	Tecan, Männedorf, CH
Microscope	Eclipse Ti2	Nikon Europe, Amstelveen, NL
Robotics system	Freedom EVO 200	Tecan, Männedorf, CH
	Liquid handler	Tecan, Männedorf, CH
	Robotic manipulator	Tecan, Männedorf, CH

Tab. 6.2. List of software used

Software	Application	Developer
BioLection V.3.17.0-testing	MBR data visualization	Beckman Coulter, Brea, US
Bletl 1.3.1	MBR data processing	see [168, 169]
CorelDRAW 2018	Image processing	Corel Corp., Ottawa, CA
Freedom EVOware 2.7	Robotics system handling	Tecan, Männedorf, CH
Matplotlib 3.5.1	Data analytics	see [170, 171]
Numpy 1.21.5	Data analytics	see [172]
Pandas 1.4.1	Data analytics	see [173, 174]

Software	Application	Developer
Python 3.9.7	Data analytics	Python Software Foundation
Seaborn 0.11.2	Data analytics	see [175, 176]
ThorCam	Image acquisition	Thorlabs, Newton, US

Tab. 6.3. List of consumables used

Consumable	Specification	Manufacturer
Centrifuge tube filter	Costar spin-x, 0.22 µm, nylon membrane	Sigma-Aldrich Steinheim, DE
Flow chamber	250 µm height (#80167)	ibidi Gräfelfing, DE
Microtiter plate	MTP-48-B MTP-48-BOH 1 MTP-MF32C-BOH 1 MTP-R48-BOH 1 MTP-RMF32C-BOH 1 Square well (#701354)	Beckman Coulter Brea, US Brand, Wertheim, DE
Pipet tips, manual	1.5 mm orifice (#17015068)	Mettler-Toledo, Columbus, US
Pipet tips, robotics system	0.8 mm orifice (#10760644)	Tecan, Männedorf, CH
Sealing foil	F-GP-10 F-GPRS48-10 F-RS48-10 F-GPRSMF32-1 F-RSMF32-1	Beckman Coulter, Brea, US
Syringe filter	0.22 µm PES	Sigma-Aldrich, Steinheim, DE

6.2. Microorganisms and strains

Strains used for this study are listed in Tab. 6.4.

Tab. 6.4. List of strains used

Strain	Specification	Source	Reference
T. reesei	QM6a (WT)	IFPEN, Rueil-Malmaison, FR	[45]
	RutC30	IFPEN, Rueil-Malmaison, FR	[45]
	RutC30 TR3158	IFPEN, Rueil-Malmaison, FR	[46]
A. niger	ANIp7-MCS-gfp2	TU Braunschweig	[55]
T. thermophilus	-	BASF SE, Ludwigshafen, DE	-

6.3. Cultivation media, reagents and buffers

Potato dextrose medium was prepared from 24 g·l^{-1} potato dextrose broth. The potato dextrose agar (PDA) was prepared from 24 g·l^{-1} potato dextrose broth and 15 g·l^{-1} agar. Both solutions were sterilized by autoclaving at 121 °C for 20 minutes.

6.3.1. Cultivation media for *T. reesei*

For MBR cultivations, two different media were used. The first one, Jourdier Medium, was prepared on the basis of the medium described by Jourdier et al. [157]. This medium consisted of a trace element solution comprising the following components: 0.4 g·l^{-1} H_3BO_3, 9 g·l^{-1} $Co(NO_3)_2 \cdot 6\ H_2O$, 3 g·l^{-1} $CuSO_4 \cdot 5\ H_2O$, 30 g·l^{-1} $FeSO_4 \cdot 7\ H_2O$, 6.4 g·l^{-1} $MnSO_4 \cdot H_2O$, 14.3 g·l^{-1} 85 % H_3PO_4(aq), 1 g·l^{-1} $Na_2MoO_4 \cdot 2\ H_2O$ and 8.4 g·l^{-1} $ZnSO_4 \cdot 7\ H_2O$. To prepare the final Jourdier Medium, 1 ml·l^{-1} trace element solution was combined with the following components: 5.6 g·l^{-1} $(NH_4)_2SO_4$, 6 g·l^{-1} 1,2,3,4-butanetetracarboxylic acid, 0.15 g·l^{-1} $CaCl_2 \cdot 2\ H_2O$, 1.5 g·l^{-1} cornsteep solids, 4.4 g·l^{-1} K_2HPO_4, 22 g·l^{-1} glucose monohydrate, 0.3 g·l^{-1} $MgSO_4 \cdot 7\ H_2O$ and 4 g·l^{-1} KOH. The pH was adjusted to 6.0 by using NaOH and the completed medium was subsequently autoclaved at 110 °C for 30 minutes.

The second medium used for MBR cultivations, adapted medium, had the same chemical composition as the Jourdier Medium, with two exceptions: KOH was excluded and $20 \cdot 10^{-3}$ g·l^{-1} Penicillin-G sodium salt was included. However, in the adapted medium, the chemicals were prepared as individual stocks, with each pH adjusted individually, and sterilized separately. The stocks used were as follows: buffer stock (60 g·l^{-1} 1,2,3,4-butanetetracarboxylic acid), cornsteep solid suspension (1.5 g·l^{-1} cornsteep solids), penicillin (20 g·l^{-1} Penicillin-G sodium salt), salt stock

(84 g·l^{-1} $(NH_4)_2SO_4$, 2.25 g·l^{-1} $CaCl_2 \cdot 2\ H_2O$, 66 g·l^{-1} K_2HPO_4, 4.5 g·l^{-1} $MgSO_4 \cdot 7\ H_2O$) and trace element solution (unaltered). Furthermore, for batch and fed-batch experiments, a 400 g·l^{-1} glucose solution was used to achieve a final concentration of 20 g·l^{-1} and 5 g·l^{-1}, respectively. For fed-batch experiments, a 150 g·l^{-1} lactose stock solution was additionally used as the feed. Sterilization was either done by autoclaving at 121 ℃ for 20 minutes (cornsteep solid suspension, salt stock, glucose stock, lactose stock) or by sterile filtration using a 0.2 µm polyethersulfone (PES) membrane (buffer stock, penicillin, trace element solution). Immediately before a cultivation, the stocks were combined to form the final medium.

6.3.2. Cultivation media for *A. niger*

The following stocks were individually prepared and sterilized: salts pH 3.8 (132 g·l^{-1} $(NH_4)_2SO_4$, 50 g·l^{-1} KH_2PO_4, 4 g·l^{-1} $MgSO_4 \cdot 7\ H_2O$, 2 g·l^{-1} $CaCl_2 \cdot 2\ H_2O$), trace elements (5 g·l^{-1} citric acid, 5 g·l^{-1} $ZnSO_4 \cdot 7\ H_2O$, 1 g·l^{-1} $(NH_4)_2Fe(SO_4)_2 \cdot 6\ H_2O$, 0.16 g·l^{-1} $CuSO_4$, 0.5 g·l^{-1} $MnCl_2 \cdot 4\ H_2O$, 0.05 g·l^{-1} H_3BO_3, 0.037 g·l^{-1} $MnSO_4 \cdot H_2O$, 0.05 g·l^{-1} $Na_2MoO_4 \cdot 2\ H_2O$), xylose (400 g·l^{-1} xylose), maltose (400 g·l^{-1} maltose). Sterilization was either done by autoclaving at 121 ℃ for 20 minutes (salts, xylose, maltose) or by sterile filtration using a 0.2 µm PES membrane (trace elements).

Vogel pre-culture medium was freshly prepared immediately before cultivation by combining the following volumes of stocks: 50 ml·l^{-1} salts pH 3.8, 1 ml·l^{-1} trace elements and 25 ml·l^{-1} xylose (equals a final concentration of 10 g·l^{-1} xylose). Additionally, 1 ml·l^{-1} cryo spore suspension and the respective amount of demineralized water was added.
Vogel main culture medium was prepared accordingly using the following volumes of stocks: 50 ml·l^{-1} salts pH 3.8, 1 ml·l^{-1} trace elements and 50 ml·l^{-1} maltose (equals a final concentration of 20 g·l^{-1} maltose). Additionally, 100 ml·l^{-1} pre-culture and the respective amount of demineralized water was added. For cultivations with reduced inoculum, the difference was supplemented with demineralized water.

6.3.3. Cultivation media for *T. thermophilus*

The following stocks were individually prepared and sterilized: salts pH 5.5 (300 g·l^{-1} $NaNO_3$, 26 g·l^{-1} KCl, 76 g·l^{-1} KH_2PO_4), glucose (50 % (m·m^{-1}) glucose), casamino acids (100 g·l^{-1} casamino acids), magnesium sulfate (246.48 g·l^{-1} $MgSO_4$ ·7 H_2O), trace elements pH 6.0 (50 g·l^{-1} EDTA, 20.05 g·l^{-1} $ZnSO_4$·7 H_2O, 3.92 g·l^{-1} $MnSO_4$·H_2O, 4.56 g·l^{-1} $FeSO_4$·7 H_2O, 1.46 g·l^{-1} $CuSO_4$·5 H_2O, 1.37 g·l^{-1} Na_2MoO_4 ·2 H_2O), antibiotics (20 g·l^{-1} penicillin, 50 g·l^{-1} streptomycin), uridine (244.20 g·l^{-1} uridine), biotin (0.06 g·l^{-1} biotin), MES pH 6.0 (213.25 g·l^{-1} MES·H_2O). MES pH 6.75 (213.25 g·l^{-1} MES·H_2O). Sterilization was either done by autoclaving at 121 °C for 20 minutes (glucose) or by sterile filtration using a 0.2 µm PES membrane (salts, casamino acids, magnesium sulfate, trace elements, antibiotics, uridine, biotin, MES).

Agar plates pH 6.5 were prepared using a basal medium (16 g·l^{-1} agar, 230 g·l^{-1} saccharose, 5 g·l^{-1} yeast extract, 1.12 g·l^{-1} uracil), which was completed after autoclaving at 121 °C for 20 minutes with the following volumes of stocks: 20 ml·l^{-1} salts, 20 ml·l^{-1} glucose, 10 ml·l^{-1} casamino acids, 2 ml·l^{-1} magnesium sulfate, 1 ml·l^{-1} trace elements, 1 ml·l^{-1} antibiotics, 10 ml·l^{-1} uridine.
Pre-culture medium consisted of a basal medium (4.66 g·l^{-1} $(NH_4)_2SO_4$, 0.49 g·l^{-1} $MgSO_4$·7 H_2O, 1.22 g·l^{-1} K_2SO_4, 0.47 g·l^{-1} $CaSO_4$·2 H_2O, 1.76 g·l^{-1} KH_2PO_4), which was completed after autoclaving at 121 °C for 20 minutes with the following volumes of stocks: 20 g·l^{-1} glucose, 10 ml·l^{-1} casamino acids, 1 ml·l^{-1} trace elements, 1 ml·l^{-1} antibiotics, 0.1 ml·l^{-1} biotin, 100 g·l^{-1} MES pH 6.0. Additionally, the respective amount of sterile demineralized water was added.
Main culture medium was prepared from a basal medium (6.99 g·l^{-1} $(NH_4)_2SO_4$, 0.49 g·l^{-1} $MgSO_4$·7 H_2O, 1.22 g·l^{-1} K_2SO_4, 0.47 g·l^{-1} $CaSO_4$·2 H_2O, 1.76 g·l^{-1} KH_2PO_4), to which the following volumes of stocks were added after autoclaving at 121 °C for 20 minutes: 1 ml·l^{-1} trace elements, 1 ml·l^{-1} antibiotics, 0.1 ml·l^{-1} biotin. Additionally, for batch experiments, 194 g·l^{-1} MES pH 6.75, 40 g·l^{-1} glucose (equals a final concentration of 20 g·l^{-1} glucose) and 300 ml·l^{-1} pre-culture were added. For fed batch experiments, 10 g·l^{-1} glucose (equals a final concentration of 5 g·l^{-1} glucose) and 300 ml·l^{-1} pre-culture were added. Finally, to all media, the respective amount of sterile demineralized water was added.

6.3.4. Reagents and buffers for cellulase assay

For the cellulase assay, the following solutions were prepared: citrate buffer pH 4.8 (23 mM citric acid monohydrate, 27 mM tri-sodium citrate dihydrate), 4-nitrophenyl-β-D-lactopyranoside (pNPL) solution (6.5 mM pNPL dissolved in citrate buffer), 4-nitrophenyl-β-D-glucopyranoside (pNPG) solution (4.98 mM pNPG dissolved in citrate buffer), 4-nitrophenol (pNP) solution (10 mM pNP dissolved in citrate buffer) and sodium carbonate solution (189 mM sodium carbonate).

6.3.5. Reagents and buffer for phytase assay

For the phytase assay, the following solutions were prepared: acetate buffer pH 4.5 (5.85 $g \cdot l^{-1}$ $CH_3COONa \cdot 3\ H_2O$, 3.24 $ml \cdot l^{-1}$ acetic acid 17.6 M), phytic acid solution pH 4.5 (4.83 $g \cdot l^{-1}$ phytic acid sodium salt hydrate dissolved in acetate buffer) and coloring solution (0.39 $g \cdot l^{-1}$ NH_4VO_3, 16.67 $g \cdot l^{-1}$ $(NH_4)_2MoO_4 \cdot 3\ H_2O$, 1.97 $ml \cdot l^{-1}$ 25 % NH_4OH, 119.25 $ml \cdot l^{-1}$ 65 % HNO_3).

6.4. Cryo preservation

For the generation of main cell banks for *T. reesei* QM6a (WT) and RutC30, a spore suspension was spread on PDA plates and incubated at 30 °C for 15-20 days. After complete sporulation, the spores were harvested with a 0.9 % ($v \cdot v^{-1}$) NaCl and 20 % ($v \cdot v^{-1}$) glycerol solution. Subsequent filtration with a wool filter removed loose mycelium. The spore suspension was adjusted to 10^8 $spores \cdot ml^{-1}$, aliquoted and stored at -80 °C until further use. Working cell banks were prepared from the master cell bank accordingly.
For *T. reesei* RutC30 TR3158, 50 ml of potato dextrose medium in a 250 ml shake flask was inoculated with a spore solution and incubated at 30 °C and 250 rpm for 2 days. After shake flask cultivation, 2 ml of the culture suspension was plated on PDA and incubated for 15-20 days at 30 °C. The subsequent spore harvest was carried out as described above for QM6a and RutC30.

For spore generation of *A. niger*, a spore suspension was spread on PDA plates and incubated at 37 °C for 5-7 days. The subsequent spore harvest was carried out as

described above for *T. reesei*.
Cryo aliquots for *T. thermophilus* were obtained by cultivation in a 2 l Erlenmeyer flask with a filling volume of 175 ml, which was incubated for 72 h at 37 °C, 80 % humidity, 900 rpm, 3 mm shaking diameter and 30 % inoculum from a pre-existing cryo. After cultivation, the cell suspension was cooled on ice water and 10 % glycerin was added. It was then split into 1 ml aliquots and stored as cryo spore suspension at -80 °C until further use.

6.5. Microbioreactor cultivation

All MBR cultivations were conducted in a BioLector II or Pro (Beckman Coulter, Brea, US). These experiments used specialized MTPs with either 48 wells for batch cultivation or 32 wells for fed batch cultivation. Each plate was sealed with a gas-permeable sealing foil to allow adequate gas exchange while maintaining sterility. Detailed specifications of the plate types and sealing foils used are given in Tab. 6.3. During cultivation, biomass concentration was monitored by measuring scattered light, while DO and pH were assessed non-invasively using built-in optodes where available. Measurements were recorded at 10-minute intervals throughout the cultivation.

6.5.1. Pre-culture procedure

For each *A. niger* cultivation run, Vogel pre-culture medium with 10 g·l^{-1} xylose (see Subsection 6.3.2) was inoculated with 10^5 spores·ml^{-1}. Then, 1 ml of inoculated pre-culture medium was transferred into every well of an FP. The plate was sealed with a gas permeable sealing foil and incubated for 44 h at 37 °C, with $\geq$85 % humidity, 21 %oxygen content of the inlet air (O_2) and 1300 rpm shaking at a 3 mm diameter. After incubation, the contents of all wells were harvested and combined to form the pre-culture.

For each *T. thermophilus* cultivation run, 100 µl cryo spore suspension was spread on an agar plate (see Subsection 6.3.3) and incubated for seven days at 37 °C until a loose white layer was visible. Then, 1 ml of pre-culture medium with 10 g·l^{-1} glucose (see Subsection 6.3.3) was transferred into every well of a 96-well square deep well plate. Using a pipet tip with a 1.5 mm orifice, a piece of overgrown agar was punched

out and added to each well. The plate was sealed with a gas permeable sealing foil and incubated for 72 h at 37 °C, with 80 % humidity and 900 rpm shaking at a 3 mm diameter. After incubation, the culture suspension of all wells were harvested and combined to form the pre-culture.

6.5.2. Main culture procedure

General MBR main culture conditions are are given in Tab. 6.5. Further cultivation conditions and media used were as follows. For *T. reesei* batch cultivations, either Jourdier medium or adapted medium containing 20 g·l^{-1} glucose was used, unless otherwise specified (see Subsection 6.3.1). For fed-batch cultivations, 2.5 g·l^{-1} glucose was used in the initial batch phase, with an additional feed of 16.6 g·l^{-1} lactose based on the initial volume. The choice of lactose concentration was made to ensure carbon-equimolarity to 15 g·l^{-1} glucose, thus providing comparable amounts of carbon sources between batch and fed-batch mode. The pH was not controlled.
For *A. niger*, Vogel main culture medium with 20 g·l^{-1} maltose was used (see Subsection 6.3.2). The pH was not controlled. For *T. thermophilus* batch experiments, main culture medium with 20 g·l^{-1} glucose was used (see Subsection 6.3.3). For fed batch experiments, main culture medium with 5 g·l^{-1} glucose was used in the initial batch phase, with an additional feed of 15 g·l^{-1} glucose based on the initial volume. In batch experiments, the O_2 was maintained at 35 %. In fed batch cultivations, the O_2 was maintained at 21 %, which was increased to 35 % during the feeding phase. In both batch and fed batch experiments, pH-setpoints were either pH 5.5 or 6.5, as detailed in the respective figures. The pH was adjusted using 3 M KOH.

Tab. 6.5. MBR cultivation conditions

Condition	***T. reesei***	***A. niger***	***T. thermophilus***
Plate type	FP or RWP	FP	FP
Rotational frequency	1000 or 1200 rpm	1400 rpm	1400 rpm
Shaking diameter	3 mm	3 mm	3 mm
Well filling volume	1 ml	0.8 ml	0.8 ml
Humidity	$\geq$85 %	$\geq$85 %	$\geq$85 %
Oxygen	21 or 35 %	35 %	21 or 35 %
Temperature	30 °C	37 °C	37 °C
Inoculum	10^5 spores·ml^{-1}	10 % pre-culture	30 % pre-culture

6.6. Automated liquid handling

A custom-configured Tecan Freedom EVO 200 (Tecan, Männedorf, CH) was used for automated biomass handling, automated microscopic analysis and product assays. Automated biomass handling included *A. niger* inoculation procedures and *T. thermophilus* main culture sampling, sample processing and microscopy. These processes required the establishment of liquid classes with tailored liquid handling parameters for managing culture suspensions. Liquid handling parameters refer to the specific settings of the robotic pipetting system to account for the unique physical and chemical characteristics of the samples. These settings are essential to ensure that the pipetting process is accurate, reproducible and efficient. Adjustable specifications include, for example, fluid aspiration and dispense speeds, the delay after aspiration and dispense and the speed at which the last drop breaks off the needle. The liquid classes used for *A. niger* inoculation procedures are detailed in Tabs. 3.1 and A.1. The liquid class used for *T. thermophilus* main culture sampling and sample processing is detailed in Tab. A.2. Details on automated microscopy of *T. thermophilus* can be found in Section 6.8.

The automated product analysis assays performed in this study included a cellulase assay for *T. reesei* cultivation samples and a phytase assay for *T. thermophilus* cultivation samples. Detailed descriptions of these assays are available in Subsections 6.7.2 and 6.7.3.

6.7. Microbioreactor sample processing and product analysis

6.7.1. Cell dry weight estimation and correlation with scattered light

The CDW was estimated using a pre-weighed centrifuge tube filter with a 0.22 µm nylon membrane. The filter was loaded with a total of 0.7 ml cell suspension in two steps and centrifuged at 13,000 rcf for three minutes. The retentate was washed twice with 0.5 ml 0.9 % NaCl. Washed filters were dried at 80 °C for 24 h and stored in a desiccator for 1 h before weighing. Then, the mass difference between the filter

containing the retentate and the empty filter was calculated. The difference in mass divided by the volume of cell suspension applied yielded the CDW.

To asses the correlation between CDW and scattered light, cultivations were conducted as specified in Section 6.5. During cultivation, main culture samples of 0.7 ml were collected as biological triplicates at various times during the steep increase in scattered light. Then, CDW and scattered light of each sample were determined. Subsequently, the CDW of each sample was plotted over its scattered light at the time of sampling. Finally, a linear regression was performed.

6.7.2. Cellulase activity measurement

The volumetric activity of two classes of cellulolytic enzymes, CBH and BGL, was determined by an automated optical assay according to a protocol adapted from Jourdier et al. [177]. CBH activity was determined vicariously by Cel7A (CBH I), which converts pNPL to β-D-lactopyranoside. In contrast, BGL activity was determined directly by the conversion of pNPG to β-D-glycopyranoside and pNP.

Prior to analysis, cultivation samples were filtered through a 0.22 µm PES membrane. The permeate was stored at 4 °C for a maximum of 7 days and, if necessary, diluted in citrate buffer. For CBH activity determination, 50 µl of pNPL solution was mixed with 50 µl of sample. For BGL activity determination, the ratio was 90 µl pNPG solution to 10 µl sample. Both mixtures were incubated at 50 °C for 30 min. Then 100 µl sodium carbonate solution was added and pNP release was detected by measuring the absorbance at 410 nm. Cellulase activity was subsequently calculated using a pNP calibration curve.
To generate the calibration line, different concentrations of pNP (0.02–5 mM) in citrate buffer were mixed with equal volumes of sodium carbonate solution. Then, the absorbance was measured at 410 nm. Linear regression of this data provided the slope and intercept of the calibration curve. These values were used to calculate the concentration of pNP released from the samples, as shown in Eq. 6.1. The determined concentration of pNP released enabled the calculation of the volumetric enzyme activity, defined as the amount of enzyme required to release 1 µmol of pNP per minute (Eqs. 6.2 and 6.3).

$$\text{concentration pNP released} \left[\frac{\mu\text{mol}}{\text{l}}\right] = \frac{\text{absorbance A [a.u.] - intercept m [a.u.]}}{\text{slope n} \left[\frac{\text{l}}{\mu\text{mol}}\right]} \tag{6.1}$$

$$\text{activity [U]} = \frac{\text{released pNP [µmol]}}{\text{t [min]}} \tag{6.2}$$

$$\text{volumetric activity} \left[\frac{\text{U}}{\text{l}}\right] = \frac{\text{concentration pNP released} \left[\frac{\mu\text{mol}}{\text{l}}\right] \cdot \text{dilution}}{\text{t [min]}} \tag{6.3}$$

6.7.3. Phytase activity measurement

The phytase activity of cultivation samples was determined by an automated optical assay adapted from the vanadate-molybdate method described by Kitson and Mellon [178]. The activity was measured in Phytase Units (FTUs). FTU is the amount of enzyme that releases 1 µmol of ortho-phosphate from sodium phytate per minute at pH 5.5 and 37 °C. Prior to analysis, samples were filtered through a 0.22 µm PES membrane and diluted in acetate buffer, if necessary.
For the assay, 180 µl phytic acid solution was mixed with 20 µl of the processed sample and incubated at 30 °C. After 3, 6, 9 and 12 min, 30 µl of the mixture was sampled and combined with 90 µl coloring solution. Following incubation for 15 min at room temperature, the absorption at 415 nm was measured.
Phytase standards ranging from 0 to 25 FTU·ml^{-1} were included in each assay and processed in the same manner as the cultivation samples. After photometric measurement, the absorption at 415 nm for both standards and samples was plotted against the assay incubation times (3, 6, 9 and 12 min) and a linear regression was performed. The slopes of the standards were then plotted against their concentrations and a second linear regression was performed. This calibration curve was used to determine the volumetric activity of the samples.

6.7.4. Space-time yield calculation

The STY was calculated by dividing the difference in activity at two points by the time difference between the same time points, according to Eq. 6.4.

$$\text{space-time yield [FTU·(ml·h)}^{-1}\text{]} = \frac{\text{activity}_{t_2}\ \text{[FTU·ml}^{-1}\text{]} - \text{activity}_{t_1}\ \text{[FTU·ml}^{-1}\text{]}}{t_2\ \text{[h]} - t_1\ \text{[h]}} \tag{6.4}$$

6.8. Automated microscopy

The complete workflow for automated microscopy involved sampling from the MBR, followed by sample dilution in 0.9 % NaCl based on the elapsed process time. After dilution, the liquid handler pipetted 250 µl of ethanol into the injection station at a dispense speed of 25 µl·s^{-1} to avoid air bubbles remaining in the chamber during sample addition. Then, 800 µl of the samples was pipetted into the injection station at a dispense speed of 3 µl·s^{-1}. The cell suspension was then pumped through the chamber at a flow rate of 3 µl·s^{-1}, during which 15 to 100 microscopy images were captured. The microscopy settings included a 150-fold magnification and phase contrast Ph1. After each sample, the chamber was rinsed with 950 µl of water, followed by a rinse with 950 µl of ethanol and a final rinse with 950 µl water, all at a flow rate of 25 µl·s^{-1}. After each procedure, samples and fluids were discarded.

6.9. Data processing and display

Data analysis and visualization were conducted using python 3.9.7, bletl 1.3.1 [168, 169], matplotlib 3.5.1 [170, 171], numpy 1.21.5 [172], pandas 1.4.1 [173, 174] and seaborn 0.11.2 [175, 176].
Cultivation plots show the mean and standard deviation for the replicates of each condition as a continuous line with a shaded area representing the standard deviation. Alternatively, the scattered light of single biological replicates is shown as a continuous line. Measurements from sampled wells were excluded from figures and calculations after sampling. Before plotting, the lowest scattered light value from

all replicates of one condition at cycle 3 was used to blank values. The scattered light measurements of each replicate were compared to this baseline and the difference was subtracted from the values. If applicable, scattered light measurements were additionally adjusted for dilution due to pH control or feeding by multiplying by the ratio of current to initial well volume. Phytase activity measurements (see Subsection 6.7.3) were volume-corrected accordingly.

References

[1] D. Moore and S. Chiu. “Fungal products as food”. In: *Bio-Exploitation of Filamentous Fungi*. Ed. by S. Pointing and K. Hyde. Fungal Diversity Press: Hong Kong, 2001, pp. 223–251.

[2] A. Fasim, V. S. More, and S. S. More. “Large-scale production of enzymes for biotechnology uses”. In: *Current Opinion in Biotechnology* 69 (2021), pp. 68–76. DOI: 10.1016/j.copbio.2020.12.002.

[3] B. Amer and E. E. K. Baidoo. “Omics-driven biotechnology for industrial applications”. In: *Frontiers in Bioengineering and Biotechnology* 9 (2021), p. 613307. DOI: 10.3389/fbioe.2021.613307.

[4] J. Steensels, B. Gallone, K. Voordeckers, and K. Verstrepen. “Domestication of industrial microbes”. In: *Current Biology* 29 (2019), R381–R393. DOI: 10.1016/j.cub.2019.04.025.

[5] P. J. Punt, N. van Biezen, A. Conesa, A. Albers, J. Mangnus, and C. van den Hondel. “Filamentous fungi as cell factories for heterologous protein production”. In: *Trends in Biotechnology* 20 (2002), pp. 200–206. DOI: 10.1016/S0167-7799(02)01933-9.

[6] T. Cocquyt. “Positioning van Leeuwenhoek’s microscopes in 17th-century microscopic practice”. In: *FEMS Microbiology Letters* 369 (2022), pp. 1–7. DOI: 10.1093/femsle/fnac031.

[7] T. C. Cairns, C. Nai, and V. Meyer. “How a fungus shapes biotechnology: 100 years of *Aspergillus niger* research”. In: *Fungal Biology and Biotechnology* 5 (2018), p. 13. DOI: 10.1186/s40694-018-0054-5.

[8] K. Ereky. *Biotechnologie der Fleisch-, Fett-, und Milcherzeugung im landwirtschaftlichen Grossbetriebe: für naturwissenschaftlich gebildete Landwirte verfasst*. Berlin, DE: P. Parey, 1919.

[9] M. Papagianni. “Advances in citric acid fermentation by *Aspergillus niger*: biochemical aspects, membrane transport and modeling”. In: *Biotechnology Advances* 25 (2007), pp. 244–263. DOI: 10.1016/j.biotechadv.2007.01.002.

[10] A. C. S. N. H. C. Landmarks. *Penicillin production through deep-tank fermentation*. URL: http://www.acs.org/content/acs/en/education/whatischemistry/landmarks/penicillin.html (visited on 07/26/2024).

[11] *Enzymes market size, share, trends & growth report, 2030*. URL: https://www.grandviewresearch.com/industry-analysis/enzymes-industry (visited on 07/07/2023).

[12] *Global enzymes market size, share, growth report [2027]*. URL: https://www.marketsandmarkets.com/Market-Reports/enzyme-market-46202020.html (visited on 07/07/2023).

[13] *Enzymes market size, growth, share, trends, report 2022-2030*. URL: https://www.precedenceresearch.com/enzymes-market (visited on 07/07/2023).

[14] H. El-Gendi, A. K. Saleh, R. Badierah, E. M. Redwan, Y. A. El-Maradny, and E. M. El-Fakharany. “A comprehensive insight into fungal enzymes: structure, classification, and their role in mankind’s challenges”. In: *Journal of Fungi* 8 (2022). DOI: 10.3390/jof8010023.

[15] H. A. B. Wösten. “Filamentous fungi for the production of enzymes, chemicals and materials”. In: *Current Opinion in Biotechnology* 59 (2019), pp. 65–70. DOI: 10.1016/j.copbio.2019.02.010.

[16] V. Meyer. “Metabolic engineering of filamentous fungi”. In: *Metabolic Engineering*. Ed. by S. Y. Lee, J. Nielsen, and G. Stephanopoulos. Vol. 13b. Weinheim, DE: WILEY-VCH GmbH, 2021, pp. 765–801.

[17] V. Meyer, E. Y. Basenko, J. P. Benz, G. H. Braus, M. X. Caddick, M. Csukai, R. P. de Vries, D. Endy, J. C. Frisvad, N. Gunde-Cimerman, T. Haarmann, Y. Hadar, K. Hansen, R. I. Johnson, N. P. Keller, N. Kraševec, U. H. Mortensen, R. Perez, A. F. J. Ram, E. Record, P. Ross, V. Shapaval, C. Steiniger, H. van den Brink, J. van Munster, O. Yarden, and H. A. B. Wösten. “Growing a circular economy with fungal biotechnology: a white paper”. In: *Fungal Biology and Biotechnology* 7 (2020), p. 5. DOI: 10.1186/s40694-020-00095-z.

[18] V. Meyer, M. R. Andersen, A. A. Brakhage, G. H. Braus, M. X. Caddick, T. C. Cairns, R. P. de Vries, T. Haarmann, K. Hansen, C. Hertz-Fowler, S. Krappmann, U. H. Mortensen, M. A. Peñalva, A. F. J. Ram, and R. M. Head. “Current challenges of research on filamentous fungi in relation to human welfare and a sustainable bio-economy: a white paper”. In: *Fungal Biology and Biotechnology* 3 (2016), p. 6. DOI: 10.1186/s40694-016-0024-8.

[19] V. Meyer. “Genetic engineering of filamentous fungi - progress, obstacles and future trends”. In: *Biotechnology Advances* 26 (2008), pp. 177–185. DOI: 10.1016/j.biotechadv.2007.12.001.

[20] S. Schmideder, L. Barthel, H. Müller, V. Meyer, and H. Briesen. “From three-dimensional morphology to effective diffusivity in filamentous fungal pellets”. In: *Biotechnology and Bioengineering* 116 (2019), pp. 3360–3371. DOI: 10.1002/bit.27166.

[21] L. Veiter, V. Rajamanickam, and C. Herwig. “The filamentous fungal pellet-relationship between morphology and productivity”. In: *Applied Microbiology and Biotechnology* 102 (2018), pp. 2997–3006. DOI: 10.1007/s00253-018-8818-7.

[22] R. Krull, T. Wucherpfennig, M. Esfandabadi, R. Walisko, G. Melzer, D. Hempel, I. Kampen, A. Kwade, and C. Wittmann. “Characterization and control of fungal morphology for improved production performance in biotechnology”. In: *Journal of Biotechnology* 163 (2013), pp. 112–123. DOI: 10.1016/j.jbiotec.2012.06.024.

[23] O. Etxebeste and E. A. Espeso. “Neurons show the path: tip-to-nucleus communication in filamentous fungal development and pathogenesis”. In: *FEMS Microbiology Reviews* 40 (2016), pp. 610–624. DOI: 10.1093/femsre/fuw021.

[24] M. Whiteway and C. Bachewich. “Fungal genetics”. In: *Fungi*. Ed. by K. Kavanagh. Hoboken, US: John Wiley & Sons, Inc., 2017, pp. 37–66.

[25] T. C. Cairns, X. Zheng, P. Zheng, J. Sun, and V. Meyer. “Moulding the mould: understanding and reprogramming filamentous fungal growth and morphogenesis for next generation cell factories”. In: *Biotechnology for Biofuels* 12 (2019), p. 77. DOI: 10.1186/s13068-019-1400-4.

[26] A. Ahamed and P. Vermette. “Effect of culture medium composition on *Trichoderma reesei*’s morphology and cellulase production”. In: *Bioresource Technology* 100 (2009), pp. 5979–5987. DOI: 10.1016/j.biortech.2009.02.070.

[27] R. P. Jansen, C. Beuck, M. Moch, B. Klein, K. Küsters, H. Morschett, W. Wiechert, and M. Oldiges. “A closer look at *Aspergillus*: online monitoring via scattered light enables reproducible phenotyping”. In: *Fungal Biology and Biotechnology* 6 (2019), p. 11. DOI: 10.1186/s40694-019-0073-x.

[28] N. Hardy, M. Moreaud, D. Guillaume, F. Augier, A. Nienow, C. Béal, and F. Ben Chaabane. “Advanced digital image analysis method dedicated to the characterization of the morphology of filamentous fungus”. In: *Journal of Microscopy* 266 (2017), pp. 126–140. DOI: 10.1111/jmi.12523.

[29] H. Giese, A. Azizan, A. Kümmel, A. Liao, C. Peter, J. Fonseca, R. Hermann, T. Duarte, and J. Büchs. “Liquid films on shake flask walls explain increasing maximum oxygen transfer capacities with elevating viscosity”. In: *Biotechnology and Bioengineering* 111 (2014), pp. 295–308. DOI: 10.1002/bit.25015.

[30] J. Büchs, S. Lotter, and C. Milbradt. “Out-of-phase operating conditions, a hitherto unknown phenomenon in shaking bioreactors”. In: *Biochemical Engineering Journal* 7 (2001), pp. 135–141. DOI: 10.1016/S1369-703X(00)00113-3.

[31] T. Wucherpfennig, K. A. Kiep, H. Driouch, C. Wittmann, and R. Krull. “Morphology and rheology in filamentous cultivations”. In: *Advances in Applied Microbiology*. Ed. by A. I. Laskin, S. Sariaslani, and G. M. Gadd. Vol. 72. Academic Press, 2010, pp. 89–136.

[32] H. Müller, L. Barthel, S. Schmideder, T. Schütze, V. Meyer, and H. Briesen. “From spores to fungal pellets: a new high-throughput image analysis highlights the structural development of *Aspergillus niger*”. In: *Biotechnology and Bioengineering* 119 (2022), pp. 2182–2195. DOI: 10.1002/bit.28124.

[33] Y. Fu, L. Yin, H. Zhu, R. Jiang, S. Li, and Q. Xu. “Effects of pellet characteristics on L-lactic acid fermentation by *R. oryzae*: pellet morphology, diameter, density, and interior structure”. In: *Applied Biochemistry and Biotechnology* 174 (2014), pp. 2019–2030. DOI: 10.1007/s12010-014-1146-1.

[34] D. J. Barry and G. A. Williams. “Microscopic characterisation of filamentous microbes: towards fully automated morphological quantification through image analysis”. In: *Journal of Microscopy* 244 (2011). DOI: 10.1111/j.1365-2818.2011.03506.x.

[35] R. Krull, C. Cordes, H. Horn, I. Kampen, A. Kwade, T. R. Neu, and B. Nörtemann. “Morphology of filamentous fungi: linking cellular biology to process engineering using *Aspergillus niger*”. In: *Advances in Biochemical Engineering/Biotechnology* 121 (2010), pp. 1–21. DOI: 10.1007/10_2009_60.

[36] S. Schmideder, L. Barthel, T. Friedrich, M. Thalhammer, T. Kovačević, L. Niessen, V. Meyer, and H. Briesen. “An X-ray microtomography-based method for detailed analysis of the three-dimensional morphology of fungal pellets”. In: *Biotechnology and Bioengineering* 116 (2019), pp. 1355–1365. DOI: 10.1002/bit.26956.

[37] M. Papagianni. “Fungal morphology and metabolite production in submerged mycelial processes”. In: *Biotechnology Advances* 22 (2004), pp. 189–259. DOI: 10.1016/j.biotechadv.2003.09.005.

[38] P. W. Cox, G. C. Paul, and C. R. Thomas. “Image analysis of the morphology of filamentous micro-organisms”. In: *Microbiology* 144 (1998), pp. 817–827. DOI: 10.1099/00221287-144-4-817.

[39] S. Pant, Ritika, P. Nag, A. Ghati, D. Chakraborty, M. R. Maximiano, O. L. Franco, A. K. Mandal, and A. Kuila. “Employment of the CRISPR/Cas9 system to improve cellulase production in *Trichoderma reesei*”. In: *Biotechnology Advances* 60 (2022), p. 108022. DOI: 10.1016/j.biotechadv.2022.108022.

[40] R. Bischof, J. Ramoni, and B. Seiboth. “Cellulases and beyond: the first 70 years of the enzyme producer *Trichoderma reesei*”. In: *Microbial Cell Factories* 15 (2016), p. 106. DOI: 10.1186/s12934-016-0507-6.

[41] H. Nevalainen, P. Suominen, and K. Taimisto. “On the safety of *Trichoderma reesei*”. In: *Journal of Biotechnology* 37 (1994), pp. 193–200. DOI: 10.1016/0168-1656(94)90126-0.

[42] D. Martinez, R. M. Berka, B. Henrissat, M. Saloheimo, M. Arvas, S. E. Baker, J. Chapman, O. Chertkov, P. M. Coutinho, D. Cullen, E. G. J. Danchin, I. V. Grigoriev, P. Harris, M. Jackson, C. P. Kubicek, C. S. Han, I. Ho, L. F. Larrondo, A. L. de Leon, J. K. Magnuson, S. Merino, M. Misra, B. Nelson, N. Putnam, B. Robbertse, A. A. Salamov, M. Schmoll, A. Terry, N. Thayer, A. Westerholm-Parvinen, C. L. Schoch, J. Yao, R. Barabote, M. A. Nelson, C. Detter, D. Bruce, C. R. Kuske, G. Xie, P. Richardson, D. S. Rokhsar, S. M. Lucas, E. M. Rubin, N. Dunn-Coleman, M. Ward, and T. S. Brettin. “Genome sequencing and analysis of the biomass-degrading fungus *Trichoderma reesei* (syn. *Hypocrea jecorina*)”. In: *Nature Biotechnology* 26 (2008), pp. 553–560. DOI: 10.1038/nbt1403.

[43] B. S. Montenecourt. “*Trichoderma reesei* cellulases”. In: *Trends in Biotechnology* 1 (1983), pp. 156–161. DOI: 10.1016/0167-7799(83)90007-0.

[44] G. B. Sperandio and E. X. F. Filho. “An overview of *Trichoderma reesei* co-cultures for the production of lignocellulolytic enzymes”. In: *Applied Microbiology and Biotechnology* 105 (2021), pp. 3019–3025. DOI: 10.1007/s00253-021-11261-7.

[45] R. Peterson and H. Nevalainen. “*Trichoderma reesei* RUT-C30 - thirty years of strain improvement”. In: *Microbiology* 158 (2012), pp. 58–68. DOI: 10.1099/mic.0.054031-0.

[46] F. Bidard-Michelot, E. Jourdier, F. Ben Chaabane, T. Aouam, and S. Prigent. “Souche de champignon ayant une viscosité diminuée”. FR3104169A1. I. É. Nouvelles. 2021.

[47] A. Fischer, S. Maiyuran, and D. Yaver. “Industrial relevance of *Trichoderma reesei* as an enzyme producer”. In: *Trichoderma reesei: Methods and Protocols*. Ed. by A. Mach-Aigner and R. Martzy. Vol. 2234. New York, US: Springer US, 2021, pp. 23–43.

[48] *List of commercial enzymes*. URL: https://amfep.org/_library/_files/Amfep_List_of_Enzymes_update_May_2015.pdf (visited on 08/28/2024).

[49] J. N. Currie. “The citric acid fermentation of *Aspergillus niger*”. In: *Journal of Biological Chemistry* 31 (1917), pp. 15–37. DOI: 10.1016/S0021-9258(18)86708-4.

[50] T. C. Cairns, L. Barthel, and V. Meyer. “Something old, something new: challenges and developments in *Aspergillus niger* biotechnology”. In: *Essays in Biochemistry* 65 (2021), pp. 213–224. DOI: 10.1042/EBC20200139.

[51] H. J. Pel, J. H. de Winde, D. B. Archer, P. S. Dyer, G. Hofmann, P. J. Schaap, G. Turner, R. P. de Vries, R. Albang, K. Albermann, M. R. Andersen, J. D. Bendtsen, J. A. E. Benen, M. van den Berg, S. Breestraat, M. X. Caddick, R. Contreras, M. Cornell, P. M. Coutinho, E. G. J. Danchin, A. J. M. Debets, P. Dekker, P. W. M. van Dijck, A. van Dijk, L. Dijkhuizen, A. J. M. Driessen, C. d’Enfert, S. Geysens, C. Goosen, G. S. P. Groot, P. W. J. de Groot, T. Guillemette, B. Henrissat, M. Herweijer, J. P. T. W. van den Hombergh, C. A. M. J. J. van den Hondel, R. T. J. M. van der Heijden, R. M. van der Kaaij, F. M. Klis, H. J. Kools, C. P. Kubicek, P. A. van Kuyk, J. Lauber, X. Lu, M. J. E. C. van der Maarel, R. Meulenberg, H. Menke, M. A. Mortimer, J. Nielsen, S. G. Oliver, M. Olsthoorn, K. Pal, N. N. M. E. van Peij, A. F. J. Ram, U. Rinas, J. A. Roubos, C. M. J. Sagt, M. Schmoll, J. Sun, D. Ussery, J. Varga, W. Vervecken, P. J. J. van de Vondervoort, H. Wedler, H. A. B. Wösten, A.-P. Zeng, A. J. J. van Ooyen, J. Visser, and H. Stam. “Genome sequencing and analysis of the versatile cell factory *Aspergillus niger* CBS 513.88”. In: *Nature Biotechnology* 25 (2007), pp. 221–231. DOI: 10.1038/nbt1282.

[52] P. L. Show, K. O. Oladele, Q. Y. Siew, F. A. Aziz Zakry, J. C.-W. Lan, and T. C. Ling. “Overview of citric acid production from *Aspergillus niger*”. In: *Frontiers in Life Science* 8 (2015), pp. 271–283. DOI: 10.1080/21553769.2015.1033653.

[53] A. M. Abdel-Azeem, M. A. Abdel-Azeem, S. Y. Abdul-Hadi, and A. G. Darwish. “*Aspergillus*: biodiversity, ecological significances, and industrial applications”. In: *Recent Advancement in White Biotechnology Through Fungi*. Ed. by A. N. Yadav, S. Mishra, S. Singh, and A. Gupta. Vol. 1. Cham, CH: Springer International Publishing, 2019, pp. 121–179.

[54] D. Lubertozzi and J. D. Keasling. “Developing *Aspergillus* as a host for heterologous expression”. In: *Biotechnology Advances* 27 (2009), pp. 53–75. DOI: 10.1016/j.biotechadv.2008.09.001.

[55] H. Driouch, A. Roth, P. Dersch, and C. Wittmann. “Optimized bioprocess for production of fructofuranosidase by recombinant *Aspergillus niger*”. In: *Applied Microbiology and Biotechnology* 87 (2010), pp. 2011–2024. DOI: 10.1007/s00253-010-2661-9.

[56] R. Jansen, H. Morschett, D. Hasenklever, M. Moch, W. Wiechert, and M. Oldiges. “Microbioreactor-assisted cultivation workflows for time-efficient phenotyping of protein producing *Aspergillus niger* in batch and fed-batch mode”. In: *Biotechnology Progress* 37 (2021), e3144. DOI: 10.1002/btpr.3144.

[57] T. Schuetze and V. Meyer. “Polycistronic gene expression in *Aspergillus niger*”. In: *Microbial Cell Factories* 16 (2017), p. 162. DOI: 10.1186/s12934-017-0780-z.

[58] E. Geib and M. Brock. “ATNT: an enhanced system for expression of polycistronic secondary metabolite gene clusters in *Aspergillus niger*”. In: *Fungal Biology and Biotechnology* 4 (2017), p. 13. DOI: 10.1186/s40694-017-0042-1.

[59] D. Liu, S. Garrigues, and R. P. de Vries. “Heterologous protein production in filamentous fungi”. In: *Applied Microbiology and Biotechnology* 107 (2023), pp. 5019–5033. DOI: 10.1007/s00253-023-12660-8.

[60] B. Siebecker, T. Schütze, S. Spohner, S. Haefner, and V. Meyer. “Transcriptomic insights into the roles of the transcription factors Clr1, Clr2 and Clr4 in lignocellulose degradation of the thermophilic fungal platform *Thermothelomyces thermophilus*”. In: *Frontiers in Bioengineering and Biotechnology* 11 (2023), pp. 1–17. DOI: 10.3389/fbioe.2023.1279146.

[61] A. E. Apinis. “Occurrence of thermophilous microfungi in certain alluvial soils near Nottingham”. In: *Nova Hedwigia* 5 (1963), pp. 57–78.

[62] A. von Klopotek. “Revision der thermophilen *Sporotrichum*-Arten: *Chrysosporium thermophilum* (Apinis) comb. nov. und *Chrysosporium fergusii* spec. nov. = status conidialis von *Corynascus thermophilus* (Fergus und Sinden) comb. nov.” In: *Archives of Microbiology* 98 (1974), pp. 365–369. DOI: 10.1007/BF00425296.

[63] C. A. Oorschot. “The genus *Myceliophthora*”. In: *Persoonia* 9 (1977), pp. 401–408.

[64] Y. Marin-Felix, A. M. Stchigel, A. N. Miller, J. Guarro, and J. F. Cano-Lira. “A re-evaluation of the genus *Myceliophthora* (Sordariales, Ascomycota): its segregation into four genera and description of *Corynascus fumimontanus* sp. nov.” In: *Mycologia* 107 (2015), pp. 619–632. DOI: 10.3852/14-228.

[65] R. M. Berka, I. V. Grigoriev, R. Otillar, A. Salamov, J. Grimwood, I. Reid, N. Ishmael, T. John, C. Darmond, M.-C. Moisan, B. Henrissat, P. M. Coutinho, V. Lombard, D. O. Natvig, E. Lindquist, J. Schmutz, S. Lucas, P. Harris, J. Powlowski, A. Bellemare, D. Taylor, G. Butler, R. P. de Vries, I. E. Allijn, J. van den Brink, S. Ushinsky, R. Storms, A. J. Powell, I. T. Paulsen, L. D. H. Elbourne, S. E. Baker, J. Magnuson, S. LaBoissiere, A. J. Clutterbuck, D. Martinez, M. Wogulis, A. L. de Leon, M. W. Rey, and A. Tsang. “Comparative genomic analysis of the thermophilic biomass-degrading fungi *Myceliophthora thermophila* and *Thielavia terrestris*”. In: *Nature Biotechnology* 29 (2011), pp. 922–927. DOI: 10.1038/nbt.1976.

[66] J. Li, L. Lin, T. Sun, J. Xu, J. Ji, Q. Liu, and C. Tian. “Direct production of commodity chemicals from lignocellulose using *Myceliophthora thermophila*”. In: *Metabolic Engineering* 61 (2020), pp. 416–426. DOI: 10.1016/j.ymben.2019.05.007.

[67] L. Viikari, M. Alapuranen, T. Puranen, J. Vehmaanperä, and M. Siika-aho. “Thermostable enzymes in lignocellulose hydrolysis”. In: *Biofuels*. Ed. by L. Olsson. Vol. 108. Berlin, Heidelberg, DE: Springer Berlin Heidelberg, 2007, pp. 121–145.

[68] M. A. Emalfarb, A. Ben-Bassat, R. P. Burlingame, V. M. Chernoglazov, O. N. Okounev, P. T. Olson, A. P. Sinitsyn, and I. V. Solovjeva. “Cellulase compositions and methods of use”. US005811381A. M. A. Emalfarb. 1998.

[69] H. Visser, V. Joosten, P. J. Punt, A. V. Gusakov, P. T. Olson, R. Joosten, J. Bartels, J. Visser, A. P. Sinitsyn, M. A. Emalfarb, J. C. Verdoes, and J. Wery. “Development of a mature fungal technology and production platform for industrial enzymes based on a *Myceliophthora thermophila* isolate, previously known as *Chrysosporium lucknowense* C1”. In: *Industrial Biotechnology* 7 (2011), pp. 214–223. DOI: 10.1089/ind.2011.7.214.

[70] B. Siebecker. “Characterization and optimization of *Thermothelomyces thermophilus* as fungal production host”. PhD thesis. Technische Universität Berlin, 2021.

[71] C. L. Pirich, G. F. Picheth, A. M. Fontes, M. Delgado-Aguilar, and L. P. Ramos. “Disruptive enzyme-based strategies to isolate nanocelluloses: a review”. In: *Cellulose* 27 (2020), pp. 5457–5475. DOI: 10.1007/s10570-020-03185-8.

[72] G. Jäger, H. Wulfhorst, E. U. Zeithammel, E. Elinidou, A. C. Spiess, and J. Büchs. “Screening of cellulases for biofuel production: online monitoring of the enzymatic hydrolysis of insoluble cellulose using high-throughput scattered light detection”. In: *Biotechnology Journal* 6 (2011), pp. 74–85. DOI: 10.1002/biot.201000387.

[73] K. R. Mihajlovski and M. D. Milić. “The role of plant cell wall degrading enzymes in biorefinery development”. In: *Lignocellulose Bioconversion Through White Biotechnology*. Ed. by A. Kumar Chandel. West Sussex, UK: John Wiley & Sons, Ltd., 2022, pp. 99–135.

[74] P. Sutaoney, S. Rai, S. Sinha, R. Choudhary, A. K. Gupta, S. Singh, and P. Banerjee. “Current perspective in research and industrial applications of microbial cellulases”. In: *International Journal of Biological Macromolecules* 264 (2024), p. 130639. DOI: 10.1016/j.ijbiomac.2024.130639.

[75] C. Derntl, L. Gudynaite-Savitch, S. Calixte, T. White, R. L. Mach, and A. R. Mach-Aigner. “Mutation of the Xylanase regulator 1 causes a glucose blind hydrolase expressing phenotype in industrially used *Trichoderma* strains”. In: *Biotechnology for Biofuels* 6 (2013), p. 62. DOI: 10.1186/1754-6834-6-62.

[76] *BRENDA*. URL: www.brenda-enzymes.org (visited on 08/05/2024).

[77] X. G. Lei and J. M. Porres. “Phytase enzymology, applications and biotechnology”. In: *Biotechnology Letters* 25 (2003), pp. 1787–1794. DOI: 10.1023/A:1026224101580.

[78] R. Greiner and U. Konietzny. “Phytase for food application”. In: *Food Technology and Biotechnology* 44 (2006), pp. 125–140.

[79] S. Rebello, L. Jose, R. Sindhu, and E. Aneesh. “Molecular advancements in the development of thermostable phytases”. In: *Applied Microbiology and Biotechnology* 101 (2017), pp. 2677–2689. DOI: 10.1007/s00253-017-8195-7.

[80] Y. Dersjant-Li, A. Awati, H. Schulze, and G. Partridge. “Phytase in non-ruminant animal nutrition: a critical review on phytase activities in the gastrointestinal tract and influencing factors”. In: *Journal of the Science of Food and Agriculture* 95 (2015), pp. 878–896. DOI: 10.1002/jsfa.6998.

[81] A. Kumar, B. Singh, P. Raigond, C. Sahu, U. N. Mishra, S. Sharma, and M. K. Lal. “Phytic acid: blessing in disguise, a prime compound required for both plant and human nutrition”. In: *Food Research International* 142 (2021), p. 110193. DOI: 10.1016/j.foodres.2021.110193.

[82] S. Kataki, H. West, M. Clarke, and D. C. Baruah. “Phosphorus recovery as struvite: recent concerns for use of seed, alternative Mg source, nitrogen conservation and fertilizer potential”. In: *Resources, Conservation and Recycling* 107 (2016), pp. 142–156. DOI: 10.1016/j.resconrec.2015.12.009.

[83] F. Di Capua, S. de Sario, A. Ferraro, A. Petrella, M. Race, F. Pirozzi, U. Fratino, and D. Spasiano. “Phosphorous removal and recovery from urban wastewater: current practices and new directions”. In: *The Science of the Total Environment* 823 (2022), p. 153750. DOI: 10.1016/j.scitotenv.2022.153750.

[84] T. Zhao, X. Yong, Z. Zhao, V. Dolce, Y. Li, and R. Curcio. “Research status of *Bacillus* phytase”. In: *3 Biotech* 11 (2021), p. 415. DOI: 10.1007/s13205-021-02964-9.

[85] E. Feizollahi, R. S. Mirmahdi, A. Zoghi, R. T. Zijlstra, M. S. Roopesh, and T. Vasanthan. “Review of the beneficial and anti-nutritional qualities of phytic acid, and procedures for removing it from food products”. In: *Food Research International* 143 (2021), p. 110284. DOI: 10.1016/j.foodres.2021.110284.

[86] *Animal feed phytase market*. URL: https://straitsresearch.com/report/animal-feed-phytase-market (visited on 08/04/2024).

[87] *Animal feed market size*. URL: https://www.gminsights.com/industry-analysis/animal-feed-phytase-market (visited on 08/04/2024).

[88] A. E. Posch, C. Herwig, and O. Spadiut. “Science-based bioprocess design for filamentous fungi”. In: *Trends in Biotechnology* 31 (2013), pp. 37–44. DOI: 10.1016/j.tibtech.2012.10.008.

[89] S. Teworte, K. Malcı, L. E. Walls, M. Halim, and L. Rios-Solis. “Recent advances in fed-batch microscale bioreactor design”. In: *Biotechnology Advances* 55 (2022), p. 107888. DOI: 10.1016/j.biotechadv.2021.107888.

[90] M. Rienzo, S. J. Jackson, L. K. Chao, T. Leaf, T. J. Schmidt, A. H. Navidi, D. C. Nadler, M. Ohler, and M. D. Leavell. “High-throughput screening for high-efficiency small-molecule biosynthesis”. In: *Metabolic Engineering* 63 (2021), pp. 102–125. DOI: 10.1016/j.ymben.2020.09.004.

[91] S. Achinas, J.-I. Heins, J. Krooneman, and G. J. W. Euverink. “Miniaturization and 3D printing of bioreactors: a technological mini review”. In: *Micromachines* 11 (2020), p. 853. DOI: 10.3390/mi11090853.

[92] M. Scheidle, M. Jeude, B. Dittrich, S. Denter, F. Kensy, M. Suckow, D. Klee, and J. Büchs. “High-throughput screening of *Hansenula polymorpha* clones in the batch compared with the controlled-release fed-batch mode on a small scale”. In: *FEMS Yeast Research* 10 (2010), pp. 83–92. DOI: 10.1111/j.1567-1364.2009.00586.x.

[93] K. Totlani, R. J. van Tatenhove-Pel, M. T. Kreutzer, W. M. van Gulik, and V. van Steijn. “Microbioreactors for nutrient-controlled microbial cultures: bridging the gap between bioprocess development and industrial use”. In: *Biotechnology Journal* 18 (2023), e2200549. DOI: 10.1002/biot.202200549.

[94] M. Funke, A. Buchenauer, U. Schnakenberg, W. Mokwa, S. Diederichs, A. Mertens, C. Müller, F. Kensy, and J. Büchs. “Microfluidic biolector - microfluidic bioprocess control in microtiter plates”. In: *Biotechnology and Bioengineering* 107 (2010), pp. 497–505. DOI: 10.1002/bit.22825.

[95] S. D. Doig, F. Baganz, and G. J. Lye. “High-throughput screening and process optimisation”. In: *Basic Biotechnology*. Ed. by C. Ratledge and B. Kristiansen. Cambridge, UK: Cambridge University Press, 2006, pp. 289–306.

[96] F. Delvigne, R. Takors, R. Mudde, W. van Gulik, and H. Noorman. “Bioprocess scale-up/down as integrative enabling technology: from fluid mechanics to systems biology and beyond”. In: *Microbial Biotechnology* 10 (2017), pp. 1267–1274. DOI: 10.1111/1751-7915.12803.

[97] L. M. Mayr and D. Bojanic. “Novel trends in high-throughput screening”. In: *Current Opinion in Pharmacology* 9 (2009), pp. 580–588. DOI: 10.1016/j.coph.2009.08.004.

[98] G. Sánchez-Orellana, S. Casas-Flores, and B. Gutiérrez-Medina. “Automated, continuous video microscopy tracking of hyphal growth”. In: *Fungal Genetics and Biology* 123 (2019), pp. 25–32. DOI: 10.1016/j.fgb.2018.11.006.

[99] C. Lattermann and J. Büchs. “Design and operation of microbioreactor systems for screening and process development”. In: *Bioreactors*. Ed. by C.-F. Mandenius. Vol. 1. Weinheim, DE: WILEY-VCH GmbH, 2016, pp. 35–76.

[100] J. Hemmerich, S. Noack, W. Wiechert, and M. Oldiges. “Microbioreactor systems for accelerated bioprocess development”. In: *Biotechnology Journal* 13 (2018). DOI: 10.1002/biot.201700141.

[101] F. Kensy, E. Zang, C. Faulhammer, R.-K. Tan, and J. Büchs. “Validation of a high-throughput fermentation system based on online monitoring of biomass and fluorescence in continuously shaken microtiter plates”. In: *Microbial Cell Factories* 8 (2009), p. 31. DOI: 10.1186/1475-2859-8-31.

[102] J. Hemmerich, N. Adelantado, J. M. Barrigón, X. Ponte, A. Hörmann, P. Ferrer, F. Kensy, and F. Valero. “Comprehensive clone screening and evaluation of fed-batch strategies in a microbioreactor and lab scale stirred tank bioreactor system: application on *Pichia pastoris* producing *Rhizopus oryzae* lipase”. In: *Microbial Cell Factories* 13 (2014), p. 36. DOI: 10.1186/1475-2859-13-36.

[103] L. M. Helleckes, C. Müller, T. Griesbach, V. Waffenschmidt, M. Moch, M. Osthege, W. Wiechert, and M. Oldiges. “Explore or exploit? A model-based screening strategy for PETase secretion by *Corynebacterium glutamicum*”. In: *Biotechnology and Bioengineering* 120 (2022), pp. 139–153. DOI: 10.1002/bit.28261.

[104] J. I. Betts and F. Baganz. “Miniature bioreactors: current practices and future opportunities”. In: *Microbial Cell Factories* 5 (2006), p. 21. DOI: 10.1186/1475-2859-5-21.

[105] *bioREACTOR (2mag)*. URL: https://2mag.de/produkte/bioreactor.html/ (visited on 09/08/2024).

[106] *BioLector (Beckman)*. URL: https://www.beckman.de/microbioreactor (visited on 09/08/2024).

[107] *Bioscreen C (Oy Growth Curves)*. URL: https://www.bioscreen.fi/ (visited on 09/08/2024).

[108] *Growth Profiler (EnzyScreen)*. URL: https://www.enzyscreen.com/article/growth-profiler/ (visited on 09/08/2024).

[109] *SensorDish Reader (PreSens Precision Sensing)*. URL: https://www.presens.de/products/detail/sdr-sensordish-reader-basic-set (visited on 09/08/2024).

[110] A. Buchenauer, M. Funke, J. Büchs, W. Mokwa, and U. Schnakenberg. “Microbioreactors with microfluidic control and a user-friendly connection to the actuator hardware”. In: *Journal of Micromechanics and Microengineering* 19 (2009), p. 074012. DOI: 10.1088/0960-1317/19/7/074012.

[111] A. Buchenauer, M. C. Hofmann, M. Funke, J. Büchs, W. Mokwa, and U. Schnakenberg. “Microbioreactors for fed-batch fermentations with integrated online monitoring and microfluidic devices”. In: *Biosensors & Bioelectronics* 24 (2009), pp. 1411–1416. DOI: 10.1016/j.bios.2008.08.043.

[112] M. Funke, A. Buchenauer, W. Mokwa, S. Kluge, L. Hein, C. Müller, F. Kensy, and J. Büchs. “Bioprocess control in microscale: scalable fermentations in disposable and user-friendly microfluidic systems”. In: *Microbial Cell Factories* 9 (2010), p. 86. DOI: 10.1186/1475-2859-9-86.

[113] M. Samorski, G. Müller-Newen, and J. Büchs. “Quasi-continuous combined scattered light and fluorescence measurements: a novel measurement technique for shaken microtiter plates”. In: *Biotechnology and Bioengineering* 92 (2005), pp. 61–68. DOI: 10.1002/bit.20573.

[114] T. Ladner, D. Flitsch, T. Schlepütz, and J. Büchs. “Online monitoring of dissolved oxygen tension in microtiter plates based on infrared fluorescent oxygen-sensitive nanoparticles”. In: *Microbial Cell Factories* 14 (2015), p. 161. DOI: 10.1186/s12934-015-0347-9.

[115] M. Funke, S. Diederichs, F. Kensy, C. Müller, and J. Büchs. “The baffled microtiter plate: increased oxygen transfer and improved online monitoring in small scale fermentations”. In: *Biotechnology and Bioengineering* 103 (2009), pp. 1118–1128. DOI: 10.1002/bit.22341.

[116] *Round well plate datasheet*. URL: https://www.m2p-labs.com/fileadmin/redakteur/Data_sheets/Microtiter_plates/Datasheet_RoundWellPlate__0121.pdf (visited on 05/25/2023).

[117] *FlowerPlate datasheet*. URL: https://www.m2p-labs.com/fileadmin/redakteur/Data_sheets/Microtiter_plates/Datasheet__FlowerPlate__0221.pdf (visited on 05/25/2023).

[118] C. Blesken, T. Olfers, A. Grimm, and N. Frische. “The microfluidic bioreactor for a new era of bioprocess development”. In: *Engineering in Life Sciences* 16 (2016), pp. 190–193. DOI: 10.1002/elsc.201500026.

[119] *Microfluidic round well plate datasheet*. URL: https://www.m2p-labs.com/fileadmin/redakteur/Data_sheets/Microtiter_plates/Datesheet__Gen2-MF_RoundWellPlate__0621.pdf (visited on 09/10/2024).

[120] *Microfluidic FlowerPlate datasheet*. URL: https://www.m2p-labs.com/fileadmin/redakteur/Data_sheets/Microtiter_plates/Datasheet__Gen2-MF_FlowerPlate__0621.pdf (visited on 09/10/2024).

[121] R. Jansen, N. Tenhaef, M. Moch, W. Wiechert, S. Noack, and M. Oldiges. “FeedER: a feedback-regulated enzyme-based slow-release system for fed-batch cultivation in microtiter plates”. In: *Bioprocess and Biosystems Engineering* 42 (2019), pp. 1843–1852. DOI: 10.1007/s00449-019-02180-z.

[122] J. Hemmerich, N. Tenhaef, C. Steffens, J. Kappelmann, M. Weiske, S. J. Reich, W. Wiechert, M. Oldiges, and S. Noack. “Less sacrifice, more insight: repeated low-volume sampling of microbioreactor cultivations enables accelerated deep phenotyping of microbial strain libraries”. In: *Biotechnology Journal* 14 (2019), e1800428. DOI: 10.1002/biot.201800428.

[123] T. C. Silva, M. Eppink, and M. Ottens. “Automation and miniaturization: enabling tools for fast, high–throughput process development in integrated continuous biomanufacturing”. In: *Journal of Chemical Technology & Biotechnology* 97 (2022), pp. 2365–2375. DOI: 10.1002/jctb.6792.

[124] S. Beutel and F. Lenk, eds. *Smart biolabs of the future*. Cham, CH: Springer International Publishing, 2022.

[125] T. Habich and S. Beutel. “Digitalization concepts in academic bioprocess development”. In: *Engineering in Life Sciences* 24 (2024), p. 2300238. DOI: 10.1002/elsc.202300238.

[126] J. Zhang, Y. Chen, L. Fu, E. Guo, B. Wang, L. Dai, and T. Si. “Accelerating strain engineering in biofuel research via build and test automation of synthetic biology”. In: *Current Opinion in Biotechnology* 67 (2021), pp. 88–98. DOI: 10.1016/j.copbio.2021.01.010.

[127] S. Sadeghi, R. B. Canty, N. Mukhin, J. Xu, F. Delgado-Licona, and M. Abolhasani. “Engineering a sustainable future: harnessing automation, robotics, and artificial intelligence with self-driving laboratories”. In: *ACS Sustainable Chemistry & Engineering* 12 (2024), pp. 12695–12707. DOI: 10.1021/acssuschemeng.4c02177.

[128] *Liquid Handling Station (Brand)*. URL: https://shop.brand.de/de/pipettierroboter-liquid-handling-station-p75.html (visited on 09/11/2024).

[129] *OT-2 (Opentrons)*. URL: https://opentrons.com/robots/ot-2 (visited on 09/11/2024).

[130] *Fluent (Tecan)*. URL: https://lifesciences.tecan.com/fluent-laboratory-automation-workstation (visited on 09/11/2024).

[131] T. M. Rosch, J. Tenhaef, T. Stoltmann, T. Redeker, D. Kösters, N. Hollmann, K. Krumbach, W. Wiechert, M. Bott, S. Matamouros, J. Marienhagen, and S. Noack. “AutoBioTech - a versatile biofoundry for automated strain engineering”. In: *ACS Synthetic Biology* 13 (2024), pp. 2227–2237. DOI: 10.1021/acssynbio.4c00298.

[132] S. Dembski, T. Schwarz, M. Oppmann, S. T. Bandesha, J. Schmid, S. Wenderoth, K. Mandel, and J. Hansmann. “Establishing and testing a robot-based platform to enable the automated production of nanoparticles in a flexible and modular way”. In: *Scientific Reports* 13 (2023), p. 11440. DOI: 10.1038/s41598-023-38535-6.

[133] A. Kusterer, C. Krause, K. Kaufmann, M. Arnold, and D. Weuster-Botz. “Fully automated single-use stirred-tank bioreactors for parallel microbial cultivations”. In: *Bioprocess and Biosystems Engineering* 31 (2008), pp. 207–215. DOI: 10.1007/s00449-007-0195-z.

[134] P. Rohe, D. Venkanna, B. Kleine, R. Freudl, and M. Oldiges. “An automated workflow for enhancing microbial bioprocess optimization on a novel microbioreactor platform”. In: *Microbial Cell Factories* 11 (2012), p. 144. DOI: 10.1186/1475-2859-11-144.

[135] B. Haby, S. Hans, E. Anane, A. Sawatzki, N. Krausch, P. Neubauer, and M. N. Cruz Bournazou. “Integrated robotic mini bioreactor platform for automated, parallel microbial cultivation with online data handling and process control”. In: *SLAS Technology* 24 (2019), pp. 569–582. DOI: 10.1177/2472630319860775.

[136] M. Osthege. “Accelerated bioprocess research by autonomous experimentation and Bayesian modeling”. PhD thesis. RWTH Aachen University, 2022.

[137] L. M. Helleckes, D. Puchta, H. Czech, H. Morschett, B. Geinitz, W. Wiechert, and M. Oldiges. “From frozen cell bank to product assay: high-throughput strain characterisation for autonomous Design-Build-Test-Learn cycles”. In: *Microbial Cell Factories* 22 (2013), p. 130. DOI: 10.1186/s12934-023-02140-z.

[138] A. Radek, N. Tenhaef, M. Müller, C. Brüsseler, W. Wiechert, J. Marienhagen, T. Polen, and S. Noack. “Miniaturized and automated adaptive laboratory evolution: evolving *Corynebacterium glutamicum* towards an improved d-xylose utilization”. In: *Bioresource Technology* 245 (2017), pp. 1377–1385. DOI: 10.1016/j.biortech.2017.05.055.

[139] R. Jansen, M. Müller, S. Schröter, J. Kappelmann, B. Klein, M. Oldiges, and S. Noack. “Parallelized disruption of prokaryotic and eukaryotic cells via miniaturized and automated bead mill”. In: *Engineering in Life Sciences* 20 (2020), pp. 350–356. DOI: 10.1002/elsc.202000002.

[140] C. Müller, P. Bakkes, P. Lenz, V. Waffenschmidt, L. Helleckes, K. Jaeger, W. Wiechert, A. Knapp, R. Freudl, and M. Oldiges. “Accelerated strain construction and characterization of *C. glutamicum* protein secretion by laboratory automation”. In: *Applied Microbiology and Biotechnology* 106 (2022), pp. 4481–4497. DOI: 10.1007/s00253-022-12017-7.

[141] F. M. Mione, L. Kaspersetz, M. F. Luna, J. Aizpuru, R. Scholz, M. Borisyak, A. Kemmer, M. T. Schermeyer, E. C. Martinez, P. Neubauer, and M. N. Cruz Bournazou. “A workflow management system for reproducible and interoperable high-throughput self-driving experiments”. In: *Computers & Chemical Engineering* 187 (2024), p. 108720. DOI: 10.1016/j.compchemeng.2024.108720.

[142] A. E. Posch, O. Spadiut, and C. Herwig. “A novel method for fast and statistically verified morphological characterization of filamentous fungi”. In: *Fungal Genetics and Biology* 49 (2012), pp. 499–510. DOI: 10.1016/j.fgb.2012.05.003.

[143] *Nucleus (Zaber)*. URL: https://www.zaber.com/products/microscopes (visited on 09/13/2024).

[144] *Mica (Leica)*. URL: https://www.leica-microsystems.com/de/produkte/p/mica/ (visited on 09/13/2024).

[145] *BioTek Lionheart FX (Agilent)*. URL: https://www.agilent.com/en/product/cell-analysis/cell-imaging-microscopy/automated-cell-imagers/biotek-lionheart-fx-automated-microscope-1623188 (visited on 09/13/2024).

[146] R. Jansen, K. Küsters, H. Morschett, W. Wiechert, and M. Oldiges. “A fully automated pipeline for the dynamic at-line morphology analysis of microscale *Aspergillus* cultivation”. In: *Fungal Biology and Biotechnology* 8 (2021), p. 2. DOI: 10.1186/s40694-021-00109-4.

[147] K. Ruzaeva, K. Küsters, W. Wiechert, B. Berkels, M. Oldiges, and K. Nöh. “Automated characterization of catalytically active inclusion body production in biotechnological screening systems”. In: *2022 44th Annual International Conference of the IEEE Engineering in Medicine & Biology Society (EMBC)*. 2022, pp. 3874–3877.

[148] H. Jeckel and K. Drescher. “Advances and opportunities in image analysis of bacterial cells and communities”. In: *FEMS Microbiology Reviews* 45 (2021), pp. 1–14. DOI: 10.1093/femsre/fuaa062.

[149] O. Ronneberger, P. Fischer, and T. Brox. “U-Net: convolutional networks for biomedical image segmentation”. In: *Medical Image Computing and Computer-Assisted Intervention – MICCAI 2015*. Ed. by N. Navab, J. Hornegger, W. M. Wells, and A. F. Frangi. Vol. 9351. Cham, CH: Springer International Publishing, 2015, pp. 234–241.

[150] C. Stringer, T. Wang, M. Michaelos, and M. Pachitariu. “Cellpose: a generalist algorithm for cellular segmentation”. In: *Nature Methods* 18 (2021), pp. 100–106. DOI: 10.1038/s41592-020-01018-x.

[151] K. Cutler, C. Stringer, T. Lo, L. Rappez, N. Stroustrup, S. Brook Peterson, P. Wiggins, and J. Mougous. “Omnipose: a high-precision morphology-independent solution for bacterial cell segmentation”. In: *Nature Methods* 19 (2022), pp. 1438–1448. DOI: 10.1038/s41592-022-01639-4.

[152] J. Seiffarth, T. Scherr, B. Wollenhaupt, O. Neumann, H. Scharr, D. Kohlheyer, R. Mikut, and K. Nöh. “ObiWan-Microbi: OMERO-based integrated workflow for annotating microbes in the cloud”. In: *SoftwareX* 26 (2024), p. 101638. DOI: 10.1016/j.softx.2024.101638.

[153] K. Rohr, L. Gremm, B. Geinitz, E. Jourdier, W. Wiechert, F. Ben Chaabane, and M. Oldiges. “Optimizing microbioreactor cultivation strategies for *Trichoderma reesei*: from batch to fed-batch operations”. In: *Microbial Cell Factories* 23 (2024), p. 112. DOI: 10.1186/s12934-024-02371-8.

[154] W. Duetz and B. Witholt. “Oxygen transfer by orbital shaking of square vessels and deepwell microtiter plates of various dimensions”. In: *Biochemical Engineering Journal* 17 (2004), pp. 181–185. DOI: 10.1016/S1369-703X(03)00177-3.

[155] R. Walisko, J. Moench-Tegeder, J. Blotenberg, T. Wucherpfennig, and R. Krull. “The taming of the shrew - controlling the morphology of filamentous eukaryotic and prokaryotic microorganisms”. In: *Filaments in Bioprocesses*. Ed. by R. Krull and T. Bley. Cham, CH: Springer International Publishing, 2015, pp. 1–27.

[156] N. Hardy, F. Augier, A. Nienow, C. Béal, and F. Ben Chaabane. “Scale-up agitation criteria for *Trichoderma reesei* fermentation”. In: *Chemical Engineering Science* 172 (2017), pp. 158–168. DOI: 10.1016/j.ces.2017.06.034.

[157] E. Jourdier, L. Poughon, C. Larroche, F. Monot, and F. Ben Chaabane. “A new stoichiometric miniaturization strategy for screening of industrial microbial strains: application to cellulase hyper-producing *Trichoderma reesei* strains”. In: *Microbial Cell Factories* 11 (2012), p. 70. DOI: 10.1186/1475-2859-11-70.

[158] E. Jourdier, F. Ben Chaabane, L. Poughon, C. Larroche, and F. Monot. “Simple kinetic model of cellulase production by *Trichoderma reesei* for productivity or yield maximization”. In: *Chemical Engineering Transactions* 27 (2012), pp. 313–318. DOI: 10.3303/CET1227053.

[159] H. Giese, P. Kruithof, K. Meier, M. Sieben, E. Antonov, R. Hommes, and J. Büchs. “Improvement and scale-down of a *Trichoderma reesei* shake flask protocol to microtiter plates enables high-throughput screening”. In: *Journal of Bioscience and Bioengineering* 118 (2014), pp. 702–709. DOI: 10.1016/j.jbiosc.2014.05.016.

[160] *Troubleshooting pipetting viscous liquids*. URL: https://www.tecan.com/knowledge-portal/troubleshooting-pipetting-viscous-liquids (visited on 06/12/2024).

[161] M. Papagianni and M. Mattey. “Morphological development of *Aspergillus niger* in submerged citric acid fermentation as a function of the spore inoculum level. Application of neural network and cluster analysis for characterization of mycelial morphology”. In: *Microbial Cell Factories* 5 (2006), p. 3. DOI: 10.1186/1475-2859-5-3.

[162] K. Tucker and C. Thomas. “Mycelial morphology: the effect of spore inoculum level”. In: *Biotechnology Letters* 14 (1992), pp. 1071–1074. DOI: 10.1007/BF01021061.

[163] M. Bizukojc and S. Ledakowicz. “The morphological and physiological evolution of *Aspergillus terreus* mycelium in the submerged culture and its relation to the formation of secondary metabolites”. In: *World Journal of Microbiology and Biotechnology* 26 (2010), pp. 41–54. DOI: 10.1007/s11274-009-0140-1.

[164] N. Hardy, M. Moreaud, and F. Ben Chaabane. “Image analysis method for the characterization of *Trichoderma reesei* during fermentations”. In: *Trichoderma reesei: Methods and Protocols*. Ed. by A. R. Mach-Aigner and R. Martzy. Vol. 2234. New York, US: Springer US, 2021, pp. 119–133.

[165] K. Rohr, B. Geinitz, J. Seiffarth, A. Anbarani, S. Bernauer, M. Moch, J. Tenhaef, W. Wiechert, K. Nöh, and M. Oldiges. “Insights into the morphology-productivity relationship of filamentous fungi through small-scale cultivation and automated microscopy of *Thermothelomyces thermophilus*”. In: *Biotechnology Progress* (2025), e3528. DOI: 10.1002/btpr.3528.

[166] M. Ganzlin and U. Rinas. “In-depth analysis of the *Aspergillus niger* glucoamylase (glaA) promoter performance using high-throughput screening and controlled bioreactor cultivation techniques”. In: *Journal of Biotechnology* 135 (2008), pp. 266–271. DOI: 10.1016/j.jbiotec.2008.04.005.

[167] T. Scherr, J. Seiffarth, B. Wollenhaupt, O. Neumann, M. P. Schilling, D. Kohlheyer, H. Scharr, K. Nöh, and R. Mikut. “microbeSEG: A deep learning software tool with OMERO data management for efficient and accurate cell segmentation”. In: *PLOS ONE* 17 (2022), e0277601. DOI: 10.1371/journal.pone.0277601.

[168] M. Osthege, N. Tenhaef, R. Zyla, C. Müller, J. Hemmerich, W. Wiechert, S. Noack, and M. Oldiges. “bletl - a Python package for integrating BioLector microcultivation devices in the Design-Build-Test-Learn cycle”. In: *Engineering in Life Sciences* 22 (2022), pp. 242–259. DOI: 10.1002/elsc.202100108.

[169] M. Osthege, N. Tenhaef, S. Noack, L. Helleckes, J. Nießer, A. Reiter, Rebecca, L. Halle, C. Müller, and simoneschito. *JuBiotech/bletl*. Version 1.3.1. 2023. DOI: 10.5281/zenodo.8059856. URL: https://doi.org/10.5281/zenodo.8059856.

[170] J. D. Hunter. “Matplotlib: a 2D graphics environment”. In: *Computing in Science & Engineering* 9 (2007), pp. 90–95. DOI: 10.1109/MCSE.2007.55.

[171] T. A. Caswell, M. Droettboom, A. Lee, E. Sales de Andrade, T. Hoffmann, J. Hunter, J. Klymak, E. Firing, D. Stansby, N. Varoquaux, J. Hedegaard Nielsen, B. Root, R. May, P. Elson, J. K. Seppänen, D. Dale, J. Lee, D. McDougall, A. Straw, P. Hobson, hannah, C. Gohlke, A. F. Vincent, T. S. Yu, E. Ma, S. Silvester, C. Moad, N. Kniazev, E. Ernest, and P. Ivanov. *matplotlib/matplotlib*. Version 3.5.1. 2021. DOI: 10.5281/zenodo.5773480. URL: https://doi.org/10.5281/zenodo.5773480.

[172] C. R. Harris, K. J. Millman, S. J. van der Walt, R. Gommers, P. Virtanen, D. Cournapeau, E. Wieser, J. Taylor, S. Berg, N. J. Smith, R. Kern, M. Picus, S. Hoyer, M. H. van Kerkwijk, M. Brett, A. Haldane, J. F. del Río, M. Wiebe, P. Peterson, P. Gérard-Marchant, K. Sheppard, T. Reddy, W. Weckesser, H. Abbasi, C. Gohlke, and T. E. Oliphant. “Array programming with NumPy”. In: *Nature* 585 (2020), pp. 357–362. DOI: 10.1038/s41586-020-2649-2.

[173] W. McKinney. “Data structures for statistical computing in Python”. In: *Proceedings of the 9th Python in Science Conference*. Ed. by S. van der Walt and J. Millman. 2010, pp. 56–61. DOI: 10.25080/Majora-92bf1922-00a.

[174] The pandas development team. *pandas-dev/pandas: Pandas*. Version 1.4.1. 2022. DOI: 10.5281/zenodo.6053272. URL: https://doi.org/10.5281/zenodo.6053272.

[175] M. L. Waskom. “Seaborn: statistical data visualization”. In: *Journal of Open Source Software* 6 (2021), p. 3021. DOI: 10.21105/joss.03021.

[176] W. Michael, M. Gelbart, O. Botvinnik, J. Ostblom, P. Hobson, S. Lukauskas, D. C. Gemperline, T. Augspurger, Y. Halchenko, J. Warmenhoven, J. B. Cole, J. de Ruiter, J. Vanderplas, S. Hoyer, C. Pye, A. Miles, C. Swain, K. Meyer, M. Martin, P. Bachant, E. Quintero, G. Kunter, S. Villalba, Brian, C. Fitzgerald, C. Evans, M. L. Williams, D. O’Kane, T. Yarkoni, and T. Brunner. *mwaskom/seaborn*. Version 0.11.2. 2021. DOI: 10.5281/zenodo.5205191. URL: https://doi.org/10.5281/zenodo.5205191.

[177] E. Jourdier, C. Cohen, L. Poughon, C. Larroche, F. Monot, and F. Ben Chaabane. “Cellulase activity mapping of *Trichoderma reesei* cultivated in sugar mixtures under fed-batch conditions”. In: *Biotechnology for Biofuels* 6 (2013), p. 79. DOI: 10.1186/1754-6834-6-79.

[178] R. E. Kitson and M. G. Mellon. “Colorimetric determination of phosphorus as molybdivanadophosphoric acid”. In: *Industrial & Engineering Chemistry Analytical Edition* 16 (1944), pp. 379–383. DOI: 10.1021/i560130a017.

List of Figures

1.1. Product groups produced by filamentous fungi 3
1.2. Life cycle of filamentous fungi 4
1.3. Morphology of filamentous fungi in submerged cultivation 6
1.4. Mechanism of action of cellulases 10
1.5. Reaction catalyzed by phytases 11
1.6. The BioLector MBR 14
1.7. Schematic of the laboratory automation platform used in this work 17
1.8. Schematic of the automated microscopy equipment used in this work . . 19
2.1. Batch cultivation of *T. reesei* in an FP 25
2.2. Batch cultivation of *T. reesei* in an RWP at 1000 rpm 27
2.3. Batch cultivation of *T. reesei* with adapted medium 30
2.4. Correlation between scattered light and CDW for *T. reesei* 32
2.5. Cellulase activities for different glucose and lactose combinations 35
2.6. Batch cultivation of *T. reesei* RutC30 with glucose and lactose 36
2.7. Fed batch cultivation of *T. reesei* RutC30 38
3.1. Schematic of the *A. niger* cultivation workflow 43
3.2. Manual reference cultivation of *A. niger* 44
3.3. Cultivation of *A. niger* with automated inoculation of individual wells . . . 47
3.4. Cultivation of *A. niger* with automated master mix inoculation 49
3.5. Manual cultivation of *A. niger* with reduced inoculum 51
3.6. Cultivation of *A. niger* with automated inoculation using wide outlet tips . 53
3.7. Comparison of 222 manual reference cultures of *A. niger* 56
3.8. Two-week schedules for *A. niger* cultivation procedures 58
4.1. Schematic of the *T. thermophilus* cultivation and analysis workflow 63
4.2. Microscopy settings for *T. thermophilus* 65
4.3. Batch cultivation of *T. thermophilus* with microfluidic pH control 67
4.4. Fed batch cultivation of *T. thermophilus* with microfluidic pH control 70
4.5. Training of the algorithm for segmentation of *T. thermophilus* biomass . . 76
4.6. Automatically extracted morphological metrics of *T. thermophilus* 78

4.7. Automatically segmented microscopy images of *T. thermophilus* 80
A.1. *A. niger* manual reference cultures and automatically inoculated cultures 124
A.2. Enlarged microscopy images of a *T. thermophilus* batch cultivation 125
A.3. Enlarged microscopy images of a *T. thermophilus* fed batch cultivation . . 126
A.4. Number of detected fungi over fungal size (pH 5.5) 127
A.5. Number of detected fungi over fungal size (pH 6.5) 128

List of Tables

3.1. Liquid classes for water and *A. niger* culture suspension 45
4.1. Key performance indicators for a fed batch cultivation of *T. thermophilus* . 72
6.1. List of devices used 89
6.2. List of software used 89
6.3. List of consumables used 90
6.4. List of strains used 91
6.5. MBR cultivation conditions 96
A.1. Liquid classes for *A. niger* culture suspension using standard robotic tips and wide outlet tips 123
A.2. Liquid classes for water and *T. thermophilus* culture suspension 129

A. Appendices

A.1. Supporting material for Chapter 3

Tab. A.1. Comparison of the liquid class for pipetting *A. niger* culture suspension with standard robotic tips (0.5 mm outlet diameter) and the liquid class for pipetting *A. niger* culture suspension with wide outlet robotic tips (0.8 mm outlet diameter).

Specification	***A. niger* liquid class Standard tips**	***A. niger* liquid class Wide outlet tips**
Aspiration speed [µl·s^{-1}]	40	380
Delay after aspiration [ms]	500	500
Dispense speed [µl·s^{-1}]	250	900
Delay after dispense [ms]	0	500
Breakoff speed [µl·s^{-1}]	250	380

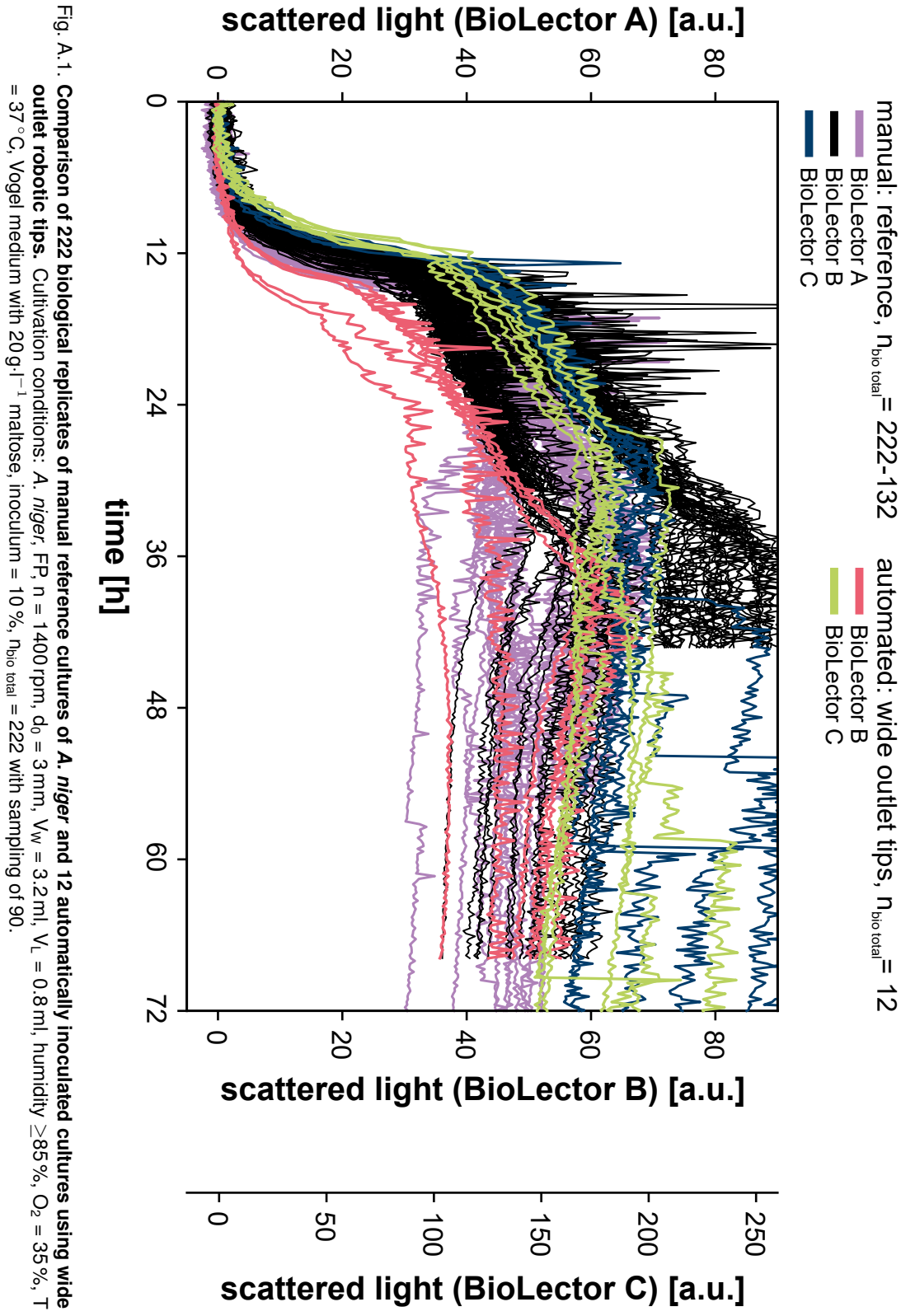

Fig. A.1. **Comparison of 222 biological replicates of manual reference cultures of *A. niger* and 12 automatically inoculated cultures using wide outlet robotic tips.** Cultivation conditions: *A. niger*, FP, n = 1400 rpm, d_0 = 3 mm, V_W = 3.2 ml, V_L = 0.8 ml, humidity $\geq$85 %, O_2 = 35 %, T = 37 °C, Vogel medium with 20 g·l^{-1} maltose, inoculum = 10 %, $n_{bio\ total}$ = 222 with sampling of 90.

A.2. Supporting material for Chapter 4

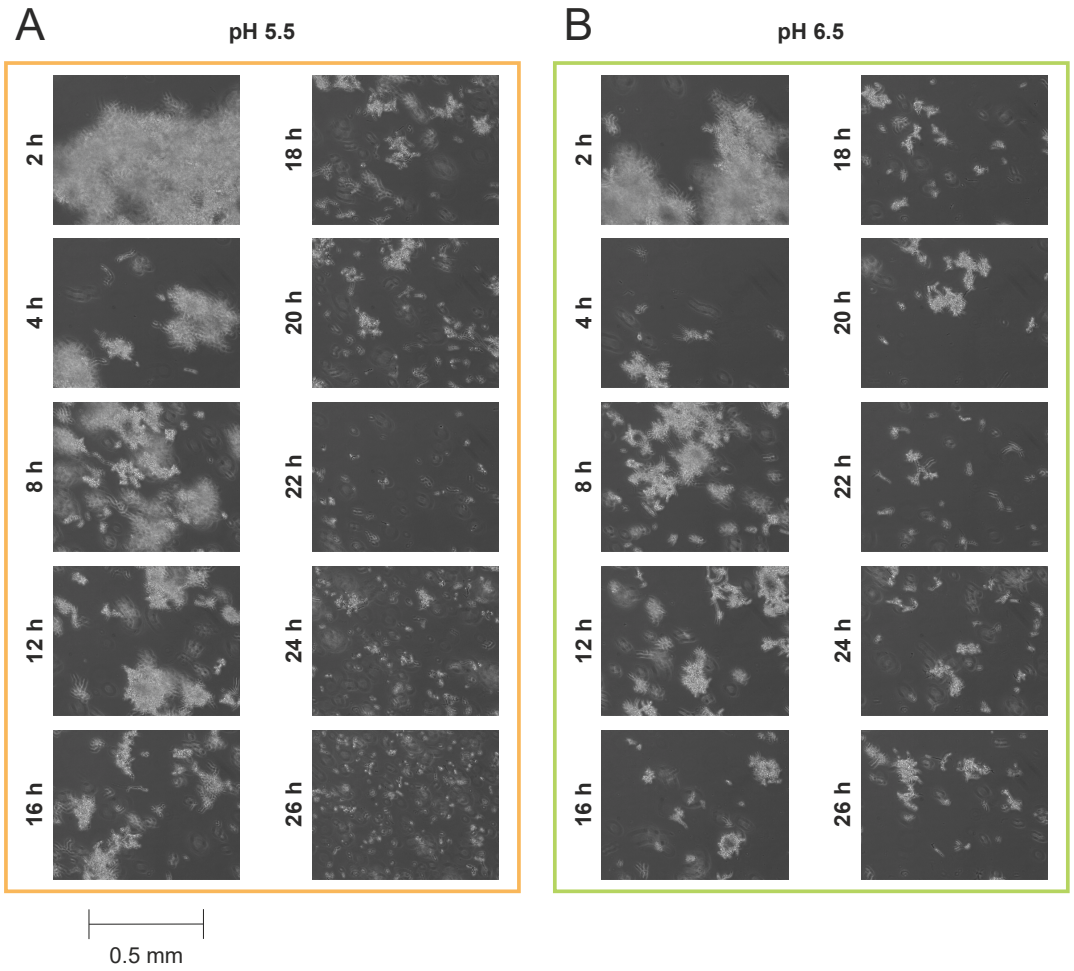

Fig. A.2. **Enlarged exemplary microscopy images taken fully automatically during batch cultivation of *T. thermophilus*.** Cultures at (A) pH 5.5 and (B) pH 6.5. Cultivation conditions: *T. thermophilus*, microfluidic FP, n = 1400 rpm, d_0 = 3 mm, V_W = 3.2 ml, V_L = 0.8 ml, humidity $\geq$85 %, O_2 = 35 %, T = 37 °C, 20 g·l^{-1} glucose, n_{bio} = 11 with sampling of 9.

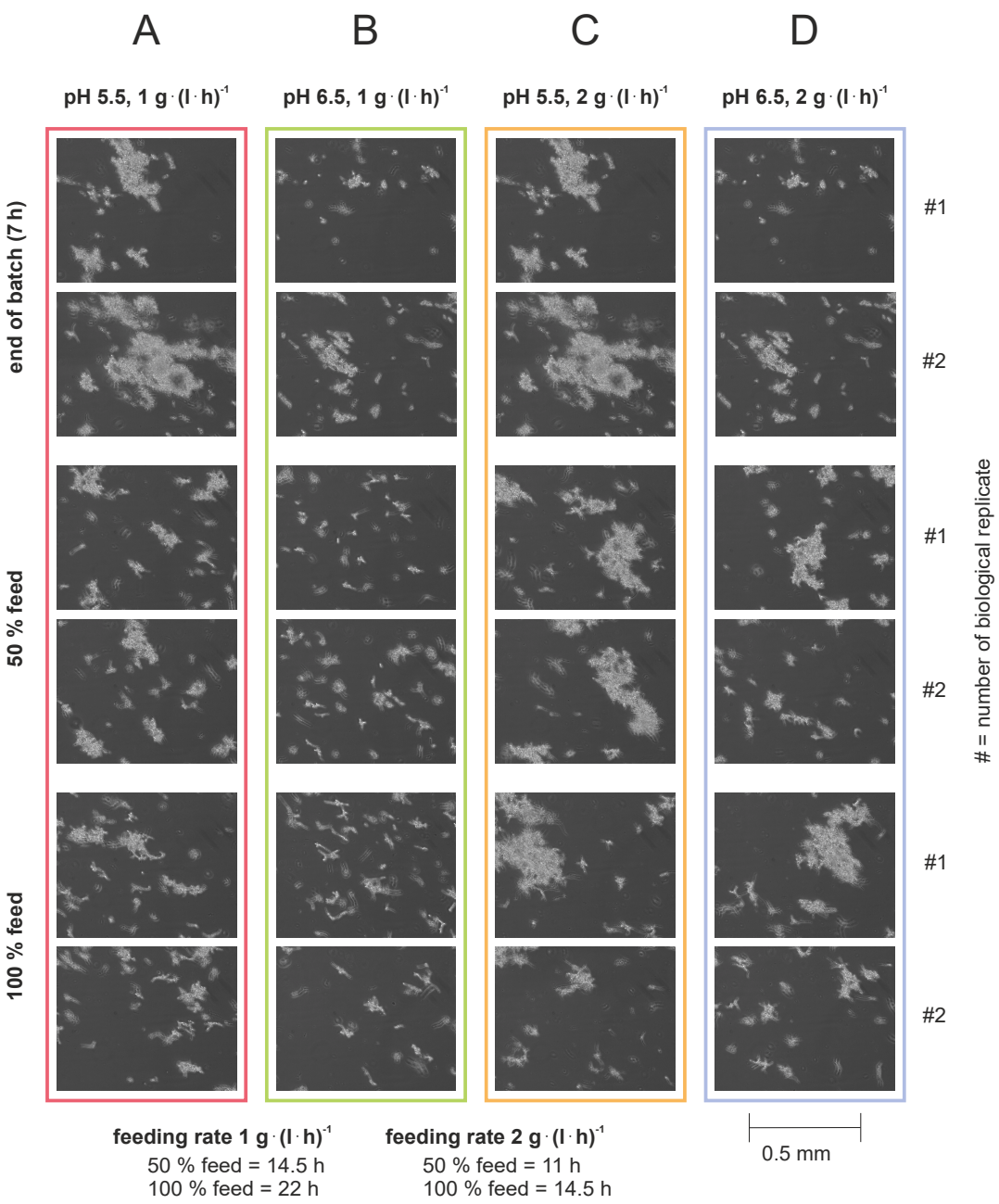

Fig. A.3. **Enlarged exemplary microscopy images taken fully automatically during fed batch cultivation of *T. thermophilus*.** Cultures at (A) pH 5.5 and (B) pH 6.5, both fed with 1 g·(l·h)$^{-1}$ glucose and cultures at (C) pH 5.5 and (D) pH 6.5, both fed with 2 g·(l·h)$^{-1}$ glucose. Cultivation conditions: *T. thermophilus*, microfluidic FP, n = 1400 rpm, d_0 = 3 mm, V_W = 3.2 ml, V_L = 0.8 ml, humidity $\geq$85 %, T = 37 °C. Batch: 5 g·l^{-1} glucose, O_2 = 21 %; fed batch: 15 g·l^{-1} glucose as a constant feed with a rate of 1 or 2 g·(l·h)$^{-1}$, O_2 = 35 %; n_{bio} = 8 with sampling of 5.

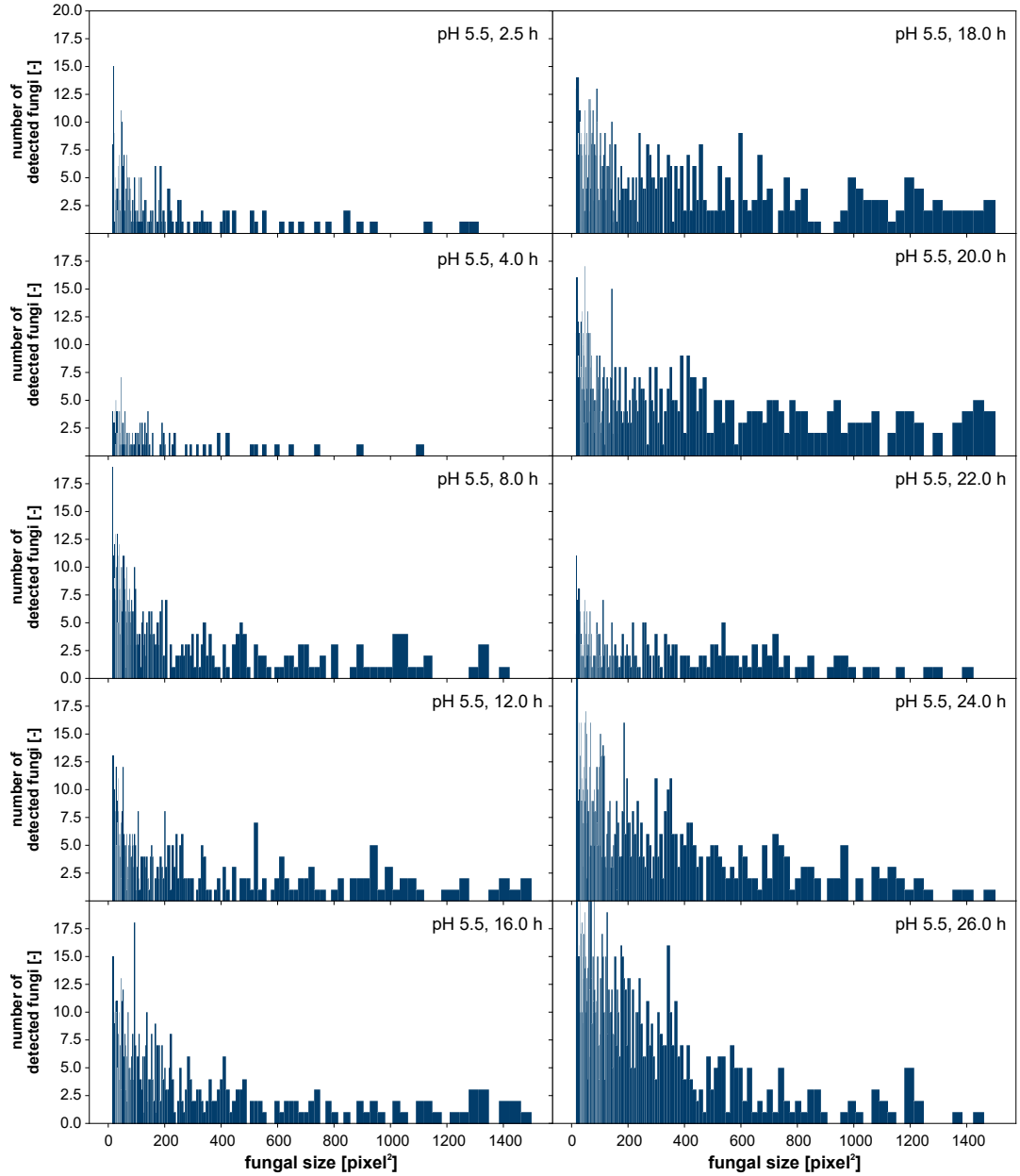

Fig. A.4. **Number of detected fungi over fungal size at pH 5.5.** Each histogram has 200 bins with logarithmically increasing bin sizes to ensure similar relative scales are covered per bin.

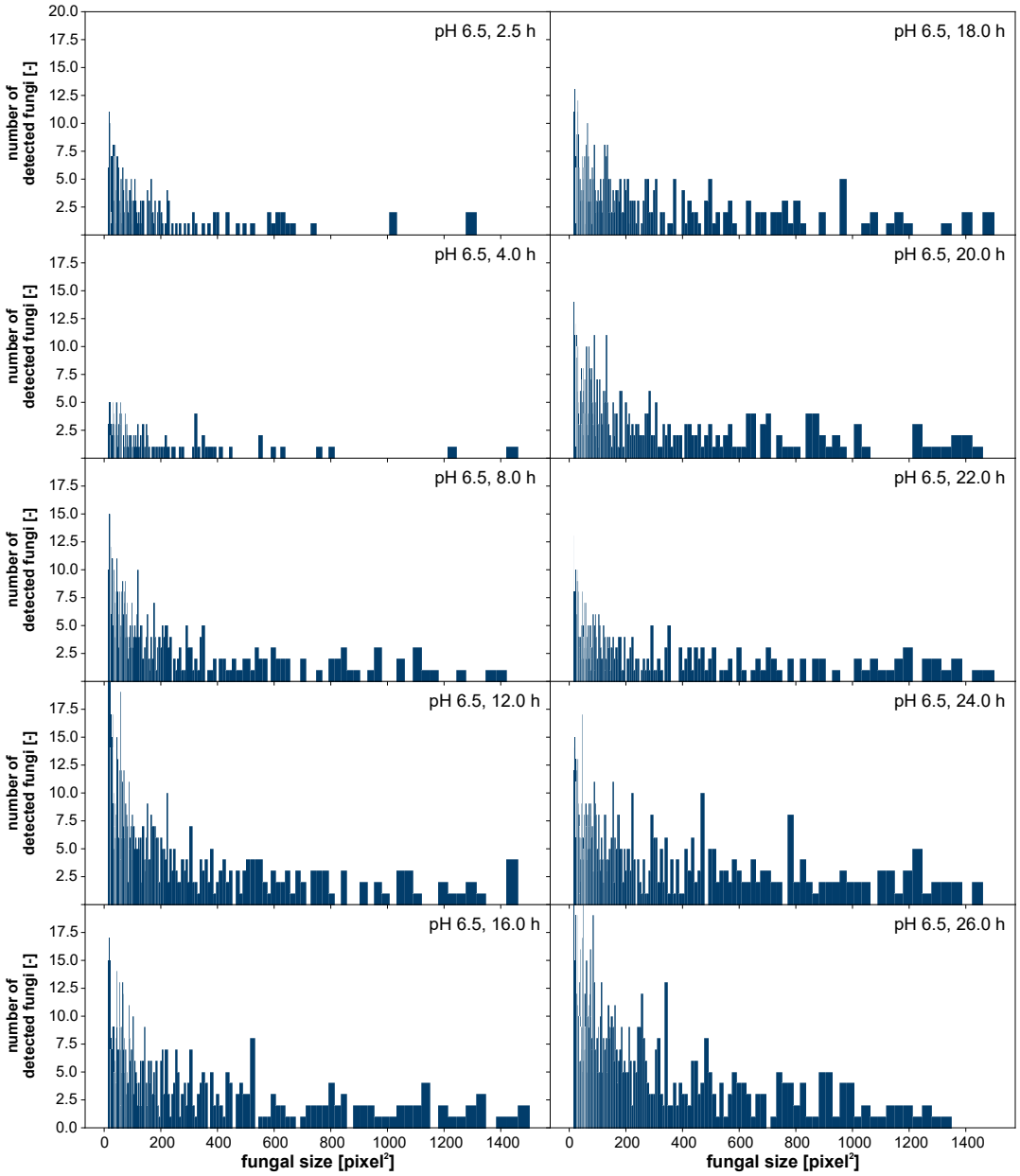

Fig. A.5. **Number of detected fungi over fungal size at pH 6.5.** Each histogram has 200 bins with logarithmically increasing bin sizes to ensure similar relative scales are covered per bin.

A.3. Supporting material for Chapter 6

Tab. A.2. Comparison of the liquid class for pipetting water with the liquid handling robotics system and the adapted liquid class for *T. thermophilus* culture suspension.

Specification	Water liquid class	*T. thermophilus* liquid class
Aspiration speed [µl·s^{-1}]	150	150
Delay after aspiration [ms]	200	200
Dispense speed [µl·s^{-1}]	600	600
Delay after dispense [ms]	0	0
Breakoff speed [µl·s^{-1}]	150	150